University of Nevada, Reno

Experimental Evaluation of Helical Piles for Underpinning Shallow Foundations on Soils Susceptible to Liquefaction using Shake Table Tests

A dissertation submitted in partial fulfillment of the
requirements for the degree of Doctor of Philosophy in
Civil and Environmental Engineering

by

Milad Jahed Orang

Dr. Ramin Motamed/Dissertation Advisor

August, 2021

THE GRADUATE SCHOOL

We recommend that the dissertation
prepared under our supervision by

MILAD JAHED ORANG

entitled

Experimental Evaluation of Helical Piles for Underpinning Shallow Foundations on Soils Susceptible to Liquefaction using Shake Table Tests

be accepted in partial fulfillment of the
requirements for the degree of

DOCTOR OF PHILOSOPHY

Ramin Motamed
Advisor

Raj Siddharthan
Committee Member

David McCallen
Committee Member

Stephen Dickenson
Committee Member

Behrooz Abbasi
Graduate School Representative

David W. Zeh, Ph.D., Dean
Graduate School

August, 2021

Abstract

The severe damage observed during past earthquakes resulting from the liquefaction of shallow saturated soil deposits underneath structures have demonstrated the necessity for further research in the area of liquefaction-induced ground movement effects. This research explores the utilization of helical piles to reduce liquefaction-induced foundation settlement and investigates their seismic performance in liquefiable grounds. Twenty-two shake table tests were conducted to examine the dynamic behavior of helical piles and their efficiency in liquefiable grounds. Among these tests, two shake table test series, one without any mitigation measures and one using helical piles, were conducted using the shake table facility at the University of California, San Diego (UCSD). The remaining shake table tests were conducted using the scaled shake table facility at the University of Nevada, Reno (UNR).

During large-scale test series at UCSD, the soil and structural components were extensively instrumented and subjected to two consistently applied shaking sequences. The model ground included a shallow liquefiable layer aimed at replicating the subsurface ground conditions observed in past earthquakes in New Zealand, Japan, and Turkey. Results from the first test series of large-scale tests (i.e., without mitigation) indicated that the flow velocity due to the hydraulic transient gradient displayed an upward flow in the loose layer, which explains the observed sand ejecta. This series of shake table tests aimed at reproducing the potential damage during liquefaction of shallow liquefiable deposits. As a result, the average foundation settlement in Shake 1 and Shake 2 were measured to be 28 cm and 42.7 cm, respectively. Measured foundation settlements were compared to the estimated foundation settlement obtained from Liu and Dobry [1997] and Bray and

Macedo's [2017] simplified procedures. The observed foundation settlement generally was higher than the estimated settlement. In the second large-scale test series, reduced excess pore-water pressure generation around the group of helical piles is mainly attributed to the increased relative density around their zone of influence as a result of installation. The foundation supported on helical piles underwent almost no differential settlement and tilt. Moreover, a significant reduction took place during the Helical Pile test compared to the Baseline test (i.e., 96% reduction on average). Liquefaction-induced settlement mechanisms are categorized as 1- shear-induced, 2- volumetric-induced, and 3- ejecta-induced. The post-shaking liquefaction-induced settlement mechanisms (i.e., volumetric and ejecta-induced mechanisms) did not affect the foundation settlement supported by helical piles. This series of large-scale shake table tests delivered a unique benchmark for calibration of numerical models, and simplified procedures to reliably estimate liquefaction-induced building settlements. Although this study introduced helical piles as a reliable and highly efficient measure to mitigate liquefaction-induced foundation tilt and settlement, the proper design and application of helical piles in seismic areas still need thorough investigation due to possible amplified superstructure response.

In the scaled shake table test series at UNR, multiple shakings were applied during each test series to evaluate the seismic behavior of the scaled helical piles and the slender shaft, taking into account various response parameters. These scaled shake table tests provided the opportunity to perform parametric study on the effects of ground motion amplitude, liquefiable layer densification, superstructure weight, and number of helices on the helical piles. Considerable ground settlements were measured during the first shaking in each test series, however negligible helical pile and slender shaft settlements were

observed during all tests. The bending moment variation showed a similar trend along the depth for the helical piles and the slender shaft: the maximum moment was consistently observed at the boundary between dense and liquefiable layers. The observed bending moments along the depth increased with increases in input motion amplitude and superstructure weight. Densification of the liquefiable layer during different test series reduced the maximum bending moment along the depth for each pile due to increased relative density. Increasing the number of helices improved the dynamic performance of the helical piles compared to the slender shaft such as maximum bending moment, maximum horizontal displacement, residual horizontal displacement, and superstructure acceleration in different ground conditions.

DEDICATION

This dissertation is dedicated to my beloved parents, Ali Asghar Jahed Orang and Maryam Farajzadeh, and to my lovely sibling, Shadi Jahed Orang, who continuously supported me on this journey. I will always be thankful for their sincere and wholehearted assistance during my life.

ACKNOWLEDGMENTS

The large-scale shake table tests were supported by funding through PEER (Pacific Earthquake Engineering Research Center) and Ram Jack. The scaled tests were funded through DFI (Deep Foundations Institute) and Ram Jack. Their generous support during this research is gratefully acknowledged.

I would like to express my sincere gratitude to my advisor Prof. Ramin Motamed for his support, assistance, and practical advice which paved the way for fruitful research during my Ph.D. studies.

I would also appreciate my dissertation committee Dr. Raj Siddharthan, Dr. David McCallen, Dr. Steve Dickenson, and Dr. Behrooz Abbasi for their suggestions and advice. Their comments and critical assessments provided salient insights through the course of this research.

Finally, I appreciate the lab staff and a group of graduate and undergraduate students at UC San Diego Powell laboratory and UNR SEM120 Laboratory especially Reza Boushehri, Fahim Mashrour Bhuyian, Andrew Sander, and Wendy Freeman for their assistance during tests preparation.

Table of Contents

List of Tables

List of Figures

1. Introduction

1.1. Statement of Research

Nowadays, the progressive research in structures and infrastructure utilities into more resilient design considerations with regards to performance-based engineering entails rigorous countermeasures related to geo-hazards. This includes liquefaction to count on the subsequent effects of geo-hazards when resiliency and post-earthquake damage recovery of infrastructures are taken into consideration. The liquefaction phenomenon is known as one of the most destructive geo-hazards, which occurs mainly in loose, sandy material and sands with some extent of fine-grained soil during an earthquake. During liquefaction, the strength of the soil reduces significantly due to the increase in the excess pore-water pressure. One of the effects of this phenomenon, known as liquefaction-induced settlement, causes catastrophic loss and damages to the structures overlain on a liquefiable ground. Post-disaster reconnaissance of areas affected by earthquakes has documented extensive damage to shallow foundations of structures within liquefaction-prone areas. For example, the 2010 and 2011 Canterbury Earthquake Sequence (CES) in New Zealand caused severe and widespread liquefaction throughout the town of Christchurch and subsequent damage to more than 20,000 residential buildings (Bray et al. [2014]). Similarly, over 27,000 buildings in Japan experienced substantial damage due to liquefaction during the 2011 Tohoku earthquake (Tokimatsu and Katsumata [2011]). Liquefaction has been extensively observed throughout California in its urban areas such as during the 1989 Loma Prieta earthquake and future earthquake events can result in similar damages to the structures. Having a good perception of the above-mentioned issues is of great importance to minimize the cost, fatality, and damage due to liquefaction.

During seismic events, foundations are deemed to have a vital role in providing integrity to the structures found in soils susceptible to liquefaction. Continuing research into the performance of foundations in seismic areas is essential to ensure that public safety is maintained. Where existing structures are to be seismically upgraded, research is needed to provide guidelines to properly design underpinning systems. Helical piles are a type of deep foundation used regularly to underpin both new and existing structures. Current practice lacks offering a cost-effective yet robust solution for underpinning residential buildings and low-story structures during earthquakes. The main goal of this research is to experimentally evaluate the performance of helical piles as an alternative solution for mitigating the settlement of shallow foundations in liquefiable soils. Additionally, this study is expected to have a broader application in the resilient design of bridges and structures by providing a more cost-effective and environmentally friendly solution in reducing the liquefaction-induced settlement effects due to earthquakes.

1.2. Motivation and Background

Previous research provided valuable insight into the liquefaction phenomenon and its subsequent effects. This included the observed behavior of foundation performance through numerous case histories around the world. The liquefaction-induced settlement mechanisms and subsequent procedures were also presented to estimate the amount of free-field and foundation settlement due to liquefaction. Additionally, various measures were introduced to minimize the associated cost and damage of the liquefaction effects including liquefaction-induced settlement and lateral spreading of the ground. All of the above-mentioned aspects are further described in detail hereafter.

Documented case histories regarding the devastating effects of liquefaction during past earthquakes have rendered valuable information to the researchers. Past earthquakes including the 1964 Niigata earthquake in Japan and the 1990 Luzon Philippine earthquake resulted in extensive damage to structures and the built environment (Yoshimi and Tokimatsu [1977]; Adachi et al. [1992]). Recent examples of these earthquakes such as the 2010-2011 Canterbury Earthquake Sequence (CES) in New Zealand and the 2011 Tohoku earthquake in Japan, also resulted in considerable liquefaction-induced damage to buildings and their foundations (Cubrinovski et al. [2010]; Yasuda et al. [2012]; Cubrinovski [2013]; Henderson [2013]). Excessive foundation settlements were observed during CES in 2010-2011, where field reconnaissance was reported differential settlements as high as 12 cm in some important buildings after the 2011 Christchurch earthquake (Bray et al. [2017]). In many cases, the foundations' differential settlement and tilt even resulted in the demolition of buildings after earthquake events (Bray et al. [2014]). Other documented case histories such as 1999 Kocaeli earthquake in Turkey (Bray and Stewart [2000]; Sancio et al. [2002]; Bray et al. [2004]) and 2010 Maule Chile earthquake (Bray and Frost [2010]; Bray et al. [2012]) also illustrated the catastrophic nature of liquefaction phenomenon and its consequent effects on the superstructures in urban areas.

Consequences of liquefaction include lateral spreading of the ground, which has been extensively documented at port facilities in Japan, as well as settlement of structures supported on shallow foundations. Liquefaction also caused extensive damage to lifeline facilities and pipeline systems due to the induced ground deformation. Lateral displacement of the soil and subsequent countermeasures to tackle this issue has been studied by 1-g shake table tests (Motamed and Towhata [2009]; Motamed et al. [2009];

Motamed et al. [2013]; Ebeido et al. [2019a]) and dynamic centrifuge experiments (Zeghal et al. [1999]; Dobry et al. [2001]; Abdoun et al. [2003]; Boulanger et al. [2003]). Liquefaction-induced movement of structures during strong motions has been further evaluated using numerical analyses, experimental studies, and field reconnaissance, which are summarized in the next section.

Past research on the behavior of shallow foundations in liquefiable soils consists of utilizing shake table tests (Yoshimi & Tokimatsu [1977]; Kokusho [1999]; Jacobs [2016]; Rasouli et al. [2016]; Toth and Motamed [2017]; Honnette [2018]; Jahed Orang et al. [2019a, b]; Bahadori et al. [2020]; Prabhakaran et al. [2020a, b]; Jahed Orang et al. [2021a, b]), centrifuge experiments (Lambe and Whitman [1985]; Liu and Dobry [1997]; Hausler [2002]; Dashti et al. [2010a,b]; Hayden et al. [2015]; Jafarian et al. [2017]; Kirkwood and Dashti [2018]; Mehrzad et al. [2018]; Tokimatsu et al. [2019]), field reconnaissance (Yoshimi and Tokimatsu [1977]; Adachi et al. [1992]; Bray and Frost [2010]; Cubrinovski et al. [2010, 2011]; Tokimatsu and Katsumata [2011]; Tokimatsu et al. [2011]; Bray et al. [2014]), and numerical simulations (Dashti and Bray [2013]; Karamitros et al. [2013]; Karimi and Dashti [2016]; Karimi et al. [2018]; Macedo and Bray [2018]). These studies have investigated the controlling mechanisms of liquefaction-induced building settlement and the effects of key parameters on the overall foundation response. The hierarchy of the highlighted research and the evolutionary progress regarding the mechanisms of the liquefaction-induced foundation settlement are summarized hereafter.

The 1964 Niigata earthquake resulted in the widespread liquefaction-induced settlement of buildings, attracting the interest of researchers in field reconnaissance followed by experimental research. During the Niigata event, 340 reinforced concrete

buildings experienced damage resulting from liquefaction. Field reconnaissance after the event estimated that liquefaction occurred to maximum depths of 20 m and the maximum building settlements reached 3.8 m (Yoshimi & Tokimatsu [1977]). In addition to the field observations, Yoshimi & Tokimatsu [1977] conducted scaled 1-g shake table tests to explore the effects of different parameters on building settlement as a result of liquefaction in sub-soils. Their study is believed to be the first experimental research focused on the behavior of shallow foundations in liquefiable soils. Based on the documented case histories from the 1964 Niigata earthquake and the complementary scaled 1-g shake table tests, Yoshimi and Tokimatsu [1977] concluded that the average settlement (S) normalized by the thickness of the liquefiable layer (D) shows an inverse relation with building width (B).

The contributing mechanisms in the liquefaction-induced settlement have been widely studied. For example, Tokimatsu and Seed [1987] and Ishihara and Yoshimine [1992] proposed empirical procedures assuming free-field conditions. One of the very first studies regarding settlement of ground due to liquefaction phenomenon was conducted by Ishihara and Yoshimine [1992], who used simple shear tests to correlate the volumetric strain (ε_v) with the relative density (D_r) of clean sand and factor of safety (FS) against liquefaction. The predicted amount of settlement based on the laboratory test results was compared to the observed settlements from the 1964 Niigata earthquake. The amount of volumetric strain for clean sand was calculated based on FS against liquefaction and relative density of each layer with a chart that leads to the calculation of overall ground settlement by integrating the volumetric strains generated within each layer. The methodology proposed by Ishihara and Yoshimine [1992] allows the calculation of ground

(i.e., free-field) settlement due to liquefaction during earthquakes and does not account for external loads (i.e., structures and foundations).

Liu and Dobry [1997] conducted eight centrifuge tests to examine settlement characteristics of circular foundations founded on liquefiable soils. They also reviewed two field case histories, which included the 1964 Niigata and the 1990 Luzon Philippine earthquakes to compare their experimental results. They reported that the degree of settlement is dependent upon foundation width and the liquefiable layer thickness, which was in line with the conclusions drawn by Yoshimi and Tokimatsu [1977].

Dashti et al. [2010a] conducted centrifuge experiments to model the mechanisms of liquefaction-induced settlement, identifying the effects of shear-induced mechanism along with partial drainage component of volumetric-induced mechanism as the dominant mechanisms contributing to the settlement of buildings in liquefiable soils. The dependency of these mechanisms on the characteristics of ground motion, subsurface conditions, and superstructure was also presented in Dashti et al. [2010a]. Later, the liquefaction-induced foundation settlement has been categorized into three main mechanisms: 1- shear-induced, 2- volumetric-induced, and 3- ejecta-induced, where each mechanism is further sub-categorized to its contributing effects which are briefly discussed here. The mechanisms contributing to the volumetric-induced settlement are partial drainage, sedimentation or solidification, and post-liquefaction reconsolidation. The shear-induced settlement is attributed to the partial bearing capacity failure of the foundation and soil-structure-interaction (SSI) induced ratcheting displacement near the edges of the foundation (Bray and Dashti [2014]). These effects can be captured using numerical simulations such as in FLAC-2D and FLAC-3D (Dashti and Bray [2013]; Karamitros et

al. [2013]) Macedo and Bray [2018]) and OpenSees (Karimi and Dashti [2016]; Karimi et al. [2018]). In a recent paper, Motamed et al. [2020] discussed the use of different numerical simulation techniques and their efficiency in predicting liquefaction-induced foundation and free field settlements. The ejecta-induced settlement is manifested by the sand boils on the ground surface. The ground failure indices, along with the correlations between ejecta volume and foundation settlement, can be used to further quantify ejecta-induced settlement (Bray and Macedo [2017]; Jahed Orang et al. [2019a]). Researchers have observed that much of the foundation settlement takes place during shaking, indicating a higher contribution of shear-induced mechanisms and partial drainage due to high hydraulic transient gradients (Dashti et al. [2010a, b]; Bray and Dashti [2014]).

In a more recent study, Bray and Macedo [2017] proposed a simplified method to estimate the shear-induced element of liquefaction-induced building settlement and provided a framework to estimate it along with the volumetric-induced settlement based on past studies. They made further recommendations on how to estimate the ejecta-induced settlement to add to the previous two components for estimating the overall settlement of buildings due to liquefaction. Lu [2017] and Bullock et al. [2018] also presented semi-empirical procedures to calculate the total settlement of the foundation due to liquefaction. In this report, Bray and Macedo's [2017] simplified procedure is employed to estimate the shake table settlement results and to compare with the observed values.

In addition to better understanding the key mechanisms of liquefaction-induced foundation settlement, it is essential to evaluate different ground improvement and foundation underpinning techniques. Several studies examined various ground improvement techniques, taking into account the contributing mechanisms of liquefaction-

induced settlement. Among these liquefaction mitigation measures are the use of ground densification methods (Liu and Dobry [1997]; Yegian et al. [2007]; Dashti et al. [2010a, b]; Olarte et al. [2017]; Rasouli et al. [2018]); drainage methods such as using underground columns (Ashford et al. [2000]; Adalier et al. [2003]; Badanagki et al. [2018]; Bahmanpour et al. [2019]), Prefabricated Vertical Drains (PVD) (Howell et al. [2012]; Olarte et al. [2017]; Paramasivam et al. [2018]; Kirkwood and Dashti [2019]), and diagonal drains (Rasouli et al. [2018]); ground bracing methods such as gravel drains (Hayden and Baez [1994]; Iai et al. [1994]; Adalier et al. [2003]), in-ground structural walls (i.e., sheet pile walls) (Olarte et al. [2017]; Rasouli et al. [2018]), and soil-cement walls (Khosravi et al. [2016]; Boulanger et al. [2018]); microbial induced calcite precipitation (MICP) (Montoya et al. [2013]; Darby et al. [2019]); induced partial saturation (Eseller-Bayat et al. [2013]; Mousavi and Ghayoomi [2019]; Mousavi and Ghayoomi [2021]); and the use of geocomposite and geogrid reinforcement (Bahadori et al. [2020]). The listed ground improvement techniques address some of the liquefaction-induced settlement mechanisms, providing varying mitigation efficiencies depending on different ground conditions and shaking intensities. In a recent study, the use of polymer injection was studied to minimize liquefaction-induced foundation settlement using large-scale shake table tests, and the results indicated the salient performance of a shallow foundation in a shallow liquefiable stratum rehabilitated with synthetic polymer (Prabhakaran et al. [2020b]). Although various methods provide some extent of efficiency in reducing foundation tilt and settlement, the cost-effectiveness and higher-order efficiencies in mitigating liquefaction-induced settlement still need further investigation.

The dynamic behavior of deep foundations has been studied through past research and considerable progress has been made to explore the seismic behavior of different types of deep foundations at various ground conditions. Experimental studies including centrifuge tests (Boulanger et al. [1999]; Wilson et al. [2000]; Ghayoomi et al. [2018]) and shake table experiments (Makris et al. [1997]; Tokimatsu et al. [2005]; Mashhoud et al. [2018]; Lim and Jeong [2018]) were used to investigate the dynamic response of single steel piles, single micropiles, and pile groups mainly in dry and unsaturated sandy, silty, and cohesive soils. The effect of multi-layer soil deposits on the seismic response of driven steel piles was studied in Wilson et al. [2000] and Abdoun et al. [2003]. Additionally, field test results garnered useful insight on soil-pile-structure interaction under dynamic loading (Novak and Grigg [1976]; El-Marsafawi et al. [1992]; Nikolaou et al. [2001]; Abd Elaziz and El Naggar [2014]; Capatti et al. [2018]; Farhangi et al. [2020]). Moreover, The behavior of pile foundations in liquefied and lateral spreading grounds has been investigated through 1g shake table experiments (Motamed and Towhata [2009]; Motamed et al. [2009]; Motamed et al. [2013]; Ebeido et al. [2019a]) and centrifuge testing (Zeghal et al. [1999]; Dobry et al. [2001]; Abdoun et al. [2003]; Boulanger et al. [2003]). Amongst several types of deep foundations studied by the researchers, there is a lack of knowledge regarding the response of helical piles in the liquefiable grounds.

Helical piles are a type of deep foundation elements which are used for underpinning foundations in existing and new construction, especially in areas with limited access and low headroom. In addition, helical piles have the benefit of fast and easy installation with minimal equipment. The main components of helical piles consist of a lead section, an extension part, helical plates, and coupling connections (Perko [2009]).

Due to the increasing demands on helical piles' utilization, evaluation of the seismic response of helical piles is of great importance. Helical piles could be a cost-effective solution for retrofitting low-story buildings in areas susceptible to liquefaction. Although the satisfactory performance of helical piles has been observed during past earthquakes in New Zealand, Japan, and the United States, design codes do not address the use of helical piles in high seismic zones (Cerato et al. [2017]). However, these observations arose the question of the dynamic behavior of helical piles in recent years.

Past published studies on the dynamic behavior of helical piles, examined the post-cyclic axial capacity taking into account various parameters such as helix number, helix size, shaft size, and helical pile type, including reinforced and unreinforced grouted pulldown micropiles (El Naggar & Abdelghany [2007a, b]; Abdelghany [2008]; Cerato & Victor [2008, 2009]). Past research has also expanded the knowledge on the behavior of helical piles under axial loading (static and dynamic) in various subsurface ground conditions. Recently, the dynamic response of different helical piles and helical pile groups in dense dry sand has been examined using shake table experiments. Recent large-scale shake table test at UCSD outdoor shake table facility (ElSawy et al. [2019a]) and scaled 1g shake table test at UNR (Jahed Orang et al. [2019b]) shed light on the adequate performance of helical piles in dry sand. ElSawy et al. [2019a, b] conducted a series of full-scale 1g shake table experiments using UCSD large high-performance outdoor shake table (LHPOST) to evaluate the dynamic behavior of different helical piles with different shaft shape, length and size with variable top weights and number of helices. Ten steel piles (9 helical piles and 1 driven pile) located within 1 m (i.e., center to center) from each other installed in a uniform dense sand layer. Two different earthquake loadings, including

Northridge (1994) and Kobe (1995), with different intensities and frequency content, were applied as input motions to assess the dynamic behavior of helical piles. All of these shake table experiments intended to examine several parameters such as the effects of loading frequency and intensity, installation methods, number of helices, pile shaft shape, and pile group damping characteristics (ElSawy et al. [2019a, b]; Jahed Orang et al. [2019b]; Shahbazi et al. [2020a, b]). Yet, the seismic performance of helical piles in liquefiable ground conditions and their efficiency in improved soil-pile-foundation response to liquefaction-induced settlement and tilt has not been well understood.

1.3. Research Objectives

Twenty-two shake table tests were conducted to evaluate the performance of a shallow foundation and helical piles in different ground conditions. Two test series were conducted at UCSD using the large-scale shake table facility located at Powell Laboratory. The first test series was conducted without any mitigation measures (i.e., Baseline test) whereas a group of helical piles was used as a liquefaction mitigation measure in the second test series (i.e., the Helical Pile test). The main purpose of this research is to evaluate the use of helical piles as a mitigation measure against liquefaction-induced shallow foundation settlement. The presence of shallow liquefiable soil deposits further encouraged the use of a large-scale 1g shake table to precisely replicate ground conditions observed in recent earthquakes in Japan, New Zealand, Turkey, and the United States (Bray et al. [2004]; Bray et al. [2014]; Luque and Bray [2017]). An overview of various objectives followed through this research are summarized below:

- Evaluate the behavior of a rigid shallow foundation underlain by near-surface liquefiable soils using a prototype soil profile.

- Provide a holistic understanding of the phenomenon of liquefaction-induced building settlement where surficial loose liquefiable soils are located at shallow depths.
- Make progress in the realization of the contribution of each liquefaction-induced mechanism during the Baseline and Helical Pile Tests.
- Evaluate the performance of helical piles in surficial liquefiable deposits while supporting a shallow foundation.
- Compare the existing remediation methods and the use of helical piles as a mitigation measure.
- Provide higher efficiencies in reducing liquefaction-induced foundation settlement and tilt.

Additional test series were conducted at the scaled shake table facility at UNR SEM120 Laboratory focusing on the seismic behavior of various helical piles with different specifications. The following goals were investigated during these test series:

- Verify the seismic performance of various helical piles with different specifications in dry ground conditions.
- Assess the effect of several parameters such as ground conditions, input motion characteristics, and structural components on the behavior of helical piles in liquefiable grounds.
- Compare the dynamic response of the different types of helical piles (i.e. difference in the number of helices) with other types of slender piles.

Overall, the achieved experimental data can be used as a baseline to validate numerical simulations of liquefaction-induced building settlement and evaluate the effectiveness of different liquefaction mitigation measures. The main scope of this study is to assess cost-effective remedial measures for liquefaction-induced foundation settlements including helical piles. This encompasses the efficiency of different methods in reducing liquefaction-induced foundation settlements along with investigating the dynamic behavior of single and group of helical piles in liquefiable grounds.

1.4. Organization of the Dissertation

This dissertation is compiled in five chapters based on three journal papers. A short summary of the title and the publication status of each paper will be provided at the end of this section.

The first chapter provides an overview of the field reconnaissance on liquefaction and its effects during past earthquakes. A literature review about liquefaction-induced mechanisms, liquefaction mitigation measures, and helical piles is also provided in this chapter. Finally, the research objectives and organization of this dissertation are explained. In the second chapter, the performance of a shallow foundation overlain on a shallow liquefiable deposit was evaluated using large scale shake table tests at the UCSD Powell Laboratory. The liquefaction-induced mechanisms were assessed through this shake table program. This series is referred to as the “Baseline” test throughout this dissertation since no mitigation measures were utilized during these test series. The third chapter describes the application of a group of helical piles to mitigate liquefaction-induced tilt and settlement. In this chapter, the same large scale shake table setup was utilized to assess the dynamic behavior of a group of helical piles along with the efficiency of this ground

improvement method in liquefaction-induced tilt and settlement mitigation. This test series is referred to as the “Helical Pile” test throughout this dissertation. The fourth chapter provides scaled shake table tests which were conducted at the UNR SEM 120 Laboratory. In this test series single helical piles with different specifications were assessed to gain a broader understanding on their dynamic performance. A comparison was also made between multiple-helix helical piles and a slender shaft throughout this study. Finally, the fifth chapter summarizes the major findings and outcomes throughout these comprehensive shake table studies and provides research recommendations for prospective studies.

Chapter 2:

Title: Large-Scale Shake Table Tests on a Shallow Foundation in Liquefiable Soils

Publication status: Published in the Journal of Geotechnical and Geoenvironmental Engineering (ASCE)

Citation: Jahed Orang, M., Motamed, R., Prabhakaran, A., & Elgamal, A. (2021). Large-Scale Shake Table Tests on a Shallow Foundation in Liquefiable Soils. *Journal of Geotechnical and Geoenvironmental Engineering*, *147*(1), 04020152.

Chapter 3:

Title: An Experimental Evaluation of Helical Piles as a Liquefaction-Induced Building Settlement Mitigation Measure

Publication status: Submitted to Soil Dynamics and Earthquake Engineering Journal

Citation: Jahed Orang, M., Boushehri, R., Motamed, R., Prabhakaran, A., & Elgamal, A. (2021). An Experimental Evaluation of Helical Piles as a Liquefaction-Induced Building Settlement Mitigation Measure (under review)

Chapter 4:

Title: Dynamic Behavior of Helical Piles in Dry and Liquefiable Soils using Scaled Shake Table Tests

Publication status: Submitted to Deep Foundations Institute (DFI) Journal

Citation: Jahed Orang, M., Motamed, R. (2021). Dynamic Behavior of Helical Piles in Dry and Liquefiable Grounds using Scaled Shaking Table Tests (under review)

1.5. References

Abd Elaziz, A. Y., & El Naggar, M. H. (2014). Group behaviour of hollow-bar micropiles in cohesive soils. *Canadian geotechnical journal*, *51*(10), 1139-1150.

Abdelghany, Y. (2008). Monotonic and cyclic behavior of helical screw piles under axial and lateral loading. University of Western Ontario Electronic Thesis and Dissertation Repository.

Abdoun, T., Dobry, R., O'Rourke, T. D., & Goh, S. H. (2003). Pile response to lateral spreads: centrifuge modeling. Journal of Geotechnical and Geoenvironmental engineering, 129(10), 869-878.

Adachi, T., Iwai, S., Yasui, M., and Sato, Y. (1992). Settlement and inclination of reinforced concrete buildings in Dagupan City due to liquefaction during 1990 Philippine earthquake. Proc. 10th World Conference on Earthquake Engineering, Vol. 2, A.A. Balkema Rotterdam, The Netherlands, 147-152.

Adalier, K., Elgamal, A., Meneses, J., & Baez, J. I. (2003). Stone columns as liquefaction countermeasure in non-plastic silty soils. Soil Dynamics and Earthquake Engineering, 23(7), 571-584.

Ashford, S. A., Rollins, K. M., Bradford, S. C., Weaver, T. J., and Baez, J. I. (2000). Liquefaction mitigation using stone columns around deep foundations: Full scale test results. Transp. Res. Rec., 1736, 110–118.

Badanagki, M., Dashti, S., & Kirkwood, P. (2018). Influence of dense granular columns on the performance of level and gently sloping liquefiable sites. Journal of Geotechnical and Geoenvironmental Engineering, 144(9), 04018065.

Bahadori, H., Motamedi, H., Hasheminezhad, A., Motamed, R. (2020). Shaking table tests on shallow foundations over geocomposite and geogrid-reinforced liquefiable soils. Soil Dyn Earthq Eng; 128:105896. https://doi.org/10.1016/j.soildyn.2019.105896.

Bahmanpour, A., Towhata, I., Sakr, M., Mahmoud, M., Yamamoto, Y., & Yamada, S. (2019). The effect of underground columns on the mitigation of liquefaction in shaking table model experiments. Soil Dynamics and Earthquake Engineering, 116, 15-30.

Borghei, A., Ghayoomi, M., & Turner, M. (2020). Centrifuge tests to evaluate seismic settlement of shallow foundations on unsaturated silty sand. In Geo-Congress 2020: Geotechnical Earthquake Engineering and Special Topics (pp. 198-207). Reston, VA: American Society of Civil Engineers.

Boulanger, R. W., Curras, C. J., Kutter, B. L., Wilson, D. W., & Abghari, A. (1999). Seismic soil-pile-structure interaction experiments and analyses. *Journal of geotechnical and geoenvironmental engineering*, *125*(9), 750-759.

Boulanger, R. W., Kutter, B. L., Brandenberg, S. J., Singh, P., & Chang, D. (2003). Pile foundations in liquefied and laterally spreading ground during earthquakes: centrifuge experiments & analyses. (No. UCD/CGM-03/01). Center for Geotechnical Modeling, Department of Civil and Environmental Engineering, University of California, Davis, California.

Boulanger, R. W., Khosravi, M., Khosravi, A., and Wilson, D. W. (2018). Remediation of liquefaction effects for an embankment using soil-cement walls: Centrifuge and numerical modeling. Soil Dynamics and Earthquake Engineering, 114(2018), 38-50, 10.1016/j.soildyn.2018.07.001.

Bray, J. D., & Stewart, J. P. (2000). Chapter 8: Damage patterns and foundation performance in Adapazari. Kocaeli, Turkey Earthquake of August 17, 1999 Reconnaissance Report, TL Youd, JP Bardet, and JD Bray, eds. Earthquake Spectra, Supplement A to, 16, 163-189.

Bray, J. D., R. B. Sancio, H.T. Durgunoglu, A. Onalp, T. L. Youd, J. P. Stewart, R. B. Seed, O.K. Cetin, E. Bol, M. B. Baturay, C. Christensen, and T. Karadayilar. (2004). Subsurface characterization at ground failure sites in Adapazari, Turkey. Journal of Geotechnical and Geoenvironmental Engineering, ASCE, Vol. 130, No. 7, pp. 673-685.

Bray, J.D., Frost, J.D. (Eds) (2010). Geo-engineering reconnaissance of the 2010 Maule, Chile earthquake. Accessed May 25, 2010.

Bray, J.D., Rollins, K., Hutchinson, T., Verdugo, R., Ledezma, C., Mylonakis, G., Assimaki, A., Montalva, G., Arduino, P., Olson, S.M., Kayen, R., Hashash, Y.M.A., Candia, G. (2012). Effects of ground failure on buildings, ports, and industrial facilities. Earthq Spectra J 28(S1):S97–S118

Bray, J. D., Cubrinovski, M., Zupan, J., & Taylor, M. (2014). Liquefaction effects on buildings in the central business district of Christchurch. Earthquake Spectra, 30(1), 85-109.

Bray, J. D. and Dashti, S. (2014). Liquefaction-induced building movements. Bulletin Earthquake Engineering, 12, 1129-1156.

Bray, J. D., & Luque, R. (2017). Seismic performance of a building affected by moderate liquefaction during the Christchurch earthquake. Soil Dynamics and Earthquake Engineering, 102, 99-111.

Bray, J. D. & Macedo, J. (2017). 6th Ishihara lecture: Simplified Procedure for estimating liquefaction-induced building settlement. Soil Dyn. Earthquake Eng., (102) 215-231 http://dx.doi.org/10.1016/j.soildyn.2017.08.026.

Bray, J.D., Markham, C.S., and Cubrinovski, M. (2017). Liquefaction Assessments at Shallow Foundation Building Sites in the Central Business District of Christchurch, New Zealand. Soil Dynamics and Earthquake Engineering J., V. 92, 153-164, http://dx.doi.org/10.1016/j.soildyn.2016.09.049.

Bullock, Z., Karimi, Z., Dashti, S., Porter, K., Liel, A. B., & Franke, K. W. (2018). A physics-informed semi-empirical probabilistic model for the settlement of shallow-founded structures on liquefiable ground. Géotechnique, 69(5), 406-419.

Bullock, Z., Dashti, S., Liel, A. B., Porter, K. A., & Karimi, Z. (2019). Assessment Supporting the Use of Outcropping Rock Evolutionary Intensity Measures for Prediction of Liquefaction Consequences. Earthquake Spectra, 35(4), 1899-1926.

Capatti, M. C., Dezi, F., Carbonari, S., & Gara, F. (2018). Full-scale experimental assessment of the dynamic horizontal behavior of micropiles in alluvial silty soils. *Soil Dynamics and Earthquake Engineering*, *113*, 58-74.

Cerato, A. B., & Victor, R. (2008). Effects of helical anchor geometry on long-term performance of small wind tower foundations subject to dynamic loads. DFI Journal-The Journal of the Deep Foundations Institute, 2(1), 30-41.

Cerato, A. B., & Victor, R. (2009). Effects of long-term dynamic loading and fluctuating water table on helical anchor performance for small wind tower foundations. Journal of performance of constructed facilities, 23(4), 251-261.

Cerato, A.B., Vargas, T.M. & Allred S.M. (2017). A critical review: state of knowledge in seismic behavior of helical piles. The Journal of the Deep Foundation Institute 11(1): 39-87.

Cetin, K. O., Bilge, H. T., Wu, J., Kammerer, A. M., & Seed, R. B. (2009). Probabilistic model for the assessment of cyclically induced reconsolidation (volumetric) settlements. Journal of Geotechnical and Geoenvironmental Engineering, 135(3), 387-398.

Cubrinovski, M., Green, R. A., Allen, J., Ashford, S., Bowman, E., Bradley, B., Cox, B., Hutchinson, T., Kavazanjian, E., Orense, R., Pender, M., Quigley, M., and Wotherspoon, L. (2010). Geotechnical reconnaissance of the 2010 Darfield (Canterbury) earthquake. Bulletin of the New Zealand Society for Earthquake Engineering 43 (4), 243–320.

Cubrinovski, M., Bray, J.D., Taylor, M., Giorgini, S., Bradley, B., Wotherspoon, L., Zupan, J. (2011). Soil liquefaction effects in the central business district during the February 2011 Christchurch earthquake. Seismol Res Lett 82(6):893–904.

Cubrinovski, M., (2013). Liquefaction-induced damage in the 2010–2011 Christchurch (New Zealand) earthquakes. Proceedings of the International Conference on Case Histories in Geotechnical Engineering. Missouri University of Science and Technology, Missouri.

Darby, K. M., Hernandez, G. L., DeJong, J. T., Boulanger, R. W., Gomez, M. G., & Wilson, D. W. (2019). Centrifuge model testing of liquefaction mitigation via microbially induced calcite precipitation. Journal of Geotechnical and Geoenvironmental Engineering, 145(10), 04019084.

Dashti, S. (2009). Toward evaluating building performance on softened ground. Ph.D. Dissertation, Dept. of Civil and Environmental Engineering, Univ. of California, Berkeley.

Dashti, S., Bray, J. D., Pestana, J. M., Riemer, M. R., and Wilson, D. (2010a). Mechanisms of the seismically-induced settlement of buildings with shallow foundations on liquefiable soil. J. Geotech. Geoenviron. Eng., 136(1), 151–164.

Dashti, S., Bray, J. D., Pestana, J. M., Riemer, M. R., and Wilson, D. (2010b). Centrifuge testing to evaluate and mitigate liquefaction-induced building settlement mechanisms. J. Geotech. Geoenviron. Eng., 136(7), 918–929.

Dashti, S. and Bray, J.D., (2013). Numerical simulation of building response on liquefiable sand. J Geotech Geoenviron Eng., 139(8):1235–49.

Dobry, R., O'Rourke, T. D., & Abdoun, T. (2001). Centrifuge-Based Evaluation of Pile Foundation Response to Lateral Spreading and Mitigation Strategies: Research Progress and Accomplishments Report. In Report MCEER-01-SP01, Multidisciplinary Center for Earthquake Engineering Research (MCEER) (Vol. 2000-2001, pp. 87-101).

Ebeido, A., Elgamal A., Tokimatsu K., Akio A., (2019a). Pile and pile group response to liquefaction-induced lateral spreading in four large-scale shake table experiments. Journal of Geotechnical & Geoenvironmental Engineering, 145(10) https://doi.org/10.1061/(ASCE)GT.1943-5606.0002142.

Ebeido, A., Elgamal, A., & Zayed, M. (2019b). Large Scale Liquefaction-Induced Lateral Spreading Shake Table Testing at the University of California San Diego. In Geo-

Congress 2019: Earthquake Engineering and Soil Dynamics (pp. 22-30). Reston, VA: American Society of Civil Engineers.

El-Marsafawi, H., Han, Y. C., & Novak, M. (1992). Dynamic experiments on two pile groups." *Journal of Geotechnical Engineering*, *118*(4), 576-592.

El Naggar, M.H. & Abdelghany, Y. (2007a). Seismic helical screw foundations systems. Proceedings of the 60th Canadian Geotechnical Conference, Ottawa, October 24-26, Paper 160.

El Naggar, M.H. & Abdelghany, Y. (2007b). Helical Screw Piles (HSP) capacity for axial cyclic loadings in cohesive soils. Proceedings of the 4th International Conference on Earthquake Geotechnical Engineering. June 25-28, Thessaloniki, Greece. Paper No. 1567.

Elsawy, M.K., El Naggar, M.H., Cerato, A., & Elgamal, A. (2019a). Seismic performance of helical piles in dry sand from large-scale shaking table tests. Géotechnique, 69(12), 1071-1085.

ElSawy, M. K., El Naggar, M. H., Cerato, A. B., & Elgamal, A. W. (2019b). Data Reduction and Dynamic p-y Curves of Helical Piles from Large-Scale Shake Table Tests. Journal of Geotechnical and Geoenvironmental Engineering, 145(10), 04019075.

Eseller-Bayat, E., Gokyer, S., Yegian, M.K., Alshawabkeh., A. (2013). Liquefaction Response of Partially Saturated Sands: An Empirical Model. ASCE Journal of Geotechnical and Geoenvironmental Engineering, 139(6), 2013, 872-879.

Farhangi, V., Karakouzian, M., & Geertsema, M. (2020). Effect of micropiles on clean sand liquefaction risk based on CPT and SPT. *Applied Sciences*, *10*(9), 3111.

Ghayoomi, M., Ghadirianniari, S., Khosravi, A., & Mirshekari, M. (2018). Seismic behavior of pile-supported systems in unsaturated sand. *Soil Dynamics and Earthquake Engineering*, *112*, 162-173.

Hausler, E.A. (2002). Influence of ground improvement on settlement and liquefaction: a study based on field case history evidence and dynamic geotechnical centrifuge tests. Ph.D. Dissertation, Dept. of Civil and Natural Resources Engineering, Univ. of California Berkeley.

Hayden RF, Baez JI. (1994). State of practice for liquefaction mitigation in North America. In: Proceedings of international workshop on remedial treatment of liquefiable soils. Tsukuba City, Japan: Public Works Research Institute.

Hayden, C. P., Zupan, J. D., Bray, J. D., Allmond, J. D., & Kutter, B. L. (2015). Centrifuge tests of adjacent mat-supported buildings affected by liquefaction. Journal of Geotechnical and Geoenvironmental Engineering, 141(3), 04014118.

Henderson, D. (2013). The Performance of House Foundations in the Canterbury earthquakes. (Master's thesis). University of Canterbury, August 2013, 1-448 http://ir.canterbury.ac.nz/handle/10092/8741.

Honnette, T. R. (2018). Measuring Liquefied Residual Strength Using Full-Scale Shake Table Cyclic Simple Shear Tests. Thesis in partial fulfillment of MS degree in Civil and Environmental Engineering, California Polytechnic State University, November.

Howell R, Rathje EM, Kamai R, Boulanger R. (2012). Centrifuge modeling of prefabricated vertical drains for liquefaction remediation. J Geotech Geoenviron Eng, 138(3):262–71.

Iai S, Matsunaga Y, Morita T, Miyata M, Sakurai, H, Oishi, H, et al. (1994). Effects of remedial measures against liquefaction at 1993 Kushiro-Oki earthquake.” In: Proceedings of 5th U.S-Japan workshop on earthquake resistant design of lifeline facilities and countermeasures against soil liquefaction. Technical Rep. NCEER-94-0026.

Ishihara, K. (1985). Stability of natural deposits during earthquakes. In Proceedings of the 11th International Conference on Soil Mechanics and Foundation Engineering, San Francisco, 12-16 AUGUST 1985. vol. 1; p. 321–376. Publication of: Balkema (AA).

Ishihara, K. and Yoshimine, M. (1992). Evaluation of settlement in deposits following liquefaction during earthquakes. Soils and Foundations, 32(1), 173-188.

Jacobs, J.S. (2016). Full-Scale Shake Table Cyclic Simple Shear Testing of Liquefiable Soil. Thesis in partial fulfillment of MS degree in Civil and Environmental Engineering, California Polytechnic State University, January: http://digitalcommons.calpoly.edu/theses/1527/.

Jafarian, Y., Mehrzad, B., Lee, C.J., Haddad, A.H. (2017). Centrifuge modeling of seismic foundation-soil-foundation interaction on liquefiable sand. Soil Dyn. Earthquake Eng., (97) 184-204 http://dx.doi.org/10.1016/j.soildyn.2017.03.019.

Jahed Orang, M., Bruketta, S., & Motamed, R. (2019a). Experimental Evaluation of Spatial Variability Effects on Liquefaction-Induced Settlements. Geo-Congress 2019: Earthquake Engineering and Soil Dynamics (pp. 294-303). Reston, VA: American Society of Civil Engineers.

Jahed Orang, M., Toth, J., and Motamed, R. (2019b). Experimental evaluation of dynamic response of helical piles in dry sand using 1g shaking table tests. VII International Conference on Earthquake Geotechnical Engineering (7ICEGE), Roma, Italy, 17-20 June 2019, pp 4226-4234.

Jahed Orang, M., Bousheri, R., Motamed, R., Prabhakaran, A., and Elgamal, A. (2020). Large-scale Shake Table Experiment on the Performance of Helical Piles in Liquefiable Soils. In Proc, DFI 45th Annual Conference on Deep Foundations, Hawthorne, NJ: Deep Foundation Institute.

Jahed Orang, M., Motamed, R., Prabhakaran, A., & Elgamal, A. (2021a). Large-Scale Shake Table Tests on a Shallow Foundation in Liquefiable Soils. Journal of Geotechnical and Geoenvironmental Engineering, 147(1), 04020152.

Jahed Orang, M., Boushehri, R., Motamed, R., Prabhakaran, A., & Elgamal, A. (2021b). An Experimental Evaluation of Helical Piles as a Liquefaction-Induced Building Settlement Mitigation Measure (Submitted to Soil Dynamics and Earthquake Engineering).

Karamitros, D. K., Bouckovalas, G. D., Chaloulos, Y. K., & Andrianopoulos, K. I. (2013). Numerical analysis of liquefaction-induced bearing capacity degradation of shallow foundations on a two-layered soil profile. Soil Dynamics and Earthquake Engineering, 44, 90-101.

Karimi, Z. and Dashti, S. (2016). Numerical and centrifuge modeling of seismic soil-foundation-structure interaction on liquefiable ground. J Geotech Geoenviron Eng., 142(1):04015061.

Karimi, Z., & Dashti, S. (2017). Ground motion intensity measures to evaluate II: the performance of shallow-founded structures on liquefiable ground. Earthquake spectra, 33(1), 277-298.

Karimi, Z., Dashti, S., Bullock, Z., Porter, K., & Liel, A. (2018). Key predictors of structure settlement on liquefiable ground: a numerical parametric study. Soil Dynamics and Earthquake Engineering, 113, 286-308.

Khosravi, M., Boulanger, R. W., Tamura, S., Wilson, D. W., Olgun, G., and Wang, Y. (2016). Dynamic centrifuge tests of soft clay reinforced by soil-cement grids. Journal of Geotechnical and Geoenvironmental Engineering, ASCE, 04016027, 10.1061/ (ASCE) GT.1943-5606.0001487.

Kirkwood, P., & Dashti, S. (2018). A centrifuge study of seismic structure-soil-structure interaction on liquefiable ground and implications for design in dense urban areas. Earthquake Spectra, 34(3), 1113-1134.

Kirkwood, P., & Dashti, S. (2019). Influence of prefabricated vertical drains on the seismic performance of similar neighboring structures founded on liquefiable deposits. Géotechnique, 1-15.

Kokusho, T. (1999). Water film in liquefied sand and its effect on lateral spread. Journal of Geotechnical and Geoenvironmental Engineering, 125(10), 817-826.

Lambe, P. C., & Whitman, R. V. (1985). Dynamic centrifugal modeling of a horizontal dry sand layer. Journal of geotechnical engineering, 111(3), 265-287.

Lim, H., & Jeong, S. (2018). Simplified p-y curves under dynamic loading in dry sand. *Soil Dynamics and Earthquake Engineering*, *113*, 101-111.

Liu, L., and Dobry, R. (1997). Seismic response of shallow foundation on liquefiable sand. J. Geotech. Geoenviron. Eng., 123(6), 557–567.

Lu, C. W. (2017). A simplified calculation method for liquefaction-induced settlement of shallow foundation. Journal of Earthquake Engineering, 21(8), 1385-1405.

Luque, R., & Bray, J. D. (2017). Dynamic analyses of two buildings founded on liquefiable soils during the Canterbury earthquake sequence. Journal of Geotechnical and Geoenvironmental Engineering, 143(9), 04017067.

Macedo, J. and Bray J.D. (2018). Key trends in liquefaction-induced building settlement. J. Geotech. Geoenviron. Eng., 144(11): 04018076.

Makris, N., Tazoh, T., Yun, X., & Fill, A. C. (1997). Prediction of the measured response of a scaled soil-pile-superstructure system. *Soil Dynamics and Earthquake Engineering*, *16*(2), 113-124.

Mashhoud, H. J., Yin, J. H., Panah, A. K., & Leung, Y. F. (2018). Shaking table test study on dynamic behavior of micropiles in loose sand. *Soil Dynamics and Earthquake Engineering*, *110*, 53-69.

Mehrzad, b., Jafarian, Y., Lee, C.J., Haddad, A.H. (2018). Centrifuge study into the effect of liquefaction extent on permanent settlement and seismic response of shallow foundations. Soils & Foundation, (58) 228–240.

Mirshekari, M., & Ghayoomi, M. (2017). Centrifuge tests to assess seismic site response of partially saturated sand layers. Soil Dynamics and Earthquake Engineering, 94, 254-265.

Montoya, B. M., DeJong, J. T., and Boulanger, R. W. (2013). Dynamic response of liquefiable sand improved by microbial induced calcite precipitation. Geotechnique, 63(4), 302-312

Moss, R. E., Seed, R. B., Kayen, R. E., Stewart, J. P., Der Kiureghian, A., & Cetin, K. O. (2006). CPT-based probabilistic and deterministic assessment of in situ seismic soil liquefaction potential. Journal of Geotechnical and Geoenvironmental Engineering, 132(8), 1032-1051.

Motamed, R., & Towhata, I. (2009). Shaking Table Model Tests on Pie Groups behind Quay Walls Subjected to Lateral Spreading. Journal of Geotechnical and Geoenvironmental Engineering, 136(3), 477-489.

Motamed, R., Towhata, I., Honda, T., Yasuda, S., Tabata, K., & Nakazawa, H. (2009). Behaviour of pile group behind a sheet pile quay wall subjected to liquefaction-induced large ground deformation observed in shaking test in E-defense project. Soils and foundations, 49(3), 459-475.

Motamed, R., Towhata, I., Honda, T., Tabata, K., & Abe, A. (2013). Pile group response to liquefaction-induced lateral spreading: E-Defense large shake table test. Soil Dyn and Earthquake Eng., 51, 35-46 http://dx.doi.org/10.1016/j.soildyn.2013.04.007.

Motamed, R., Orang, M. J., Parayancode, A., & Elgamal, A. (2020). Results of a Class C Blind Prediction Competition on the Numerical Simulation of a Large-Scale Liquefaction Shaking Table Test. In Geo-Congress 2020: Foundations, Soil Improvement, and Erosion (pp. 334-342). Reston, VA: American Society of Civil Engineers.

Mousavi, S., & Ghayoomi, M. (2019). Liquefaction mitigation of silty sands via microbial induced partial saturation. In Geo-Congress 2019: Earthquake Engineering and Soil Dynamics (pp. 304-312). Reston, VA: American Society of Civil Engineers.

Mousavi, S., & Ghayoomi, M. (2021). Liquefaction mitigation of sands with nonplastic fines via microbial-induced partial saturation. Journal of Geotechnical and Geoenvironmental Engineering, 147(2), 04020156.

Nikolaou, S., Mylonakis, G., Gazetas, G., & Tazoh, T. (2001). Kinematic pile bending during earthquakes: analysis and field measurements. *Geotechnique*, *51*(5), 425-440.

Novak, M., & F. Grigg, R. (1976). Dynamic experiments with small pile foundations. *Canadian Geotechnical Journal*, *13*(4), 372-385.

Olarte, J., Paramasivam, B., Dashti, S., Liel, A., & Zannin, J. (2017). Centrifuge modeling of mitigation-soil-foundation-structure interaction on liquefiable ground. Soil Dynamics and Earthquake Engineering, 97, 304-323.

Paramasivam, B., Dashti, S., & Liel, A. (2018). Influence of prefabricated vertical drains on the seismic performance of structures founded on liquefiable soils.” Journal of Geotechnical and Geoenvironmental Engineering, 144(10), 04018070.

Perko, H.A. (2009). Helical piles: a practical guide to design and installation. New York, NY, USA: John Wiley & Sons.

Prabhakaran, A., Kyungtae, K., Ebeido, A., Jahed Orang, M., Motamed, R., Elgamal, A., and Frazao, C. (2020a). Polymer injection and associated site liquefaction remediation mechanisms. 17th World Conference on Earthquake Engineering, 17WCEE, Sendai, Japan – September 13-18., Paper no: 4b-0024

Prabhakaran, A., Kyungtae, K., Jahed Orang, M., Qiu, Z., Ebeido, A., Zayed, M., Boushehri, R., Motamed, R., Elgamal, A., and Frazao, C. (2020b). Polymer injection and liquefaction-induced foundation settlement: a shake table test investigation. In Geo-Congress 2020: Geotechnical Earthquake Engineering and Special Topics (pp. 1-9). Reston, VA: American Society of Civil Engineers.

Rasouli, R., I. Towhata, and T. Akima. (2016). Experimental evaluation of drainage pipes as a mitigation against liquefaction-induced settlement of structures. J. Geotech. Geoenviron. Eng. 142 (9): 04016041. https://doi.org/10.1061/ (ASCE) GT.1943-5606.0001509.

Rasouli, R., Towhata, I., Rattez, H., & Vonaesch, R. (2018). Mitigation of nonuniform settlement of structures due to seismic liquefaction. Journal of Geotechnical and Geoenvironmental Engineering, 144(11), 04018079.

Sancio R.B., Bray J.D., Stewart J.P., Youd T.L., Durgunoglu H.T., Onalp A., Seed R.B., Christensen C., Baturay M.B., Karadayilar T. (2002). Correlation between ground failure and soil conditions in Adapazari, Turkey. Soil Dyn Earthq Eng 22(9–12):1093–1102

Shahbazi, M., Cerato, A. B., Allred, S., El Naggar, M. H., & Elgamal, A. (2020a). Damping characteristics of full-scale grouped helical piles in dense sands subjected to small and large shaking events. Canadian Geotechnical Journal, 57(6), 801-814.

Shahbazi, M., Cerato, A. B., El Naggar, H. M., and Elgamal, A. (2020b) Evaluation of Seismic Soil–Structure Interaction of Full-Scale Grouped Helical Piles in Dense Sand. International Journal of Geomechanics, 20(12), 04020228.

Tokimatsu, K., and Seed, H. B. (1987). Evaluation of settlements in sands due to earthquake shaking. J. Geotech. Eng., 10.1061/(ASCE)0733-9410(1987)113:8(861), 861–878.

Tokimatsu, K., Suzuki, H., & Sato, M. (2005). Effects of inertial and kinematic interaction on seismic behavior of pile with embedded foundation. *Soil Dynamics and Earthquake Engineering*, *25*(7-10), 753-762.

Tokimatsu, K., et al., (2011). Quick report on geotechnical problems in the 2011 Tohoku Pacific Ocean earthquake. Research reports on earthquake engineering, CUEE, Tokyo Institute of Technology, #118, pp 21–47 (in Japanese)

Tokimatsu, K., & Katsumata, K. (2011). Liquefaction-induced damage to buildings in Urayasu city during the 2011 Tohoku Pacific earthquake. In proceedings of the international symposium on engineering lessons learned from the (pp. 665-674).

Tokimatsu, K., Hino, K., Suzuki, H., Ohno, K., Tamura, S., & Suzuki, Y. (2019). Liquefaction-induced settlement and tilting of buildings with shallow foundations based on field and laboratory observation. Soil Dynamics and Earthquake Engineering, 124, 268-279. https://doi.org/10.1016/j.soildyn.2018.04.054.

Toth, J. A. W., and R. Motamed. (2017). Parametric study on liquefaction-induced building settlements using 1-g shake table experiments. In Proc., 3rd Int. Conf. on Performance Based Design in Earthquake Geotechnical Engineering. London: International Society for Soil Mechanics and Geotechnical Engineering.

Wilson, D. W., Boulanger, R. W., & Kutter, B. L. (2000). Observed seismic lateral resistance of liquefying sand. *Journal of Geotechnical and Geoenvironmental Engineering*, *126*(10), 898-906.

Yasuda, S., Harada, K., Ishikawa, K., and Kanemaru, Y. (2012). Characteristics of liquefaction in Tokyo Bay area by the 2011 Great East Japan Earthquake. Soils and Foundations, 52(5): 793-810.

Yegian, M. K., Eseller-Bayat, E., Alshawabkeh, A., Ali, S. (2007). Induced Partial Saturation for Liquefaction Mitigation: Experimental Investigation. Journal of Geotechnical and Geoenvironmental Engineering, ASCE, 133 (4).

Yoshimi, Y., and Tokimatsu, K. (1977). Settlement of buildings on saturated sand during earthquakes. Soils & Foundation, 17(1), 23–38.

Zeghal, M., & Elgamal, A. W. (1994). Analysis of site liquefaction using earthquake records. Journal of geotechnical engineering, 120(6), 996-1017.

Zeghal, M., Elgamal, A. W., Zeng, X., & Arulmoli, K. (1999). Mechanism of liquefaction response in sand–silt dynamic centrifuge tests. Soil Dynamics and Earthquake Engineering, 18(1), 71-85.

2. Large-Scale Shake Table Tests on a Shallow Foundation in Liquefiable Soils

ABSTRACT

The significant damage observed during recent earthquakes resulting from liquefaction of shallow saturated soil deposits beneath structures has illustrated the need for further research in the area of liquefaction-induced ground movement effects. This study used the shake table facility at the University of California, San Diego to evaluate the liquefaction-induced settlement of a shallow foundation founded on top of liquefiable ground conditions. To study the seismic performance of a shallow rigid foundation, two large-scale shake table tests were conducted using different input motions with varying peak accelerations. The experimental model comprised three soil layers and included a shallow foundation seated over an unsaturated crust layer underlain by saturated loose and dense layers. The model ground was based on similar subsurface ground conditions observed in recent earthquakes in New Zealand, Japan and Turkey. The seismic response of the model foundation and the soil was captured through intensive instrumentation. The main purpose of this study is to better understand the contributing mechanisms in liquefaction-induced settlement of buildings during strong shaking. Results from this series of tests were used to explore different liquefaction mitigation countermeasures; this study served as a baseline for two follow-on shake table tests which are not discussed in this paper. Detailed discussions on the excess pore-water pressure generation and dissipation, and its effect on the contributing mechanisms of liquefaction-induced settlement are presented, along with the application of standardized cumulative absolute velocity as an intensity measure to

estimate the amount of liquefaction-induced settlement. The flow velocity calculation due to hydraulic transient gradient indicated an upward flow in the loose layer, which explains the observed sand ejecta. Measured and estimated foundation settlements were compared using simplified procedures. The observed foundation settlement generally was higher than the estimated settlement. This series of large-scale shake table tests provides a unique benchmark for calibration of numerical models, and simplified procedures to reliably estimate liquefaction-induced building settlements. Future mitigation tests can be evaluated using the results of this baseline experimental study.

2.1. Introduction

Documented case histories on the phenomenon of liquefaction have been useful to researchers studying the devastating effects of liquefaction during past earthquakes. The 1964 Niigata and 1990 Luzon Philippine earthquakes resulted in extensive damage to structures and the built environment [Yoshimi and Tokimatsu 1977; Adachi et al. 1992]. More recently, the 2010-2011 Canterbury Earthquake Sequence (CES) in New Zealand and the 2011 Tohoku earthquake in Japan generated widespread liquefaction-induced damage to structures and their foundation systems [Cubrinovski et al. 2010; Yasuda et al. 2012; Cubrinovski 2013; Henderson 2013]. Consequences of liquefaction include lateral spreading of the ground, which has been extensively documented at port facilities in Japan, as well as settlement of structures supported on shallow foundations. Liquefaction also caused extensive damage to lifeline facilities and pipeline systems due to the induced ground deformation. Lateral displacement of the soil and subsequent countermeasures to tackle this issue have been studied by 1-g shake table tests [Motamed and Towhata 2009; Motamed et al. 2013; Ebeido et al. 2019a] and dynamic centrifuge experiments [Zeghal et

al. 1999; Dobry et al. 2001; Abdoun et al. 2003; Boulanger et al. 2003]. Liquefaction-induced movement of structures during strong motion has been further evaluated using numerical analyses, experimental studies, and field reconnaissance to gain further insight into the controlling mechanisms summarized in this paper.

The 1964 Niigata earthquake resulted in widespread liquefaction-induced settlement of buildings, attracting the interest of researchers in field reconnaissance followed by experimental research. During the Niigata event, 340 reinforced concrete buildings experienced damage resulting from liquefaction. Field reconnaissance after the event estimated that liquefaction occurred to maximum depths of 20 m and the maximum building settlements reached 3.8 m [Yoshimi & Tokimatsu 1977]. In addition to the field observations, Yoshimi & Tokimatsu (1977) conducted scaled 1-g shake table tests to explore the effects of different parameters on building settlement as a result of liquefaction in sub-soils. Their study is believed to be the first experimental research focused on the behavior of shallow foundations in liquefiable soils. Based on the documented case histories from the 1964 Niigata earthquake and the complementary scaled 1-g shake table tests, Yoshimi and Tokimatsu (1977) concluded that the average settlement (S) normalized by the thickness of liquefiable layer (D) shows an inverse relation with building width (B).

The contributing mechanisms in liquefaction-induced settlement have been widely studied. For example, Tokimatsu and Seed (1987) and Ishihara and Yoshimine (1992) proposed empirical procedures assuming free-field conditions. One of the very first studies regarding settlement of ground due to liquefaction phenomenon was conducted by Ishihara and Yoshimine (1992), who used simple shear tests to correlate the volumetric strain (ε_v) with the relative density (D_r) of clean sand and factor of safety (FS) against liquefaction.

The predicted amount of settlement based on the laboratory test results was compared to the observed settlements from the 1964 Niigata earthquake. The amount of volumetric strain for clean sand was calculated based on FS against liquefaction and relative density of each layer [Ishihara and Yoshimine 1992] with a chart that leads to the calculation of overall ground settlement by integrating the volumetric strains generated within each layer. The methodology proposed by Ishihara and Yoshimine (1992) allows the calculation of ground (i.e. free-field) settlement due to liquefaction during earthquakes and does not account for external loads (i.e. structures and foundations).

Past research on the behavior of shallow foundations in liquefiable soils consists of utilizing shake table tests [Jacobs 2016; Toth and Motamed 2017; Honnette 2018; Orang et al. 2019], centrifuge experiments [Liu and Dobry 1997; Hausler 2002; Dashti et al. 2010a; Dashti et al. 2010b; Jafarian et al. 2017; Mehrzad et al. 2018; Tokimatsu et al. 2018; Kirkwood and Dashti 2018] and field reconnaissance [Bray and Frost 2010; Cubrinovski et al. 2010; Cubrinovski et al. 2011; Tokimatsu et al. 2011; Bray et al. 2014]. Liu and Dobry (1997) conducted eight centrifuge tests to examine settlement characteristics of circular foundations founded on liquefiable soils. They also reviewed two field case histories, which included the 1964 Niigata and the 1990 Luzon Philippine earthquakes to compare their experimental results. The result of their study indicated that degree of settlement is dependent upon width of foundation and thickness of liquefiable layer, which was in line with the conclusions drawn by Yoshimi and Tokimatsu (1977). Dashti et al. (2010a) conducted centrifuge experiments to model the mechanisms of liquefaction-induced settlement, identifying the effects of shear-induced mechanism along with partial drainage component of volumetric-induced mechanism as the dominant mechanisms

contributing to the settlement of buildings in liquefiable soils. The dependency of these mechanisms on the characteristics of ground motion, subsurface conditions, and superstructure was also presented in Dashti et al. (2010a).

Liquefaction-induced building movement was then defined to consist of volumetric-induced and shear-induced deformations, where each category included different mechanisms. Further details regarding mechanisms of liquefaction-induced structure settlement were presented in Bray and Dashti (2014). The results from their study indicated that much of the building settlement occurs during strong ground motion due to the shear-induced movement of the foundation (i.e., soil-structure-interaction (SSI)-induced ratcheting and partial bearing capacity failure) as well as localized drainage (volumetric-induced) resulting from high transient hydraulic gradients generated in all directions in soil media. These effects can be captured using numerical simulations such as in FLAC-2D and FLAC-3D [Karamitros et al. 2013; Dashti and Bray 2014; Macedo and Bray 2018] and OpenSees [Karimi and Dashti 2016; Karimi et al. 2018]. In a recent paper, Motamed et al. (2020) discussed the use of different numerical simulation techniques and their efficiency in predicting liquefaction-induced foundation and free field settlements. Incorporation of all these mechanisms in estimating liquefaction-induced building settlement is extremely important due to the fact that past simplified procedures for liquefaction-induced settlement evaluation are limited to only capturing the free-field ground settlements. Bray and Dashti (2014) also provided recommendations for further evaluation of liquefaction-induced building movement considering the contribution of the above-mentioned controlling mechanisms. Their study highlighted the contribution of sand ejecta to the settlement of structures during earthquakes. However, there is no well-

documented procedure to estimate the contribution of ejecta in liquefaction-induced building displacement. In a more recent study, Bray and Macedo (2017) proposed a simplified method to estimate the shear-induced element of liquefaction-induced building settlement and provided a framework to estimate it along with the volumetric-induced settlement based on past studies. They made further recommendations on how to estimate the ejecta-induced settlement to add to the previous two components for estimating the overall settlement of buildings due to liquefaction. Lu (2017) and Bullock et al. (2018) also presented semi-empirical procedures to calculate total settlement of the foundation due to liquefaction. In this study, Bray and Macedo's (2017) simplified procedure is employed to estimate the shake table settlement results and to compare with the observed values.

The purpose of this research is to study the behavior of a rigid shallow foundation underlain by near surface liquefiable soils using a prototype soil profile patterned after past earthquakes. The large-scale shake table facility at the University of California, San Diego (UCSD) Powell laboratory was used with a 2.9 m tall laminar soil box. This experimental study provides an improved understanding of the phenomenon of liquefaction-induced building settlement where surficial loose liquefiable soils are located at shallow depths. In addition, the experimental data can be used as a baseline to validate numerical simulations of liquefaction-induced building settlement and evaluate the effectiveness of different liquefaction mitigation measures such as stone columns and prefabricated vertical drains [Paramasivam et al. 2018; Badanagki et al. 2018; Kirkwood and Dashti 2019; Bahmanpour et al. 2019]. The results of this study have been used as a baseline to evaluate the effectiveness of two countermeasures in mitigating liquefaction-induced settlement of the

foundation including polymer injection and helical piles, which will be presented in follow-up publications.

2.2. Large-Scale Shake Table Testing Program

A series of large-scale shake table tests were conducted at the shake table facility at the University of California San Diego (Powell Laboratory) in June 2018 to evaluate the effects of liquefaction-induced settlement on shallow foundations. The facility is equipped with a large laminar soil box with internal dimensions of 3.9 m (L) by 1.8 m (W) by 2.9 m (H), shown in Figure 2.1, which was used to conduct a two-phase liquefaction experimental study sponsored by the Pacific Earthquake Engineering Research (PEER). The first phase, which included no mitigation strategy, is presented here and is referred to as the "baseline" test throughout this paper, while the second phase consisted of a group of helical piles as a countermeasure. This paper only focuses on the results of the first phase of the large-scale tests, which is intended to establish a baseline for future shake table tests with different mitigation measures. A three-layer soil model was tested, consisting of saturated dense and loose layers overlain by medium dense, unsaturated crust layer. The physical ground model simulates prototype ground conditions representative of soil profiles with shallow liquefiable layers observed at specific locations during the Adapazari 1999 Kocaeli earthquake [Bray et al. 2004] and Christchurch 2010-2011 Canterbury Earthquake Sequence (CES) where FTG-7 and CTUC buildings were located [Bray et al. 2014; Luque and Bray 2017]. The input motion sequences (Shake 1-1 and Shake 1-2) were applied, with peak acceleration ranging from 0.53 g to 0.66 g and a constant frequency of 2 Hz for 15 seconds including 6 seconds cyclic ramp up followed by 6 seconds of uniform amplitude motion and finally 3 seconds of tapering down. These input motions were as recorded

motions without any filtering. Table 2.1 provides a summary of the target and achieved peak accelerations of the input motions in the shake table tests as well as some additional parameters. The target input motions were somewhat lower than the achieved table motion (table feedback). Although the table's actual motions were higher, the achieved input motions were approximately similar to the motions recorded during the Christchurch event at two different stations in terms of PGAs. The table acceleration time histories are illustrated in Figure 2.2. Table 2.2 presents the achieved relative densities of soil layers, depth of ground water, and foundation dimensions. Further details about the model configuration, instrumentation, soil properties, and shaking sequences are discussed in the following sections.

Figure 2.1. Shake table facility and laminar soil box at UC San Diego Powell Laboratory

Table 2.1. Shaking sequences and motion parameters for the baseline test

Parameters	Shake 1-1	Shake 1-2
Target peak acceleration (g)	0.15	0.30
Achieved peak acceleration (g)	0.53	0.66
I_a (m/sec)	3.42	9.21
CAV [*](g.sec)	1.35	2.36
CAV_{dp} (g.sec)	1.28	2.28
$D_{5\text{-}95}$ (sec)	10.10	9.74
$D_{5\text{-}75}$ (sec)	7.97	7.62

[*]for 25 seconds of recorded data.

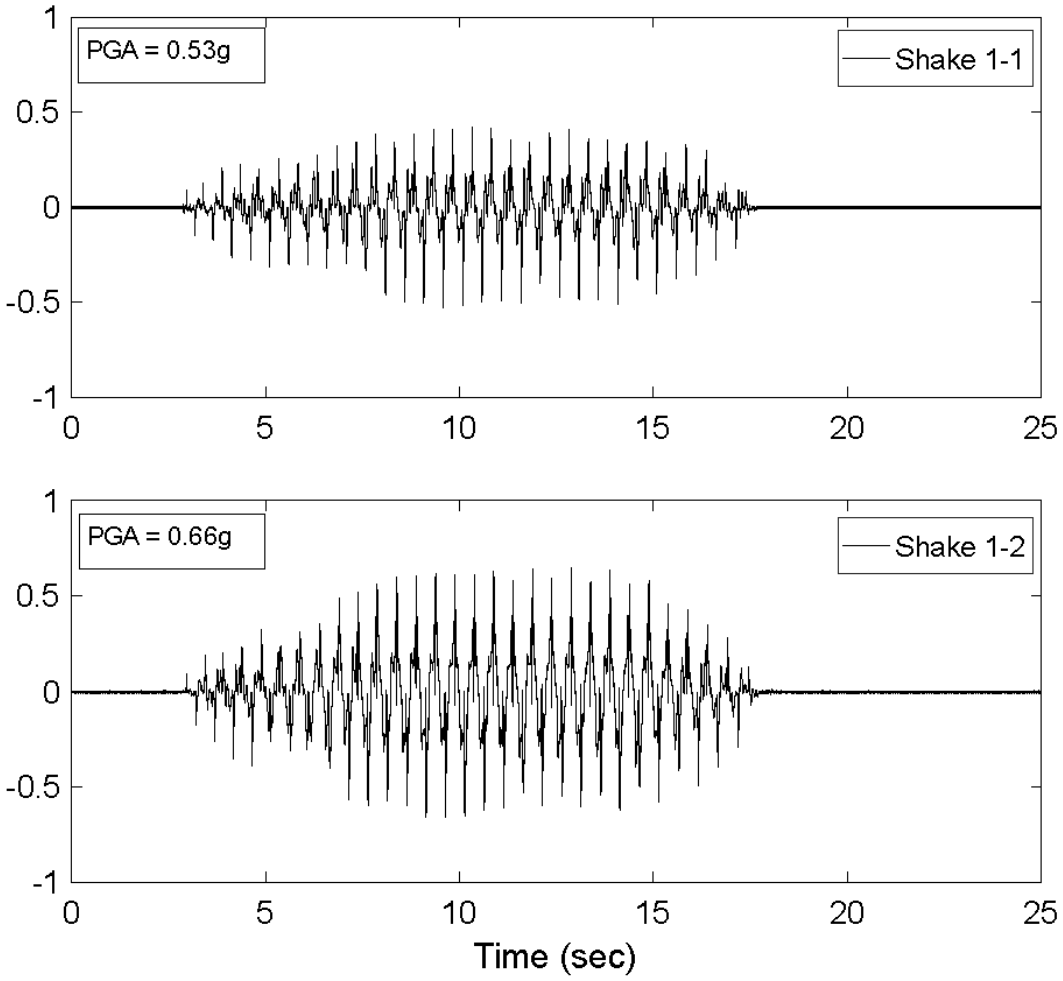

Figure 2.2. Acceleration time histories for shaking sequences.

Table 2.2. Relative density and ground water level for the baseline test

Layer	D_r (%)	Foundation dimensions (L*W*H) (m)	G.W. Level below ground (m)
Crust	50-55	1.3*0.6*0.4	-0.6
Liquefiable	40-45		
Dense	85-90		

2.2.1. Model Preparation and Instrumentation

This study aimed at reproducing a realistic prototype model ground in the shake table testing program which included shallow liquefiable soils. Some of the field case studies used to develop the model ground profile in the experiments are briefly reviewed hereafter. For example, Bray et al. (2014) documented that the critical liquefiable soil layer thicknesses under the southern part of CTUC building and the northern part of the SA building during CES were 2.5 m and 0.7 m, respectively. Additionally, Bray et al. (2004) found shallow layers of liquefiable material (i.e. only a meter or so in thickness) during the 1999 Kocaeli earthquake in Adapazari, Turkey. These case studies, which highlighted the importance of shallow surficial liquefiable soil layers on liquefaction-induced building settlements, were carefully reviewed and utilized to establish a representative model ground in this research using the large-scale laminar soil box at UCSD. The 2.9 m high laminar box at UCSD allowed a realistic model ground to be prepared to reproduce all the mechanisms of liquefaction-induced settlement of a shallow foundation including sand ejecta and evaluate its performance during strong ground shakings.

The laminar soil box is made of 43 steel frames with a total mass of 4229 kg mounted on 16 cold-rolled steel pipes allowing to minimize the boundary effects [Ebeido et al. 2019b]. The model ground consisted of three layers; dense, loose-liquefiable, and unsaturated crust. A 1 m thick dense layer was overlain by a 1.3 m thick liquefiable loose sand layer, underlying 0.6 m of medium dense crust layer. The achieved relative densities for these layers are presented in Table 2.2. The soil used to build the model was Ottawa F-65 sand in three different layers with varying relative densities (D_r). A summary of properties of Ottawa F-65 sand is presented in Table 2.3, and more details can be found in

Bastidas (2016). The dense layer was compacted in a moisture-conditioned state in three equal lifts, using a handheld vibratory compactor. The achieved relative density for the dense layer was about 85-90%. After reaching the desired thickness for the dense layer, saturation was achieved by adding water through two vertically positioned pipes located at each corner of the laminar box. The vertical pipes were conjoined using a system of horizontally-connected perforated pipes positioned at the base of the soil box. Care was taken to ensure that the dense layer was not subjected to boiling conditions during saturation. During saturation, the initial water level was raised to one-third of the anticipated height of the loose layer for the next step of model preparation. As the middle liquefiable layer was being constructed, a free water level was maintained to ensure full saturation. Before construction of the loose liquefiable layer, ten white noise motions were applied for further densify the dense layer. The loose liquefiable layer was built by pluviating dry Ottawa F65 sand through two sets of screens (one below the sand hopper and one on top of recent layer with reasonable offset, ensuring a constant height of fall) into the water. Relative density of the loose layer was about 40-45% based on weight-volume calculations. Finally, the top crust layer was built through the air pluviation method using only one screen below the hopper. The foundation was placed on the soil model after the thickness of crust layer reached 20 cm. Final thickness of the crust was about 60 cm, and the achieved relative density of crust layer was about 50-55%. The initial water content of crust layer material (5%) along with the capillary rise of the water inside this layer resulted in an unsaturated crust layer. All the presented relative densities in Table 2 were calculated based on the weight of the soil used to build the layer and its corresponding volume occupied in the laminar box. Dynamic cone penetrometer test (DCPT) was

conducted to estimate relative densities for each layer. The calculation of relative density based on the DCPT data yielded reasonable results only for the dense layer, about 83%, because the cone tip penetrated into crust and loose layer with its weight without the application of any force.

Table 2.3. Ottawa F-65 sand properties

Parameter	Value
Specific Gravity	2.65
Maximum Void Ratio (e_{max})	0.853
Minimum Void Ratio (e_{min})	0.503
Coefficient of curvature (C_c)	0.96
Coefficient of uniformity (C_u)	1.61
Maximum mass density, ρ_{max} (kg/m^3)	1759
Minimum mass density, ρ_{min}, (kg/m^3)	1446
Hydraulic conductivity of loose specimen, k_{loose} (cm/s)	0.022
Hydraulic conductivity of dense specimen, k_{dense} (cm/s)	0.016

Source: Data from Bastidas (2016).

To assess the dynamic response of superstructure and three-layered model ground, extensive instrumentation was installed to measure displacements, pore-water pressure, and accelerations at different depths. A total of 134 instruments were used in this study to capture the seismic performance of the soil-foundation-structure system. Table 2.4 presents a breakdown of the employed instruments and Figure 2.3 illustrates the instrumentation layout. As shown in Figure 2.3, three arrays of accelerometers and pore pressure sensors were utilized in north of, south of, and below the foundation to capture acceleration and

pore-water pressure. A total of 13 string potentiometers were also employed to capture the horizontal displacement of the laminar box at different depths. Four string potentiometers and four linear potentiometers were used to measure the foundation and free-field ground settlements, respectively.

Table 2.4. Type and number of instruments for the baseline test

Type	Number
Accelerometer	35
High resolution accelerometer	28
PWP sensors	47
String potentiometer	18
Linear potentiometer	6
Total	134

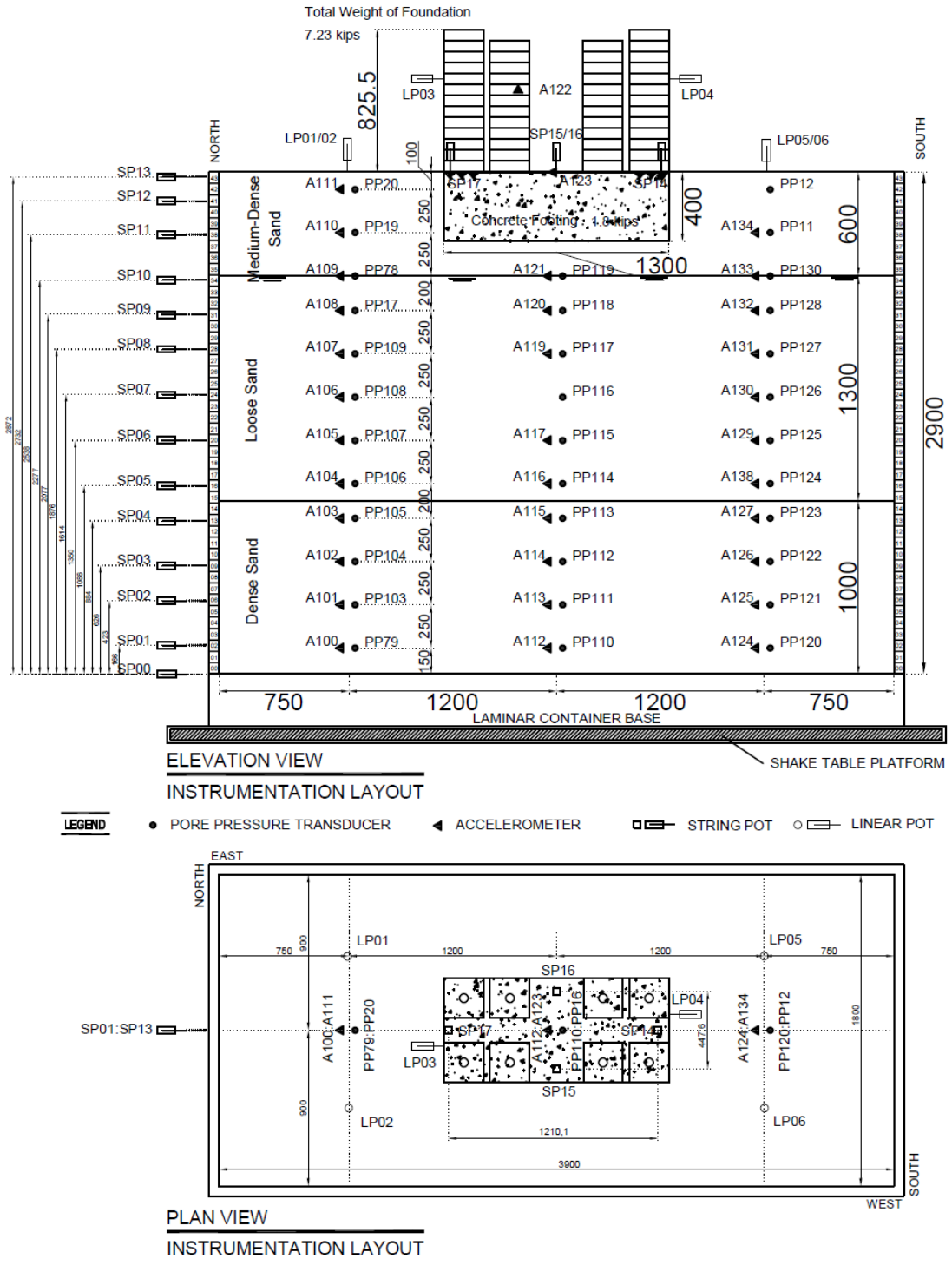

Figure 2.3. Elevation and plan view of instrumentation layout for the baseline test (all units are in mm). Three arrays of accelerometers and pore water pressure sensors were installed, two at free-field (north and south) and one under the foundation.

2.2.2. System Identification

A number of high-resolution accelerometers (PCB333B50, PCB PIEZOTRONICS, Depew, NY, USA) were installed in the model ground in the form of arrays to measure the shear wave velocity profile before the shaking sequences. These accelerometers have a broadband resolution of 0.00005 m/s^2 root-mean-square (RMS) amplitude, with a frequency range from 0.5 to 3000 Hz. A total of 28 high resolution accelerometers were installed in two different arrays to capture the travelling shear waves in the form of acceleration time histories during white noise shakings prior to the main shaking. Figure 2.4 presents the configuration of the high-resolution accelerometers used for this study. The frequency of data acquisition for these accelerometers was 25600 Hz which facilitated the observation of arrival time and time difference between two consecutive sensors which, in turn, resulted in a shear wave velocity profile with depth.

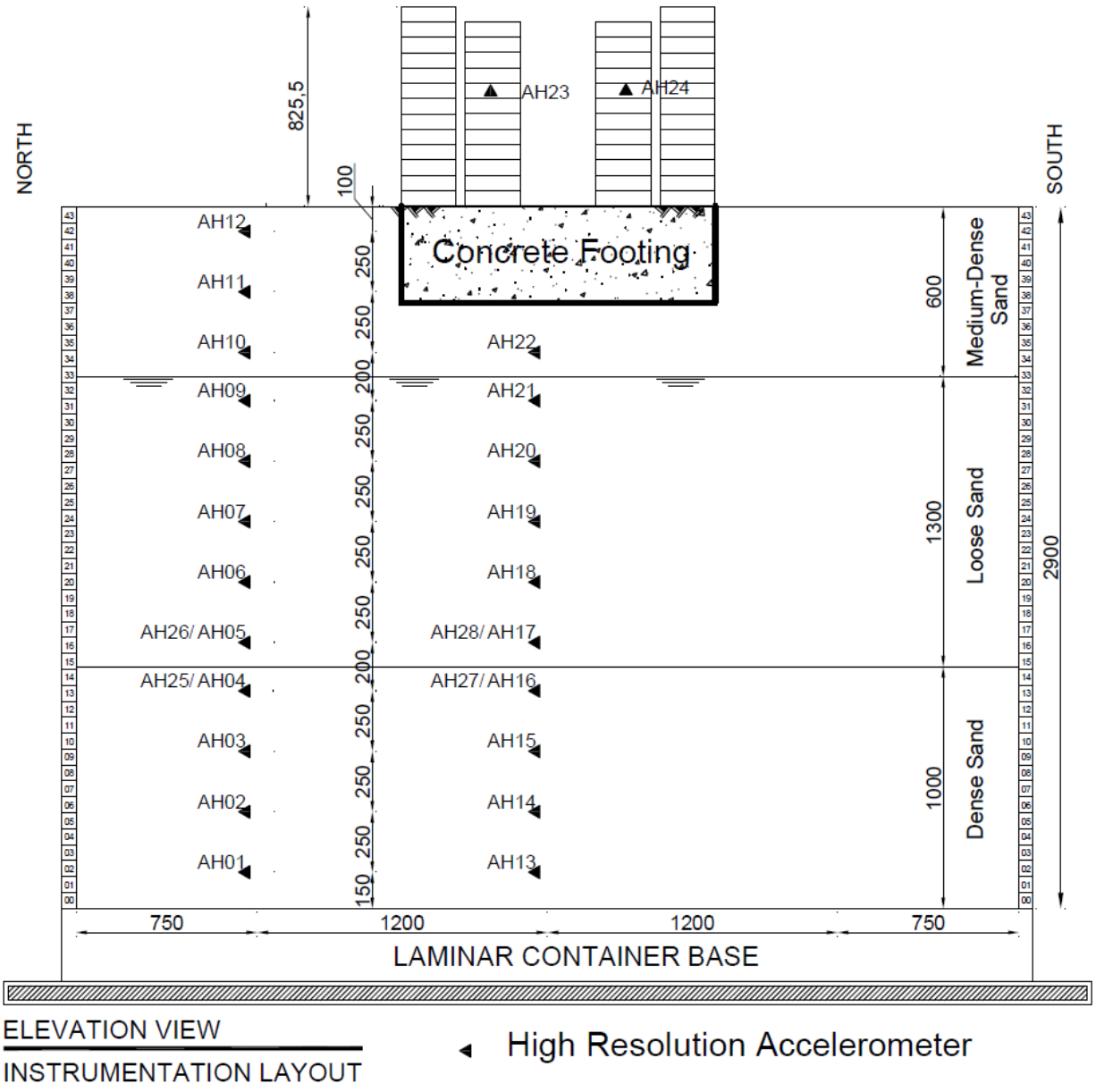

Figure 2.4. Instrumentation layout for high resolution accelerometers (all units are in mm). Two arrays of accelerometers were installed, one at free-field (north) and one beneath the foundation.

White noise motion was applied to capture the predominant frequency of the soil model before each strong shaking for 6 seconds with an amplitude of 0.05 g and frequency between 5 to 20 Hz. The Fourier Amplitude Spectra and the resulted transfer functions are presented in Figures 2.5 and 2.6 for white noise shake before the main Shake 1-1. The predominant frequency (first mode) of the soil model based on these results ranges from 4.78 to 5.10 Hz (0.21 to 0.19 sec).

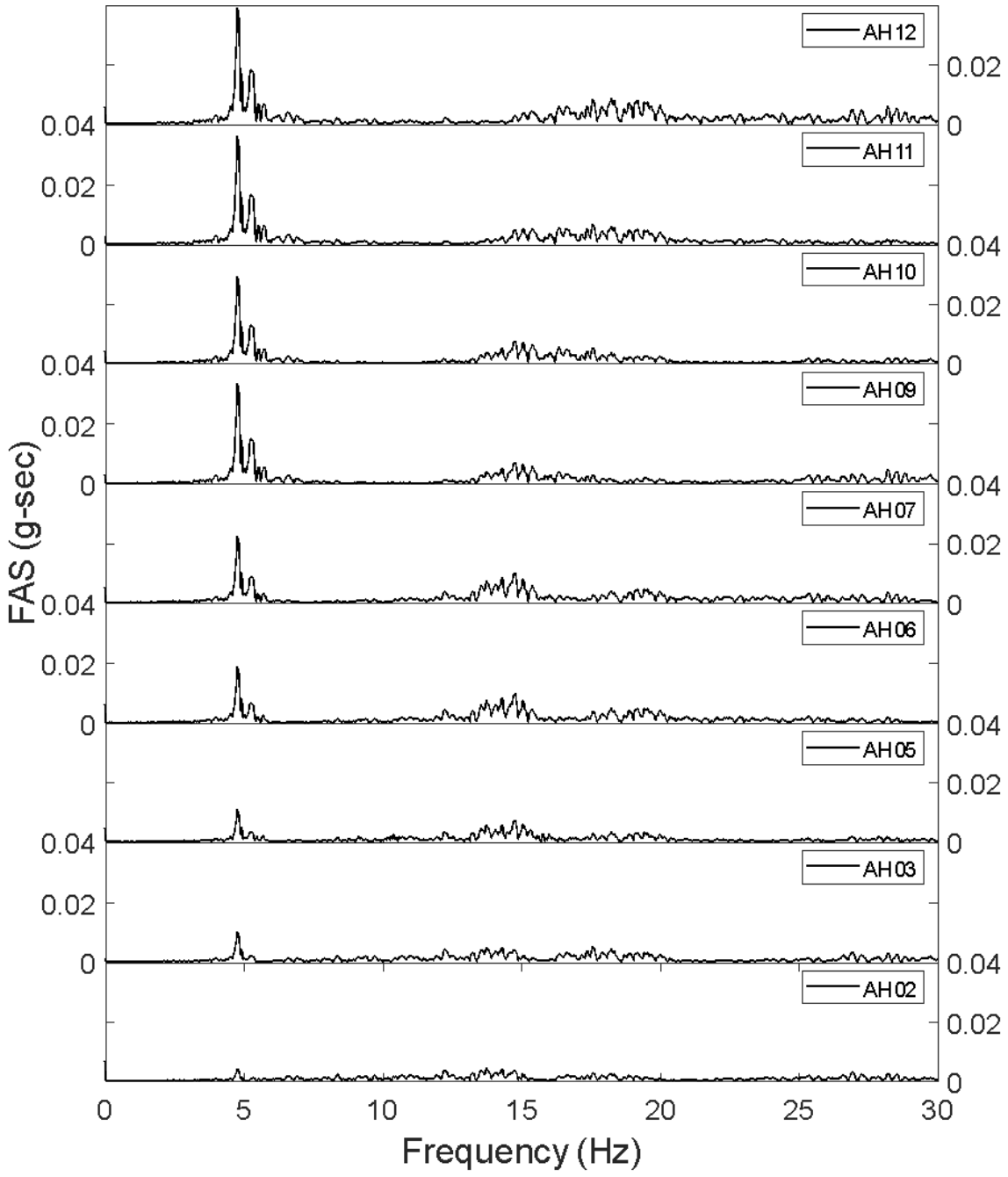

Figure 2.5. Fourier Amplitude Spectra based on high resolution accelerometer data (free-field array) prior to Shake 1-1.

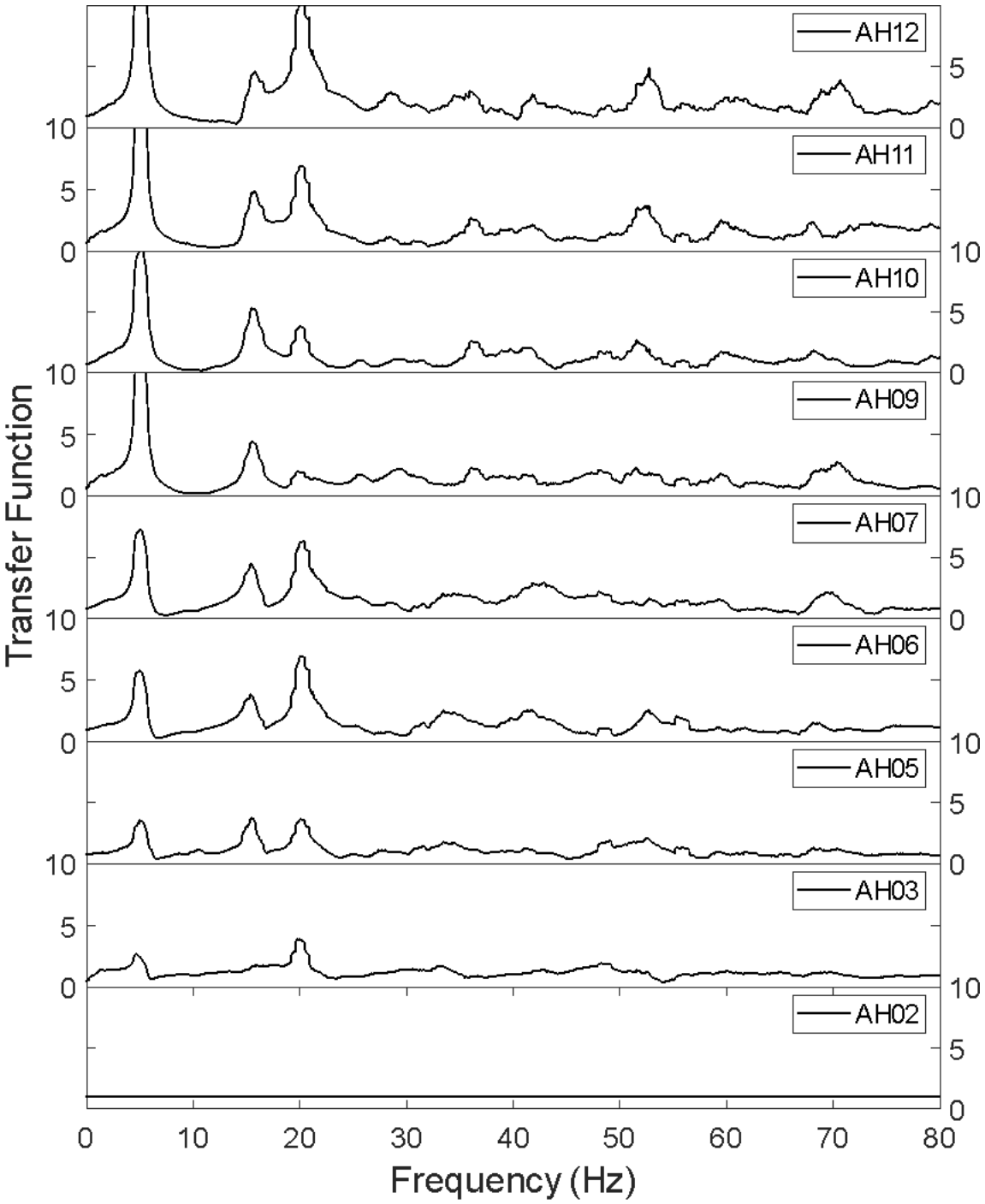

Figure 2.6. Transfer functions based on high resolution accelerometer data (free-field array) prior to Shake 1-1.

Based on the white noise motion arrival time and the time difference between two consecutive high-resolution accelerometers, the shear wave velocity profile for the constructed ground model was calculated. Figure 2.7 illustrates the shear wave velocity profile for the soil model measured before Shake 1-1. The results of the shear wave velocity calculation are also tabulated in Table 2.5. The depth of each sensor is measured from surface, and the distance between sensors is depicted in Figure 2.4 ranging between 0.2 to 0.25 m. The shear wave velocity profile indicates higher shear wave velocities in the dense layer compared to the loose and crust layer.

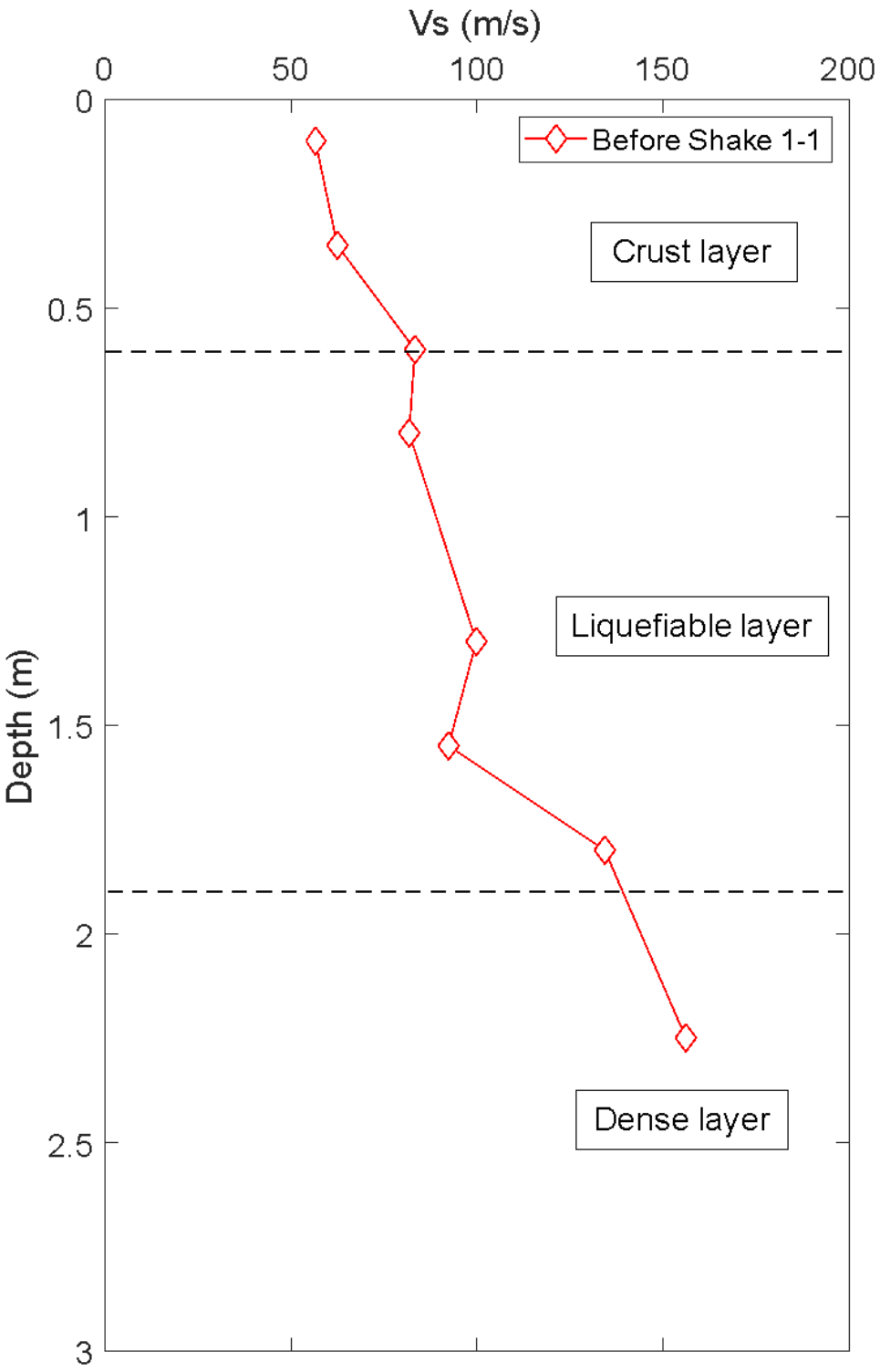

Figure 2.7. Shear wave velocity profile along depth of the soil model before Shake 1-1.

Table 2.5. Measured shear wave velocity profile along depth of model ground before Shake 1-1

Depth (m)	Arrival Time (s)	V_s (m/s)	Layer
0.1	7.5882	56.8	Crust
0.35	7.5838	62.5	Crust
0.60	7.5798	83.3	Crust
0.80	7.5774	82	Liquefiable
1.3	7.5713	100	Liquefiable
1.55	7.5688	92.6	Liquefiable
1.8	7.5661	134.6	Dense
2.25	7.5625	156.25	Dense

2.2.3. Shaking Sequences

During testing, a series of input motions were used to assess the dynamic response of shallow foundation along with free-field ground model for this baseline test. As mentioned earlier in Section 2.2, these two shaking sequences had different peak accelerations but with the same duration and frequency. Sufficient time was allowed between these two shakings for the generated pore-water pressure to dissipate. The acceleration response spectra for Shake 1-1 are presented in Figure 2.8, including response spectra for the base motion, foundation, and free-field surface ground motions. The predominant period of the input motion is shown to be 0.5 seconds, and the spectral acceleration of the foundation and surface free-field were de-amplified due to the 1.3 m liquefiable layer, resulting in lower responses of the foundation and the surrounding ground surface.

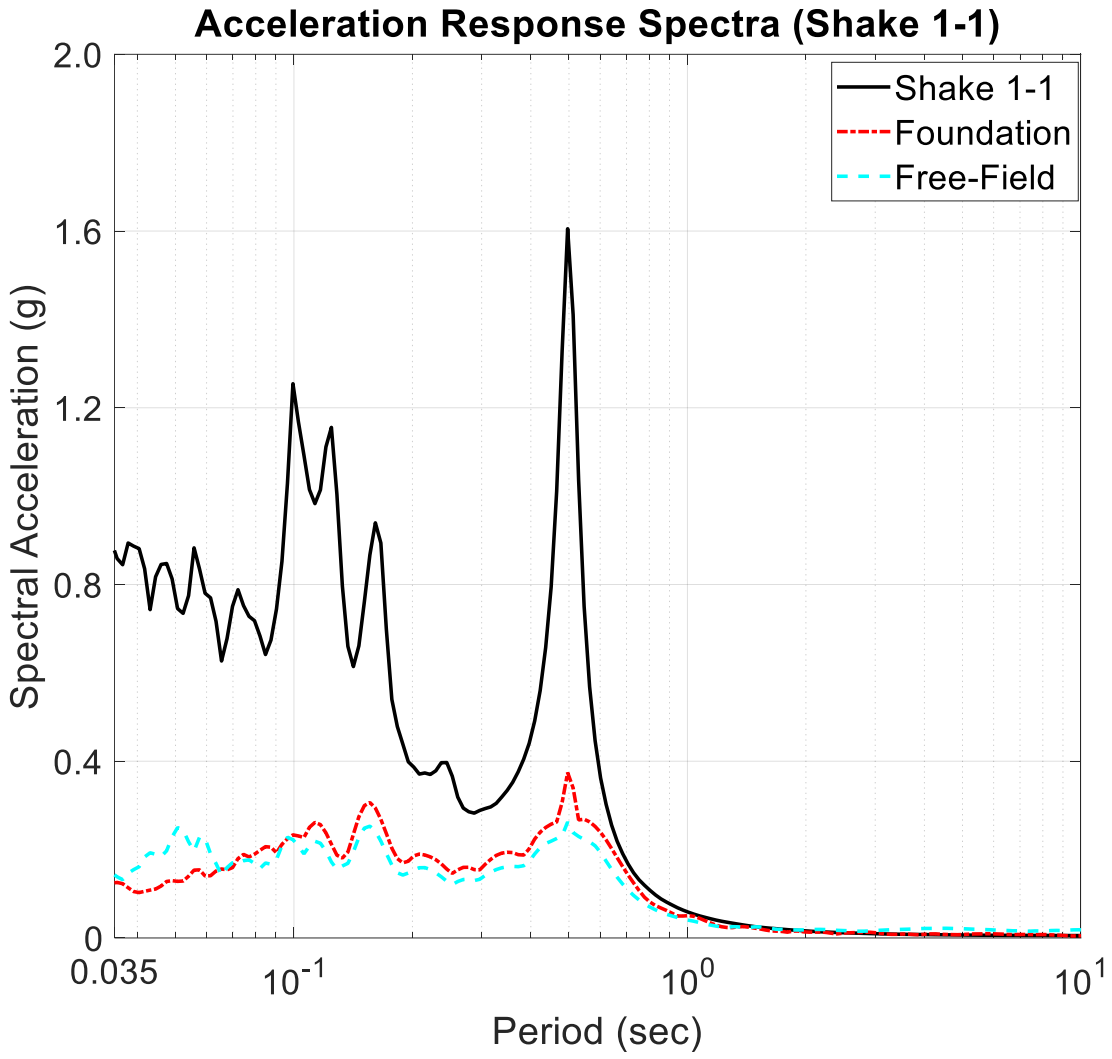

Figure 2.8. Acceleration response spectra (5% damped) for Shake 1-1.

2.3. Experimental Results

The 1g shake table testing at this scale provides an opportunity to further investigate the behavior of shallow foundation systems located on ground with surficial liquefiable layers which have been observed in several past earthquakes without the need to worry about scaling and its effect on the results. The results of excess pore-water pressure (EPWP) generation due to liquefaction in different layers is thoroughly evaluated followed by relevant discussion on hydraulic gradient and its effect on observed sand ejecta. The effect

of damage potential cumulative absolute velocity (CAV_{dp}) as an intensity measure is also discussed in the following section. Finally, the observed settlement of the shallow foundation and free-field conditions during the two shaking sequences are also discussed. It is worth noting that due to page limitations, the results of Shake 1-1 are mainly presented, while the Shake 1-2 results are included in the summary tables and figures.

Figure 2.9 shows the subset of sensors used in this paper to display representative results such as acceleration, excess pore-water pressure, and settlement time histories. As shown in Figure 2.3, three arrays of accelerometers and pore-pressure transducers were embedded in the model ground, however, only two arrays, “free-field” and “below foundation”, were selected to be presented, as shown in Figure 2.9. The soil surrounding the foundation at 0.6 m from edge of the foundation on each side is referred to as “free-field” condition through this paper. Two pairs of sensors in the middle of dense layer were selected to illustrate acceleration and pore-water pressure results for that layer. Example sensors at the bottom, middle, and top of the loose layer indicated as “bottom of liq. layer”, “mid. of liq. layer” and “top of liq. layer,” were selected to present the results for the loose layer.

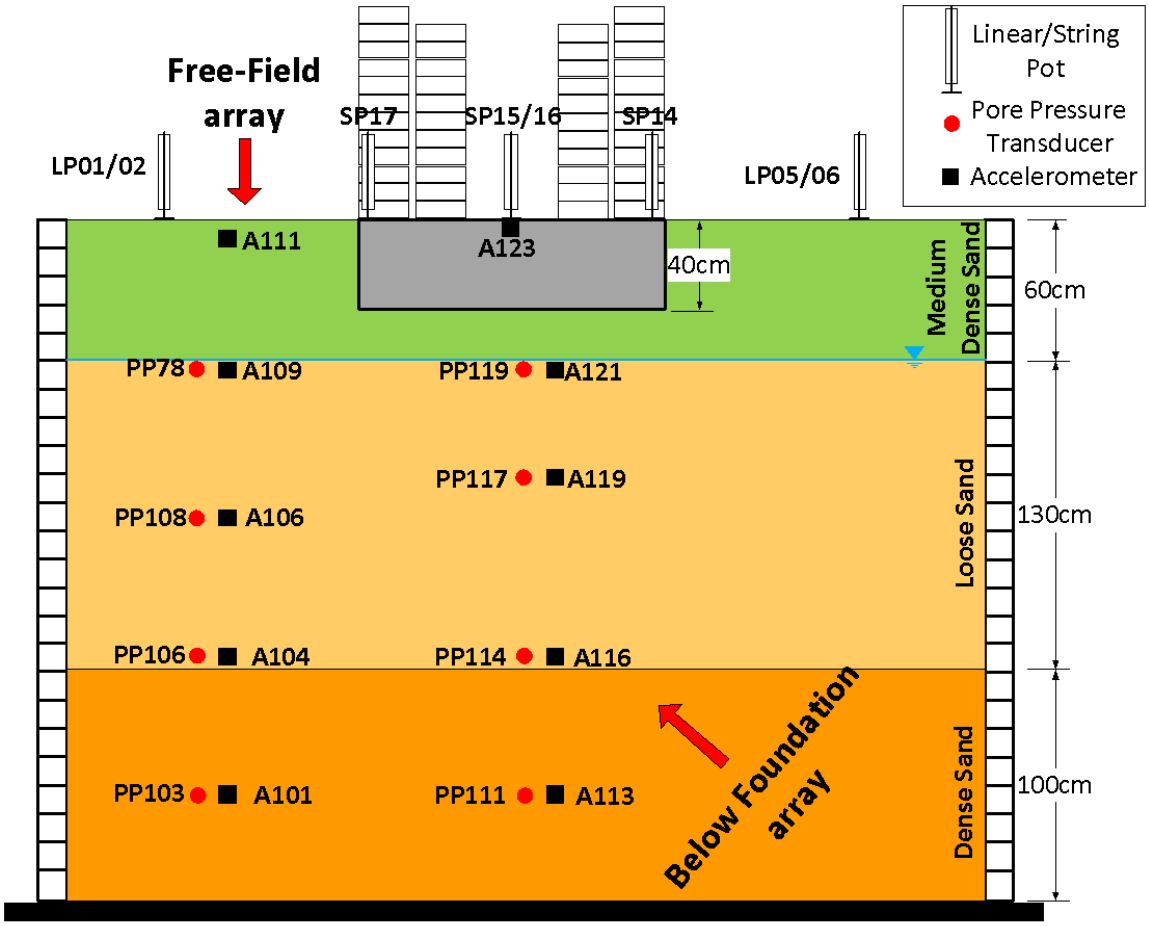

Figure 2.9. Cross-section view of sensors used for data processing of the baseline test.

2.3.1. Excess Pore-Water Pressure Generation

The liquefaction-induced settlement mechanisms introduced by Bray et al. (2014) highlighted the importance of pore-water pressure generation/dissipation, transient hydraulic gradients generated during strong shaking, and bearing capacity failure of shallow foundation due to strength reduction as contributing causes in different liquefaction-induced settlement mechanisms. As a result, the extensive instrumentation of pore-water pressure transducers was used to monitor the generation and dissipation of excess pore-water pressure in the shake table tests discussed here.

Figures 2.10 and 2.11 present the generated pore water pressure and acceleration time histories at the free-field and below the foundation arrays during Shake 1-1, respectively. The presented acceleration time histories were as recorded time histories without any filtering. These time histories are shown at different depths which include bottom, top, and middle of liquefiable layer and also the middle of the dense layer. The dashed lines represent the case in which excess pore-water pressure ratio (r_u) corresponds to unity (i.e. 1.0) at different depths and locations. When calculating the r_u values, the effect of vertical stress due to the foundation pressure was also incorporated using the 2:1 stress distribution method below the foundations. For the free-field case (Figure 2.10), the observed trend for excess pore-water pressure generation/dissipation is similar at bottom and middle of the liquefiable layer, where a drastic increase was observed in EPWP during strong shaking which was then followed by a gradual dissipation of EPWP once the shaking ceased. The rate of generation/dissipation is comparable in these depths. On the contrary, the observed EPWP trend in the upper part of the liquefiable layer and middle of the dense layer indicate a steady increase during the shaking which continued even after the shaking phase. This behavior was more pronounced in the middle of the dense layer. The reason for this progressive, though less significant, increase after the shaking could be due to the direction of pore-water pressure dissipation path at the bottom and middle of the liquefiable layer. The drainage paths created after the shaking most likely resulted in continuation of pore-water pressure buildup in the middle of dense layer and top of loose layer. This hypothesis is tested by the results presented in the next section. Results presented in Figure 2.10 show that the EPWP values reached the initial effective stress (dashed lines) in all three depths inside the liquefiable layer indicating the occurrence of

liquefaction. The pore-pressure ratio at the middle of the dense layer increased up to 0.4 as expected for a dense sandy medium, however, based on Bray and Macedo (2017), it is projected that the dense saturated sandy soil still contributed to the liquefaction-induced settlement. The highest generated EPWP during Shake 1-1 is the same for free-field and below foundation arrays at the comparable depths, potentially due to the redistribution of EPWP and the proximity of the sensors.

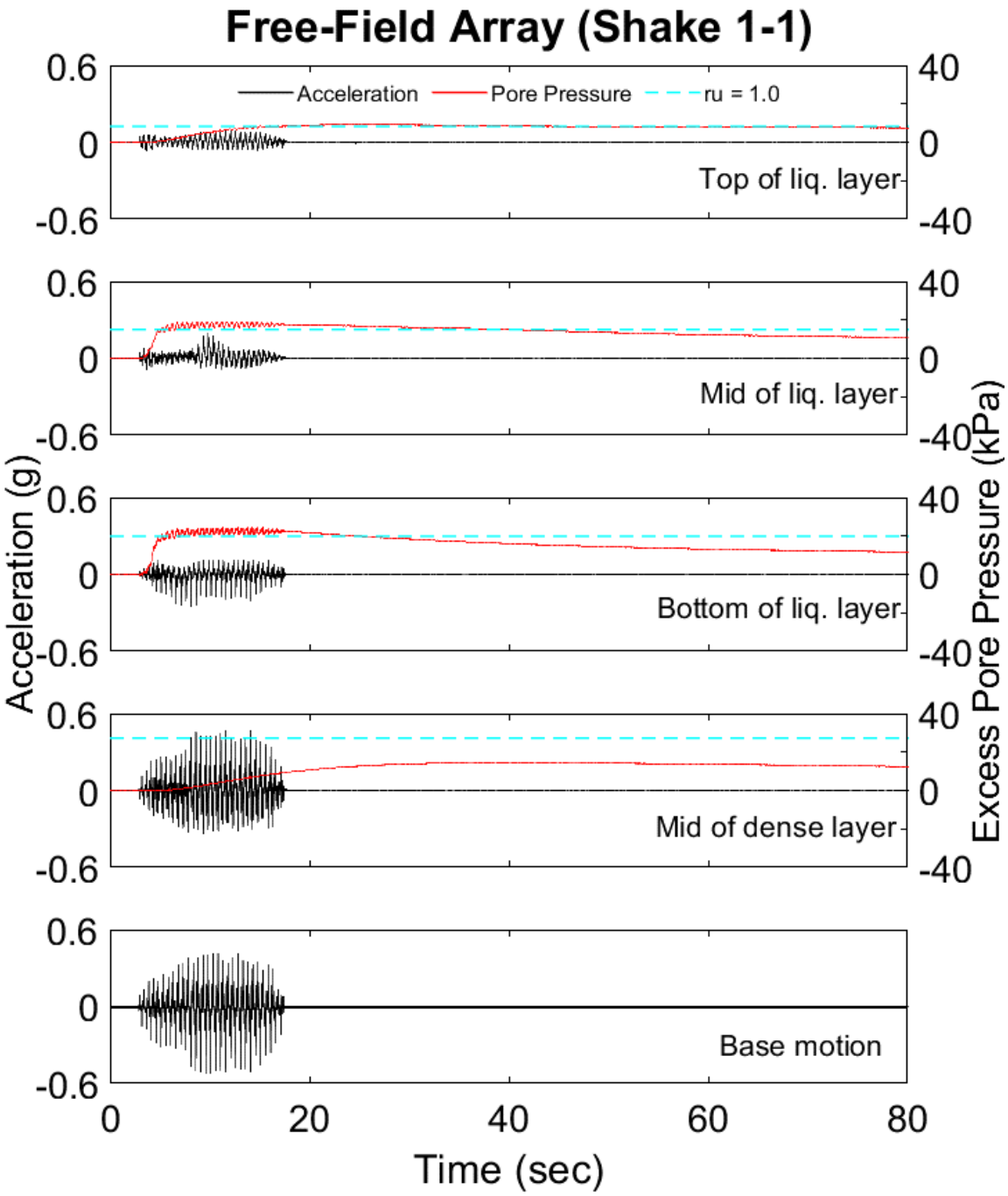

Figure 2.10. Excess pore water pressure and acceleration time histories during Shake 1-1 at different depths in the free-field array (dashed lines indicating pore pressure ratio equal to 1 at different depths.).

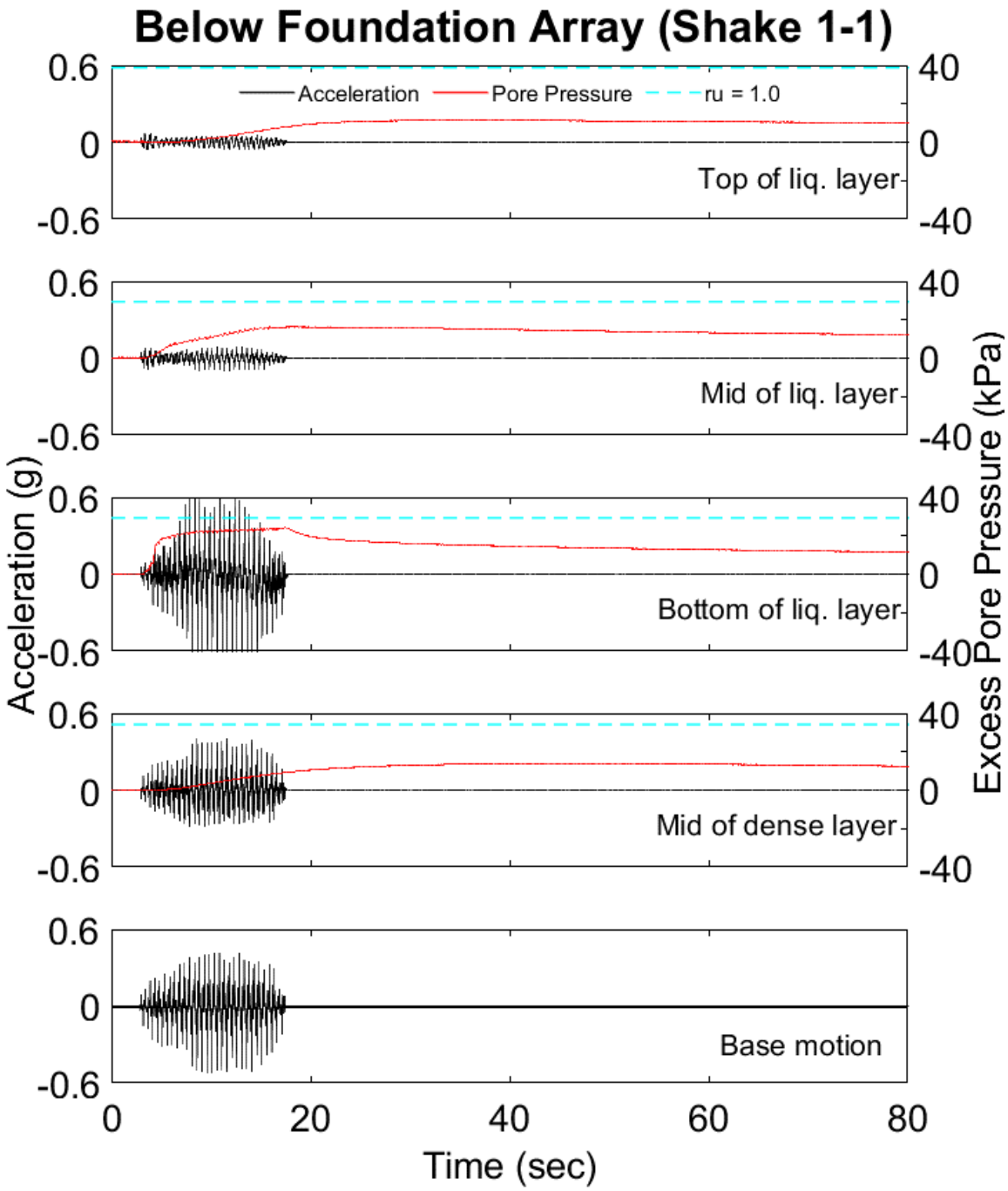

Figure 2.11. Excess pore water pressure and acceleration time histories during Shake 1-1 at different depths below the foundation (dashed lines indicating pore pressure ratio equal to 1 at different depths.).

The observations in the array under the foundation (Figure 2.11) were very similar to the free-field array presented in Figure 2.10, except for the fact that EPWP generation in the middle of liquefiable layer is not as steep as it was in the free-field array. This could be due to the added foundation pressure at top of the liquefiable layer, although the decreasing trend in EPWP just started after the ground shaking ceased. The above discussion is also valid for the drainage paths which resulted in a continued, although in a very insignificant manner, excess-pore pressure buildup at mid dense and top liquefiable level below the foundation after the shaking ceased. In addition, the r_u values (Figure 2.11, dashed lines) were lower than unity within the liquefiable layer under the foundation due to the added foundation pressure and its effect on the increased initial effective vertical stress. As illustrated in Figure 2.11, the r_u values were 1.5-2.0 times higher than their corresponding values in the free-field array (Figure 2.10). The results for Shake 1-2 are not presented in this study for the case of acceleration and pore water pressure time histories due to page limitation, but similar observations were obtained for Shake 1-2, which had higher peak acceleration than Shake 1-1.

Example EPWP time histories are presented in Figures 2.10 and 2.11, while data from all other sensors were used to present the EPWP isochrones in Figure 2.12 for Shake 1-1 along depth of the soil model from 0.6 to 2.9 m (i.e. within liquefiable and dense layers). All of the pore-water pressure sensors in both arrays were used to generate these EPWP isochrones (a total of 20 pore pressure transducers). The observed trends of the isochrones provided some valuable insight into the generation and dissipation of EPWP data. As illustrated in Figure 2.12, the EPWP data in each depth inside the liquefiable layer seemed to increase during shaking (up to 20 seconds) and followed a dissipative trend

afterward. This trend was more profound at the bottom of the liquefiable layer. On the other hand, the EPWP isochrones inside the dense layer continued to increase even after the shaking ceased (up to 50 seconds). The pore-pressure dissipation within the dense layer initiated much later, after t = 50 seconds, resulting in high pore-water pressure within the dense layer after the shaking had ceased (i.e. t = 20 seconds). Another important observation based on Figure 2.12 was the stabilization of EPWP starting from t = 50 seconds yielding relatively uniform values along depth in both of the arrays after 50 seconds.

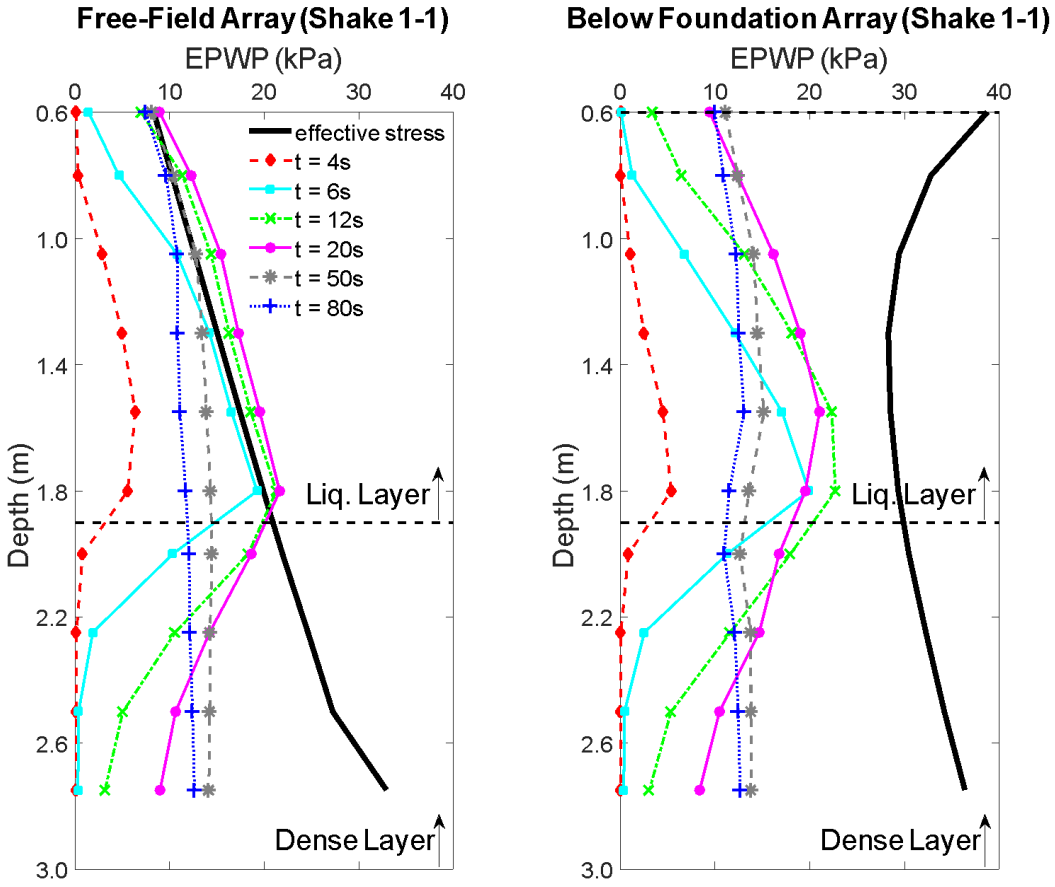

Figure 2.12. Excess pore water pressure isochrones along depth of the soil profile for Shake 1-1 at free-field and below foundation arrays.

2.3.2. Effect of Transient Hydraulic Gradient

The generated EPWP during strong shakings would result in high transient hydraulic gradients. Based on Darcy's law, the velocity of pore-water is calculated using equation $V = k*i$ in which V is the velocity of pore-water, k is the hydraulic conductivity of the soil, and i is the hydraulic gradient. Before shaking the model in the experiment, there was no difference between total heads of any two points in the model ground. The generation of EPWP during liquefaction caused the total head difference at different depths inside the model ground. Assuming 1D flow along the model depth, the total head difference generated the flow of pore-water in vertical direction. According to this assumption, the flow velocity of pore-water during Shake 1-1 was calculated between consecutive PWP sensors in different depths and locations. Results of the calculated flow velocity time histories are presented in Figure 2.13 for the case of free-field (i.e. dashed red lines) and below foundation (black continuous lines) arrays. The positive velocity between two PWP sensors indicates downward flow, while the negative velocity represents upward flow. As can be seen in Figure 2.13, the maximum absolute flow velocity occurred in the boundary of dense and loose layers, indicating significant difference in EPWP between dense and loose layers at the early stage of Shake 1-1. This observation is consistent with the presented data in Figures 2.10 and 2.11, where the rate of EPWP generation in the bottom of the loose layer was higher than the rates in the middle of the dense layer. The direction of flow at the top of the dense layer and at the boundary of the dense/loose layer was toward the dense layer (downward flow), whereas inside the loose layer, the direction of flow was upward. These observations can shed light on the fact that EPWP dissipation happened sooner in the loose layer compared to the dense layer. In addition, the direction of upward

flow coincides with the surface manifestation of sand ejecta, which happened approximately after the shaking ceased. Multiple GoPro cameras (San Mateo, CA, USA) were utilized to capture the occurrence of ejecta which indicated that the surface manifestation of ejecta started right after the shaking ceased. The observed sand boil after Shake 1-1 is depicted in Figure 2.14, but there was no direct measurement of the volume of sand ejecta due to the excess water puddling on the ground surface after each shaking sequence.

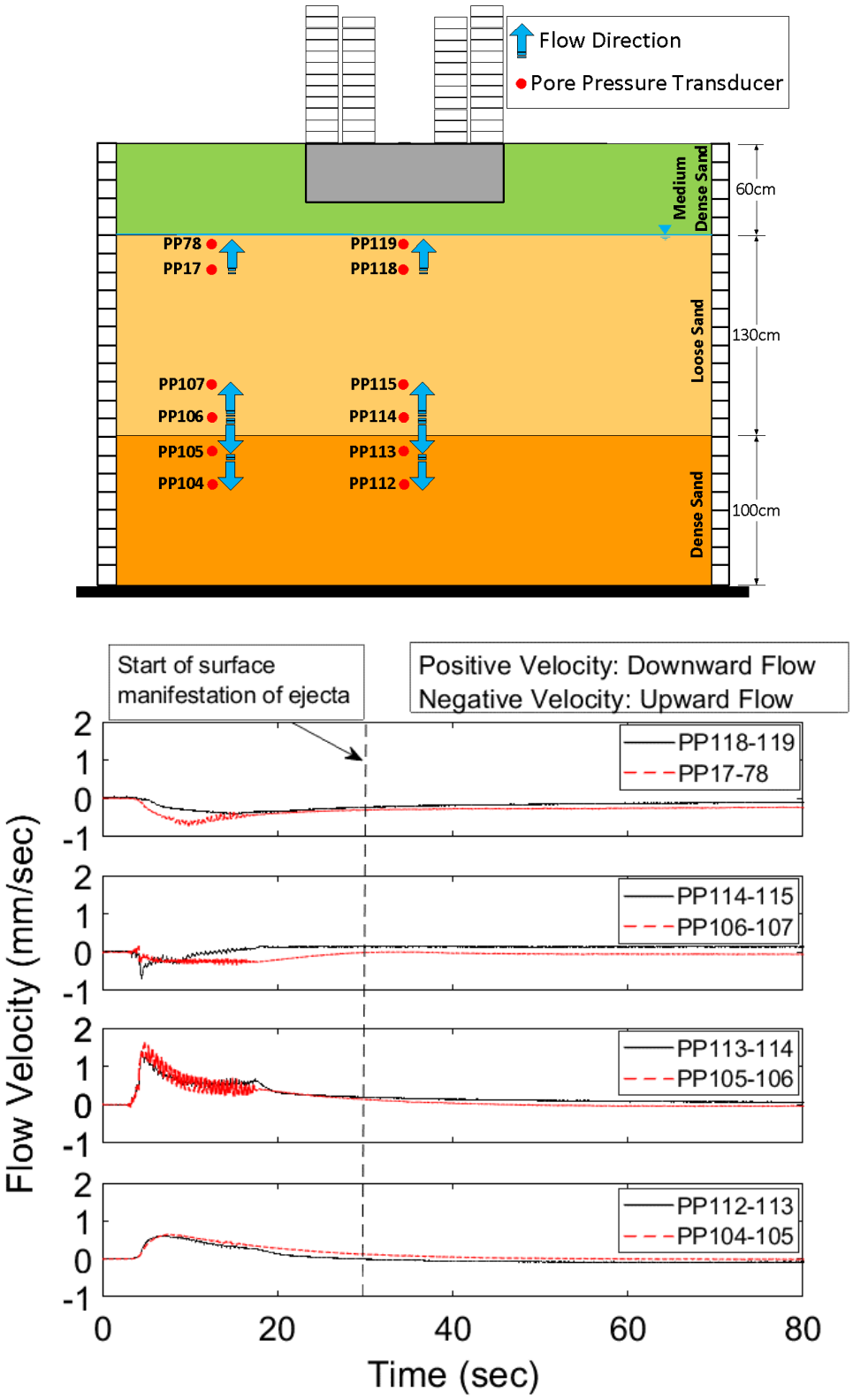

Figure 2.13. Flow velocity between two consecutive PWP sensors during Shake 1-1.

Figure 2.14. Observed sand ejecta after Shake 1-1.

2.3.3. Shear Stress-Strain Hysteresis Response

The shear stress and strain time histories and hysteresis loops were calculated using the acceleration records following the procedure outline by Zeghal and Elgamal (1994), and the results are presented in Figure 2.15 and 16 for the middle of the loose and dense layers, respectively. In this method, the shear strain time histories were directly back calculated from the acceleration records; whereas, the shear stress values were obtained assuming shear beam condition in the free-field. Higher shear stresses were generated at the middle of the dense layer compared to the middle of the liquefiable layer. The range of shear strains in the middle of both layers reached a maximum absolute value of 0.7%. Selected shear stress-strain hysteresis loops are also presented in Figures 2.15 and 2.16 at different time

steps during Shake 1-1. The stress-strain behavior in the middle of the liquefiable layer (Figure 2.15) indicated reduced stiffness after about 5 seconds when the EPWP buildup became significant. Figure 2.16, on the other hand, illustrated no reduction in stiffness at the middle of the dense layer during selected time steps in Shake 1-1, mainly attributed to the lower level of EPWP buildup.

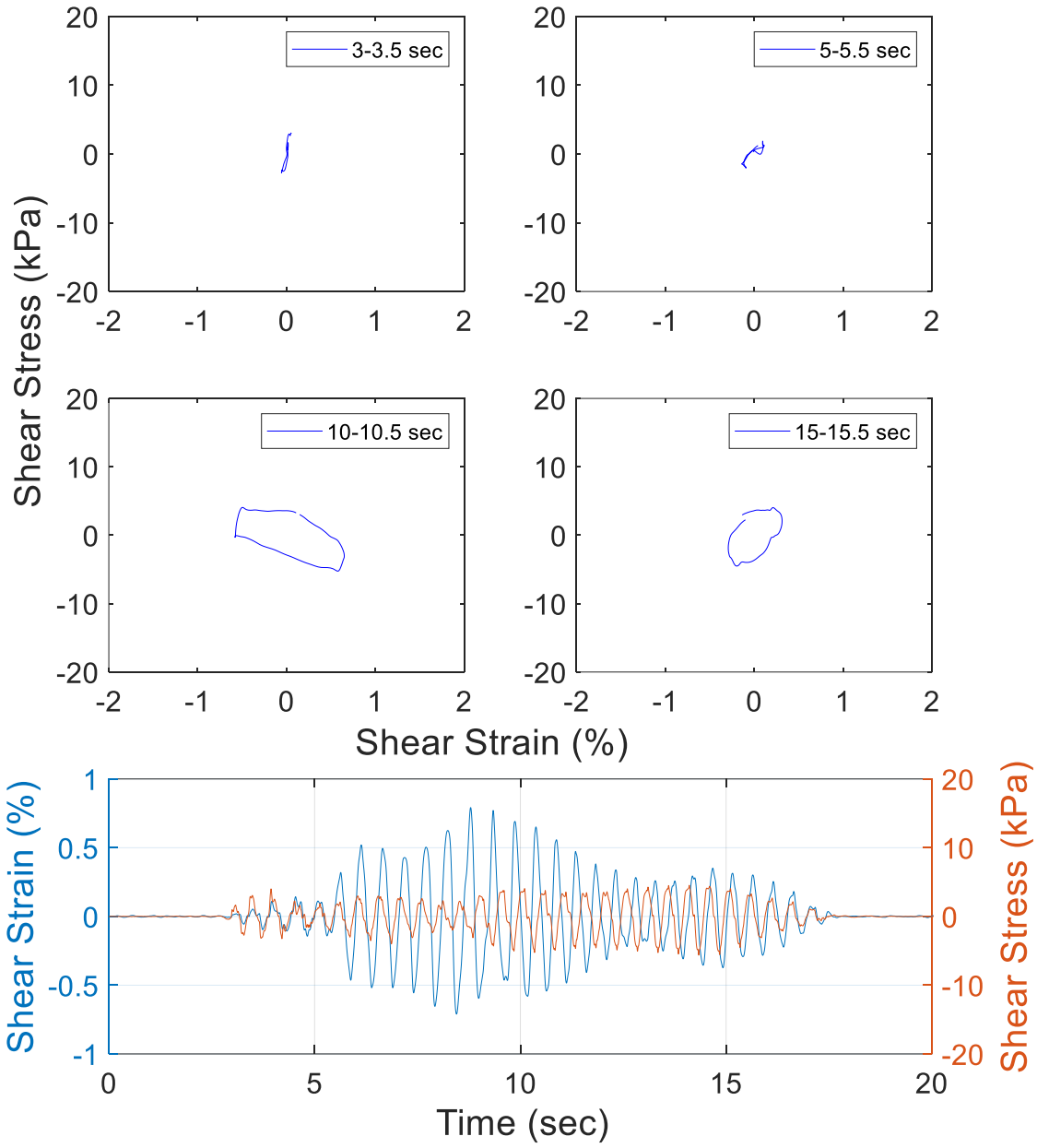

Figure 2.15. Stress-strain loops generated at the middle of loose layer at selected time spans.

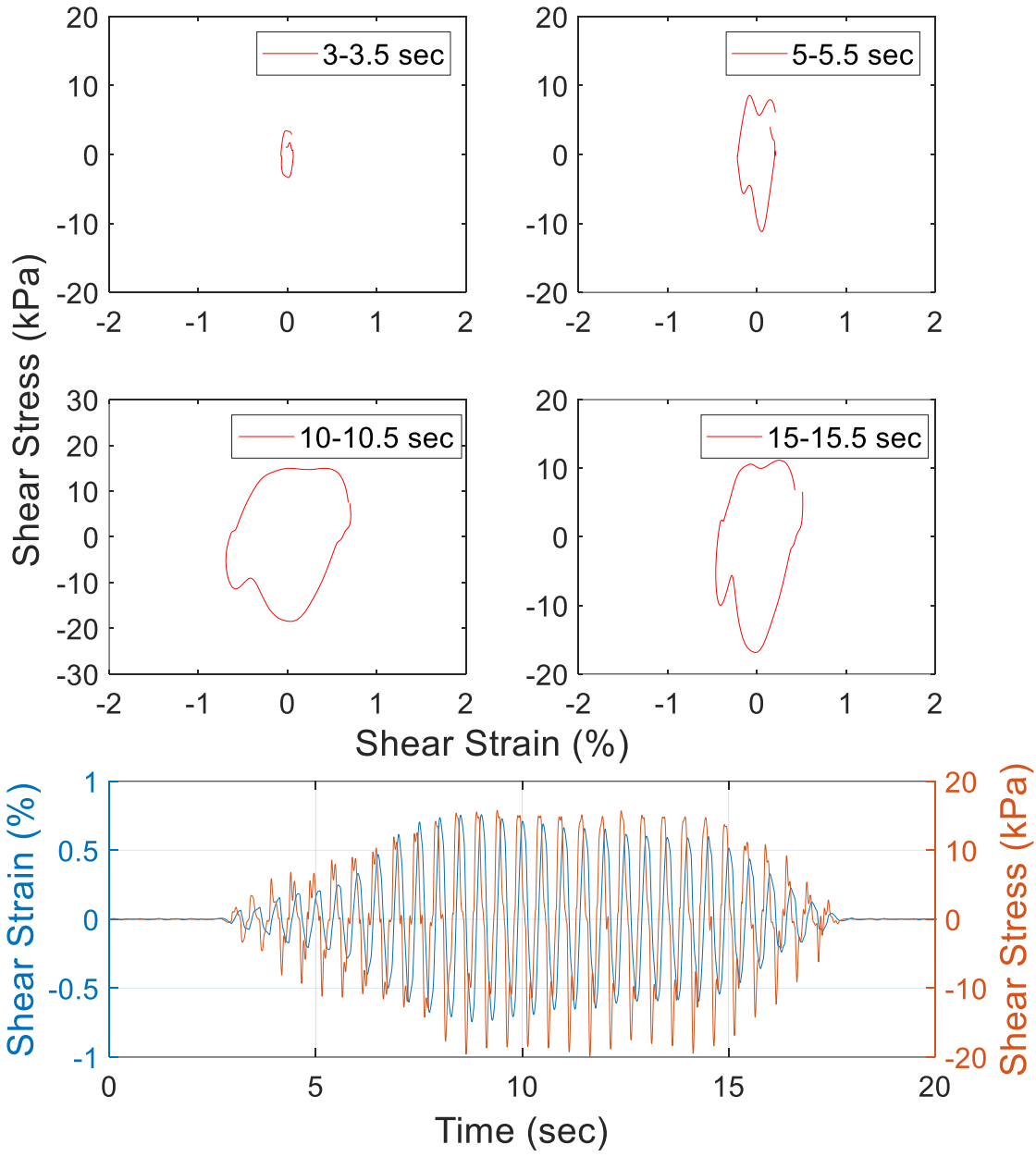

Figure 2.16. Stress-strain loops generated at the middle of dense layer at selected time spans.

2.3.4. Discussions of Damage Potential Cumulative Absolute Velocity

Several intensity measures have been evaluated to relate the effect of ground motions on the liquefaction-induced foundation settlements. Recent research evaluated the use of different intensity measures (*IM*s) in liquefaction-induced foundation settlement calculation and reported that plain *CAV* is a better predictor compared to other *IM*s [Karimi and Dashti 2017; Bullock et al. 2019]. Bray and Macedo (2017) however considered damage potential cumulative absolute velocity (CAV_{dp}) as the most relevant intensity measure to evaluate the amount of liquefaction-induced settlement. Bray and Macedo (2017) provided a simplified procedure to predict the amount of liquefaction-induced building settlement. This procedure includes CAV_{dp} as an intensity measure to calculate shear-induced settlement of the foundation. In this study, the values of CAV_{dp} were calculated at different depths for both free-field and below foundation arrays during Shake 1-1 to further investigate on the effect of this intensity measure on the amount of liquefaction-induced settlement.

Damage potential cumulative absolute velocity (CAV_{dp}) is defined in Campbell and Bozorgnia (2011) as:

$$CAV_{dp} = \sum_{i=1}^{N}(H(PGA_i - 0.025) \int_{i-1}^{i}|a(t)|dt \quad (2.1)$$

where N is the number of discrete 1-s time intervals, PGA_i is peak ground acceleration (g) in ith time interval, and $H(x)$ is the Heaviside Step Function ($H(x) = 0$ for $x < 0$ and $H(x) = 1$ for $x \geq 1$). The CAV_{dp} is taken to be zero if S_a is less than 0.2 g for periods between 0.2 and 0.5 seconds, and S_v less than 15.34 cm/s for periods ranging from 0.5 to 1 second. The CAV_{dp} only utilizes a single component of a three-component acceleration record. In this study, the acceleration records were applied and measured only in a single horizontal

direction along the model length. Using the above equation and the acceleration time histories at different depths, the CAV_{dp} time histories were calculated and are presented in Figures 2.17 and 2.18 at the free-field and below foundation arrays. In the case of the free-field array, the maximum generated CAV_{dp} is at the middle of the dense layer, while the corresponding maximum value for the array located below the foundation is at the bottom of the liquefiable layer. This indicates higher energy at similar depths in each array, which is in line with the acceleration time histories presented in Figures 2.10 and 2.11. The calculated CAV_{dp} for all other depths, including ground surface and the foundation itself, resulted in values lower than 0.5 *g*.s. The importance of using damage potential cumulative absolute velocity as an intensity measure to calculate settlement due to liquefaction is discussed in detail in Bray and Macedo (2017), and the calculated CAV_{dp} values (i.e. at different depths and arrays) were used in this study to evaluate the liquefaction-induced settlement following the simplified procedure proposed by Bray and Macedo (2017), which will be discussed in detail in Section 2.4.2 of this paper.

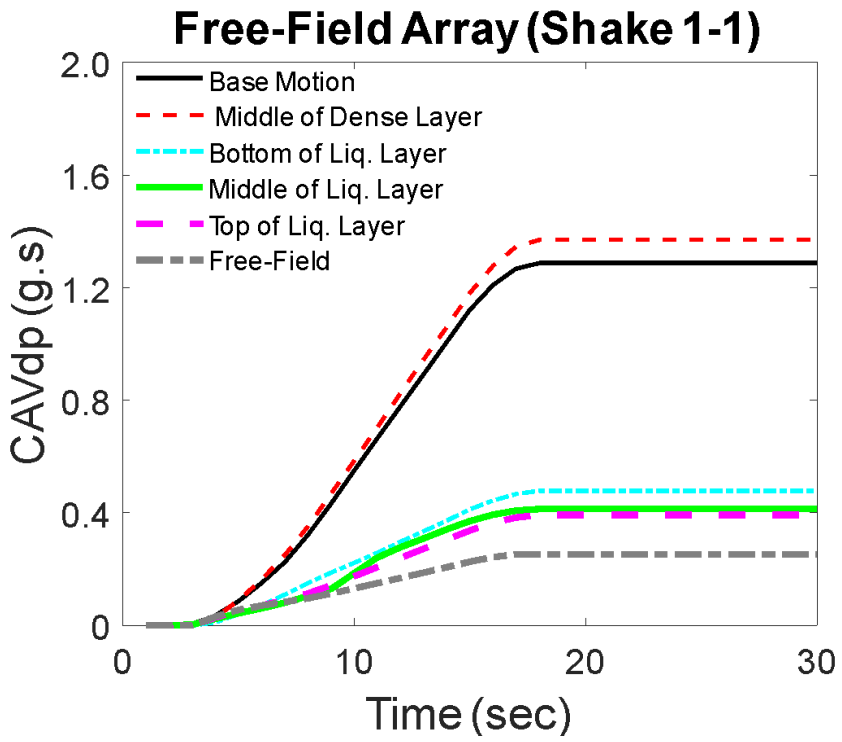

Figure 2.17. CAV_{dp} at different depths along free-field ground during Shake 1-1.

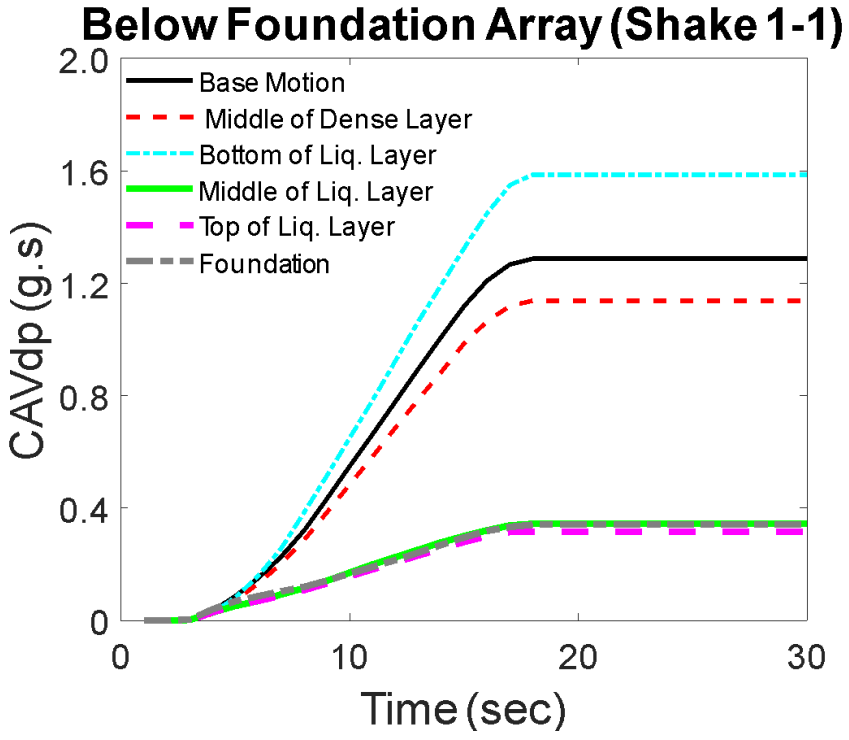

Figure 2.18. CAV_{dp} at different depths below foundation during Shake 1-1.

2.3.5. Liquefaction-Induced Foundation and Free-Field Settlements

Extensive foundation settlement was observed in this series of shake table tests. Figure 2.19(a) depicts the completed model just before the shaking sequence started, and the effects of Shake 1-1 and 1-2 are shown in Figure 2.19(b) and 2.19(c), respectively. The shallow foundation tilted about 2 degrees in-plane and punched into the soil after Shake 1-1 (Figure 2.19(b)), resulting in heave and significant cracks at the soil surface in the free-field. The in-plane and out-of-plane differential settlement were 4.9 and 2 cm, respectively [Jahed Orang et al. 2020]. Excessive amount of settlement was also noted during Shake 1-2 (Figure 2.19(c)).

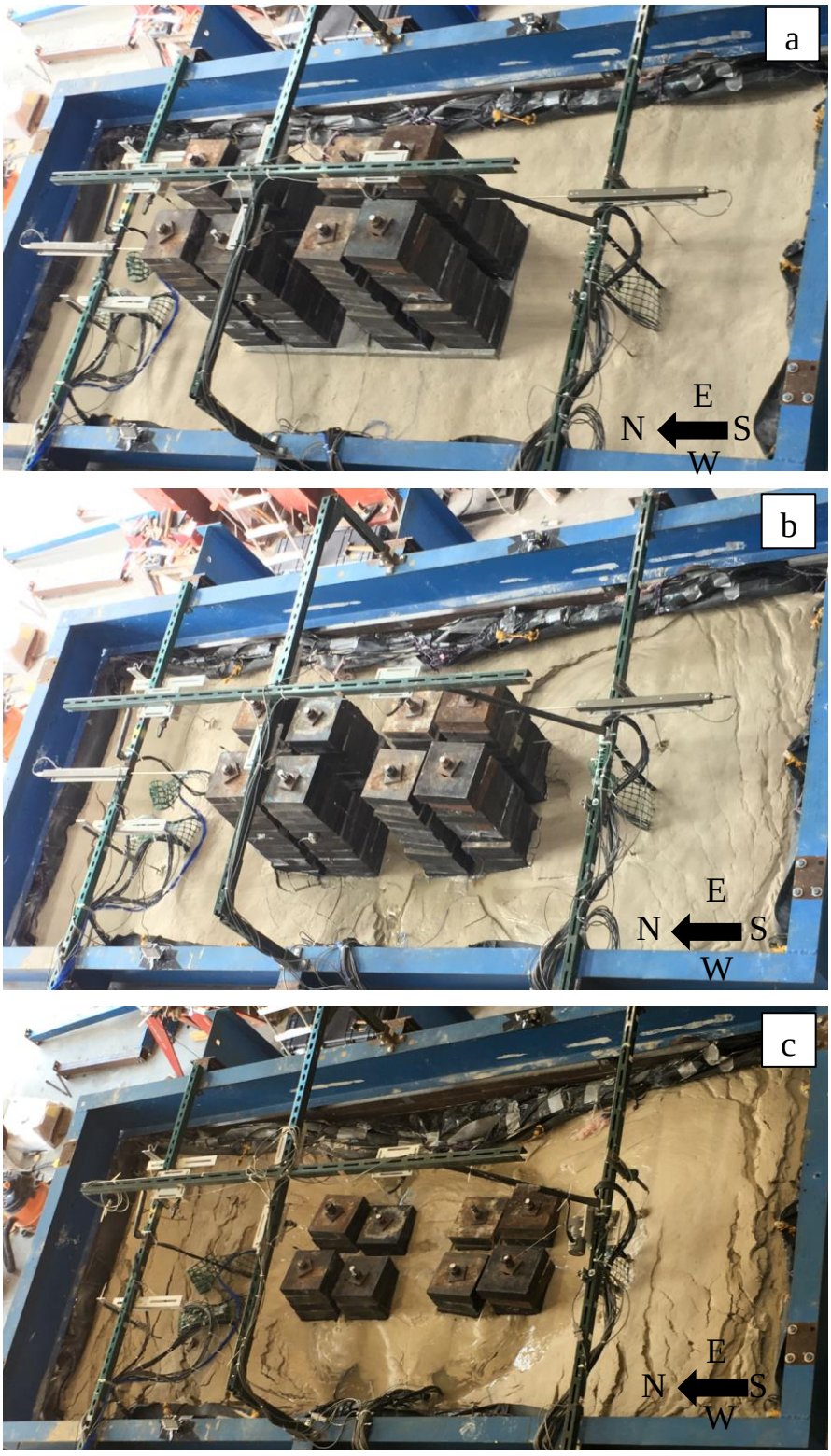

Figure 2.19. Photos of baseline model: (a) before Shake 1-1 (b) after Shake 1-1; and (c) after Shake 1-2.

The settlement-time histories of the foundation and ground surface (free-field) for Shake1-1 and 1-2 are presented in Figures 2.20 and 2.21, respectively. The recorded foundation settlement using string potentiometer on each corner of the foundation for Shake 1-1 and 1-2 is summarized in Tables 2.6 and 2.7. The foundation and ground surface settlement measurements during both shakings were achieved using four string potentiometers and four linear potentiometers. The location of the settlement transducers is indicated in Figure 2.3. For both shakings, the trends for settlement-time histories were similar in that the foundation started to sink inside the ground with the initiation of shaking and continued to settle in a relatively linear manner with respect to time until the shaking ceased. The settlement of the foundation continued even after the shaking ended, but the rate of settlement significantly decreased until it reached an asymptotic value, which was regarded as the total foundation settlement due to the liquefaction. The post shaking settlement of the foundation with respect to the total settlement of the foundation is presented in Figure 2.22 for both shakings ranging on average17 % and 7%, respectively. These percentages are attributed to mechanisms such as ground loss due to ejecta as well as post-liquefaction consolidation of liquefied soils. In the case of Shake 1-1, the post shaking settlement to the total settlement ratio (17%) was higher compared to Shake 1-2 (7%). Similar behavior was also reported in the previous studies, such as Bray and Dashti (2014), which elaborated on the liquefaction-induced settlement and contributing components such as shear-induced, volumetric-induced, and ejecta-induced mechanisms.

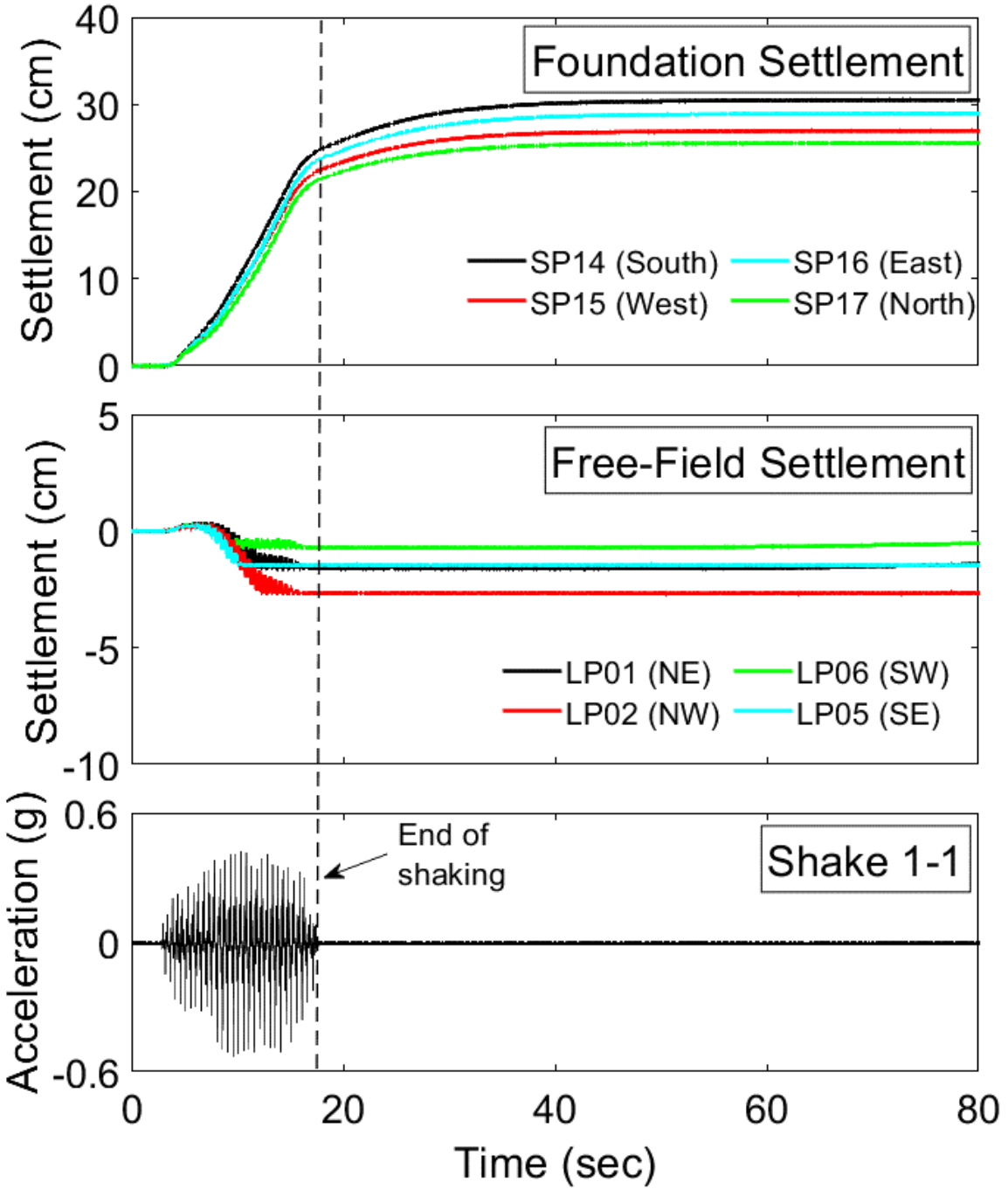

Figure 2.20. Settlement time histories at the foundation and surface free-field level during Shake 1-1 (negative settlement values indicate heave in free-field settlements.).

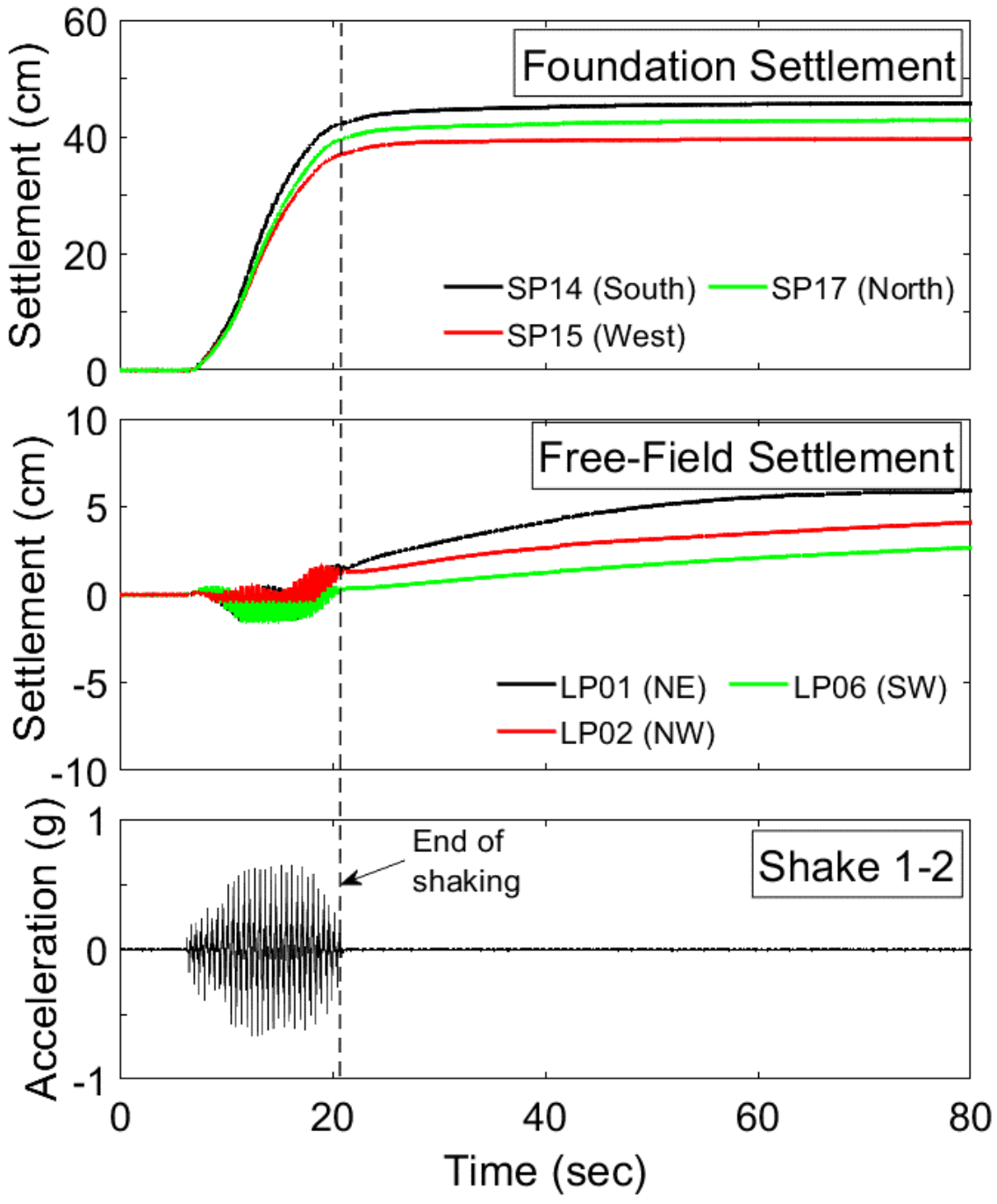

Figure 2.21. Settlement time histories at the foundation and surface free-field level during Shake 1-2.

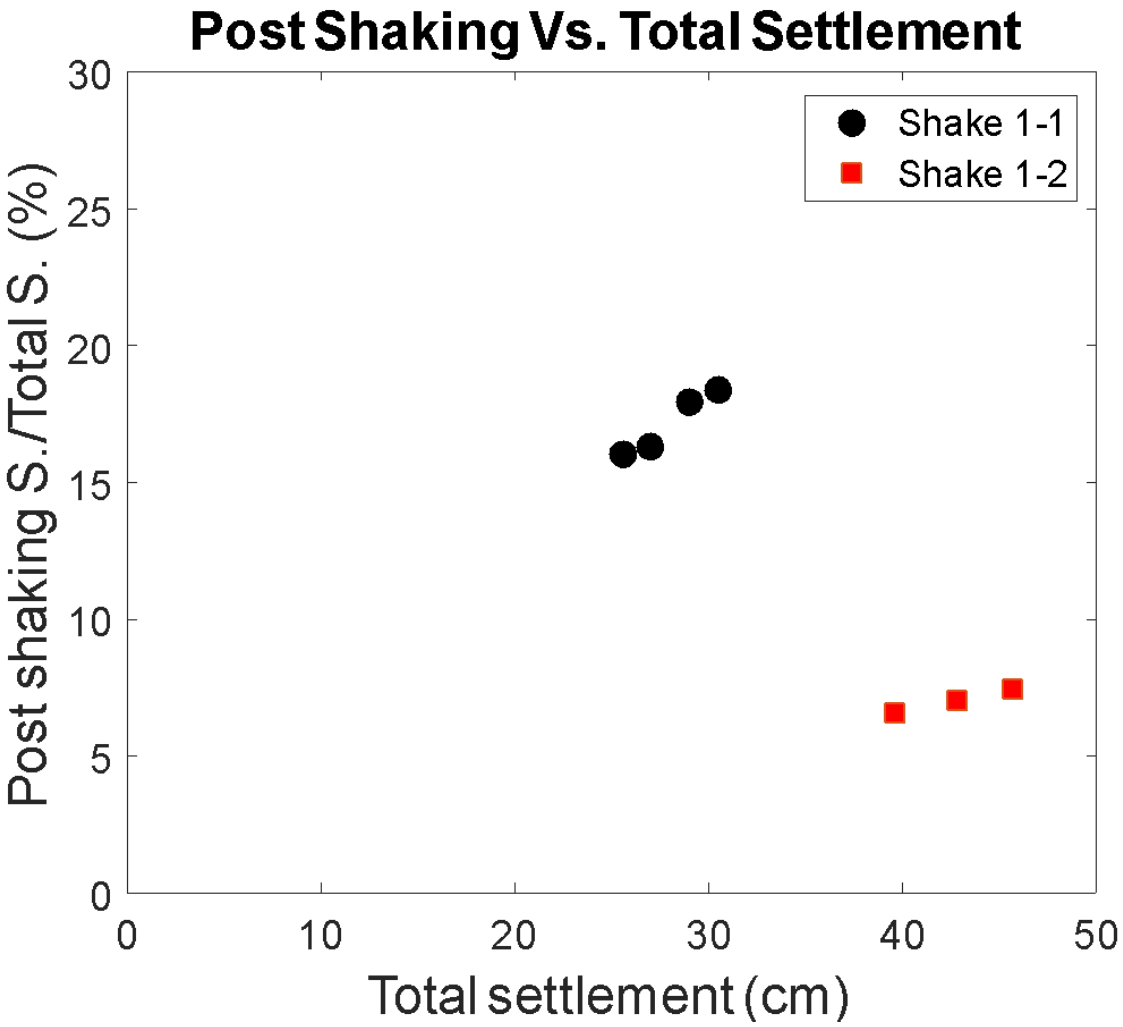

Figure 2.22. Post-shaking foundation settlement ratio with respect to total foundation settlement for Shakes 1-1 and 1-2.

Table 2.6. Measured foundation settlement values for Shake 1-1 (cm)

String pot. #	Total settlement	Settlement during shaking	Post shaking settlement
SP15	27.0	22.6	4.4
SP16	29.0	23.8	5.2
SP14	30.5	24.9	5.6
SP17	25.6	21.5	4.1
S_{avg}	28.0	23.2	4.8

Table 2.7. Measured foundation settlement values for Shake 1-2 (cm)

String pot. #	Total settlement	Settlement during shaking	Post shaking settlement
SP15	39.6	37.0	2.6
SP14	45.7	42.3	3.4
SP17	42.8	39.8	3.0
S_{avg}	42.7	39.7	3.0

The free-field settlement during both shaking events is also presented in Figures 2.20 and 2.21. During Shake 1-1, there was some permanent heave due to the foundation bearing capacity failure. The average of four linear potentiometer measurements indicated a 1.6 cm heave during Shake 1-1. However, in the case of Shake 1-2, the average free-field settlement was 4.3 cm. Measured settlement values for the free-field ground at the location of each linear potentiometer are also summarized in Table 2.8.

Table 2.8. Measured free-field settlement values for Shake 1-1 and 1-2 (cm)

Linear pot.	Total settlement		Settlement during shaking		Post shaking settlement	
	Shake 1-1	Shake 1-2	Shake 1-1	Shake 1-2	Shake 1-1	Shake 1-2
LP01	-1.6	6.0	-1.6	1.5	0	4.5
LP02	-2.7	4.2	-2.7	1.3	0	2.9
LP05	-1.5	2.7	-1.5	0.3	0	2.4
LP06	-0.7	-	-0.7	-	0	-
S_{avg}	-1.6	4.3	-1.6	1.0	0	3.3

Shake 1-1 had a lower peak acceleration compared to Shake 1-2, resulting in lower total settlement of the foundation. The amount of settlement during Shake 1-2 was strongly affected by the bearing capacity failure of the shallow foundation as well as the consequent variation of the ground condition during Shake 1-1. Based on the chart presented by Vesic (1973), showing the modes of foundation failure in sand based on relative density and D_f to B^* ratio where D_f is the embedment depth and $B^* = (2BL)/(B+L)$, local shear failure of the foundation bearing capacity took place. In this study, embedment depth, foundation length, and width were 0.4 m, 1.3 m, and 0.4 m, respectively. Consequently, the D_f/B^* ratio was 0.61 and relative density for the crust layer was 53%, resulting in local shear failure type based on Vesic's (1973) chart, consistent with the experimental observation and the heave at the free-field ground after Shake 1-1.

2.4. Liquefaction-Induced Building Settlement Estimation

2.4.1. Volumetric-Induced Settlement

The volumetric-induced settlement (D_v) was calculated based on the Ishihara and Yoshmine (1992) methodology, in which the post-liquefaction volumetric strain is obtained based on factor of safety against liquefaction (FS_L) for different relative densities of clean sand. Calculation for the volumetric-induced settlement was made using the achieved relative densities for each soil layer, as presented in Table 2. A high factor of safety against liquefaction ($FS_L > 1$) was assumed for the dense layer, while the factors of safety against liquefaction for the liquefiable layer was 0.80 based on calculated τ_{cyc} and $\tau_{cyc,L}$. The pore pressure sensors in unsaturated crust layer indicated no EPWP generation which means liquefaction was not triggered in the unsaturated crust layer during Shake 1-1. The presence of unsaturated crust can lead to lower foundation settlement. Several past research indicated that lowering the groundwater level (i.e. unsaturated top layer) resulted in lower foundation settlement compared to saturated and dry ground model condition [Mirshekari and Ghayoomi 2017; Borghei et al. 2020]. Consequently, a high factor of safety ($FS_L > 1$) was also assumed for the top crust layer in the volumetric-induced settlement calculations. The volumetric strain in each layer was subsequently multiplied by its corresponding layer thickness, resulting in 5.5 cm of volumetric-induced settlement for the baseline test during Shake 1-1.

2.4.2. Simplified Procedure by Bray and Macedo (2017) for Shear-Induced Settlement

Bray and Macedo (2017) recently introduced a simplified procedure to calculate the liquefaction-induced building settlement. The simplified procedure was suggested to

calculate the amount of shear-induced settlement (D_s) based on the results of 1300 analyses conducted using FLAC Version 7.0 with PM4Sand as the constitutive model in Bray and Macedo (2017). The final form of the equation for shear-induced settlement is:

$$Ln(Ds) = c1 + 4.59 * Ln(Q) - 0.42 * Ln(Q)^2 + c2 * LBS + 0.58 * Ln\left(Tanh\left(\frac{HL}{6}\right)\right) - 0.02 * B + 0.84 * Ln(CAVdp) + 0.41 * Ln(Sa1) + \varepsilon \quad (2.2)$$

where the variables in Equation 2.2 are defined in the notation list. The liquefaction building settlement index is calculated as:

$$LBS = \int_{0.6}^{1.9} W * \frac{\varepsilon_{shear}}{z} dz \quad (2.3)$$

Description of the variables used to calculate *LBS* is provided in Bray and Macedo (2017). The upper and lower bounds in Equation 3 indicate the depth of the top and bottom of the liquefiable layer measured from the ground surface. In order to calculate ε_{shear}, the factor of safety against liquefaction (FS_L) is required. The factor of safety against liquefaction for Shake 1-1 was 0.80. The estimated shear-induced settlement based on this simplified procedure is presented in Table 2.9. The presented values for CAV_{dp} and S_{a1} intensity measures were calculated based on equivalent linear analysis assuming no liquefaction in free-field ground condition using DEEPSOIL V7.0 [Hashash et al. 2020], consistent with the recommendations by the Bray and Macedo's simplified procedure. According to the calculated results the mean D_s was 3.3 cm based on FS_L = 0.80 (Table 2.9). The D_s in this case varies from 2 cm to 5.4 cm due to the error term variation (i.e. $-0.5 \leq \varepsilon \leq 0.5$). It is worth mentioning that if the presented CAV_{dp} values in Section 2.3.4 were used in this procedure, the calculated settlements were even lower. The lower-than-usual Sa1 value in this study is attributed to the simplified harmonic input motion used in

this series of shake table experiments, with a dominant frequency of 2 Hz (0.5 s), which resulted in unrealistically low spectral accelerations at other response periods.

Table 2.9. Details of parameters used to estimate shear-induced settlement for Shake 1-1

Variable	FS_L = 0.80		
ε_{shear} (%)	51.2		
LBS	79.7		
c1	-7.84		
c2	0.014		
Q (kPa)	41.6		
B (m)	1.3		
H_L (m)	1.55		
CAV_{dp} (*g*.s)	1.82		
S_{a1} (*g*)	0.07		
ε	-0.5	0.0	0.5
D_s (cm)	2[a]	3.3[b]	5.4[c]

[a]Mean - σ

[b]Mean

[c]Mean + σ

The variation of estimated D_s was strongly affected by the first three terms in Equation 2. The terms *c1* and *c2* are based on the calculated LBS and are important variables in shear-induced settlement calculation. Another important factor is the error term

(ε), which varies between -0.5 and 0.5, and its effect on the estimated D_s is presented in Table 2.9.

2.4.3. Comparison of Observed and Estimated Foundation Settlements

Liu and Dobry (1997) presented upper and lower boundaries for the normalized settlement data based on field observations from the 1964 Niigata and 1990 Luzon Philippine earthquakes against normalized building width. In this study, the normalized building width ratio (B/H_L) was 1.0 (B = 1.3 m and H_L = 1.3 m). The range of normalized settlement (S_t/H_L) based on the illustrated upper and lower bounds presented in Liu and Dobry (1997) was from 0.02 to 0.175. The estimated settlement based on these limits are in the range of 2.6 to 22.7 cm for Shake 1-1. The measured total settlement of the foundation in case of Shake 1-1 was 28 cm, which was 19% larger than the upper limit recommended by Liu and Dobry (1997).

In addition, Bray and Macedo's simplified procedure was used to estimate the liquefaction-induced foundation settlement for Shake 1-1. The total liquefaction-induced building settlement is the sum of volumetric-induced (D_v), shear-induced (D_s) and ejecta-induced settlement (D_e), as presented in Bray and Macedo (2017):

$$D_t = D_e + D_v + D_s \quad (2.4)$$

The volumetric-induced settlement was calculated based on Ishihara and Yoshimine's chart [Ishihara and Yoshmine 1992], and the shear-induced settlement of the foundation was obtained using Bray and Macedo's simplified method, described above. The effect of ejecta-induced settlement is still not well quantified; ground failure indices or Ishihara's ground failure design chart [Ishihara, 1985] can help to estimate the amount of ground loss due to ejecta formation (D_e) [Bray and Macedo 2017]. Recently, an

exploratory study based on a series of medium-scale shake table tests was conducted at UNR to correlate the volume of the ejecta to the total settlement of the foundation. The results indicated a linear relationship between ejecta volume and total foundation settlement up to a threshold volume of ejecta, beyond which the increase in the volume of ejecta had no significant impact on total liquefaction-induced foundation settlement [Orang et al. 2019]. In this study, it was difficult to measure the amount of ejecta due to the significant water flow to the ground surface, however based on post shaking foundation settlement measurement, the ejecta appears to contribute up to 17% of the total settlement (i.e. 4.8 cm out of 28 cm). Nonetheless, there is still no well calibrated correlation to estimate the amount and contribution percentage of ejecta-induced settlement.

A detailed summary of the estimated and measured total settlement of the foundation for Shake 1-1 is provided in Tables 2.10 and 2.11 and Figure 2.23. The estimated settlement values in Table 2.10 are based on FS_L = 0.80, ranging from 7.5 cm to 10.9 cm depending on the error term (i.e. $-0.5 \leq \varepsilon \leq 0.5$). The estimated total settlement value based on $\varepsilon = 0.5$ had the least deviation from the measured total settlement of the foundation (Figure 2.23). The estimated settlement values excluded the effect of sediment ejecta (D_e), and its inclusion can increase the estimated settlement values accordingly. Additionally, probabilistic-based methods such as Moss (2006) and Cetin et al. (2009) can be used to calculate the volumetric component of liquefaction-induced settlement which can increase the confidence interval around the total settlement calculation. Overall, the average estimated liquefaction-induced foundation settlement based on Bray and Macedo (2017) underestimated the observed foundation settlement in this study by 68%. Bray and Luque (2017) employed this simplified procedure for a building in Christchurch Central

Business District and reported conservative estimations, while the measured settlement values based on centrifuge tests conducted by Dashti (2009), reported underestimation of measured settlement values compared to the estimated values based on Bray and Macedo's (2017) simplified procedure. The range of uncertainty for the estimated settlement is mainly due to the assumptions made in this simplified procedure, as well as to the unrealistically low S_{a1} value generated in this series of experiments.

Table 2.10. Estimated settlement for Shake 1-1 (cm)

Parameter	Mean - σ	Mean	Mean + σ
D_v	5.5	5.5	5.5
D_s[a]	2.0	3.3	5.4
$D_t = D_v + D_s$	7.5	8.8	10.9

[a]Based on calculated FS_L = 0.80.

Table 2.11. Measured settlement during Shake 1-1 (cm)

Parameter	Value
Settlement during shaking	23.2
Post shaking settlement	4.8
Total Settlement *Dt*	28.0

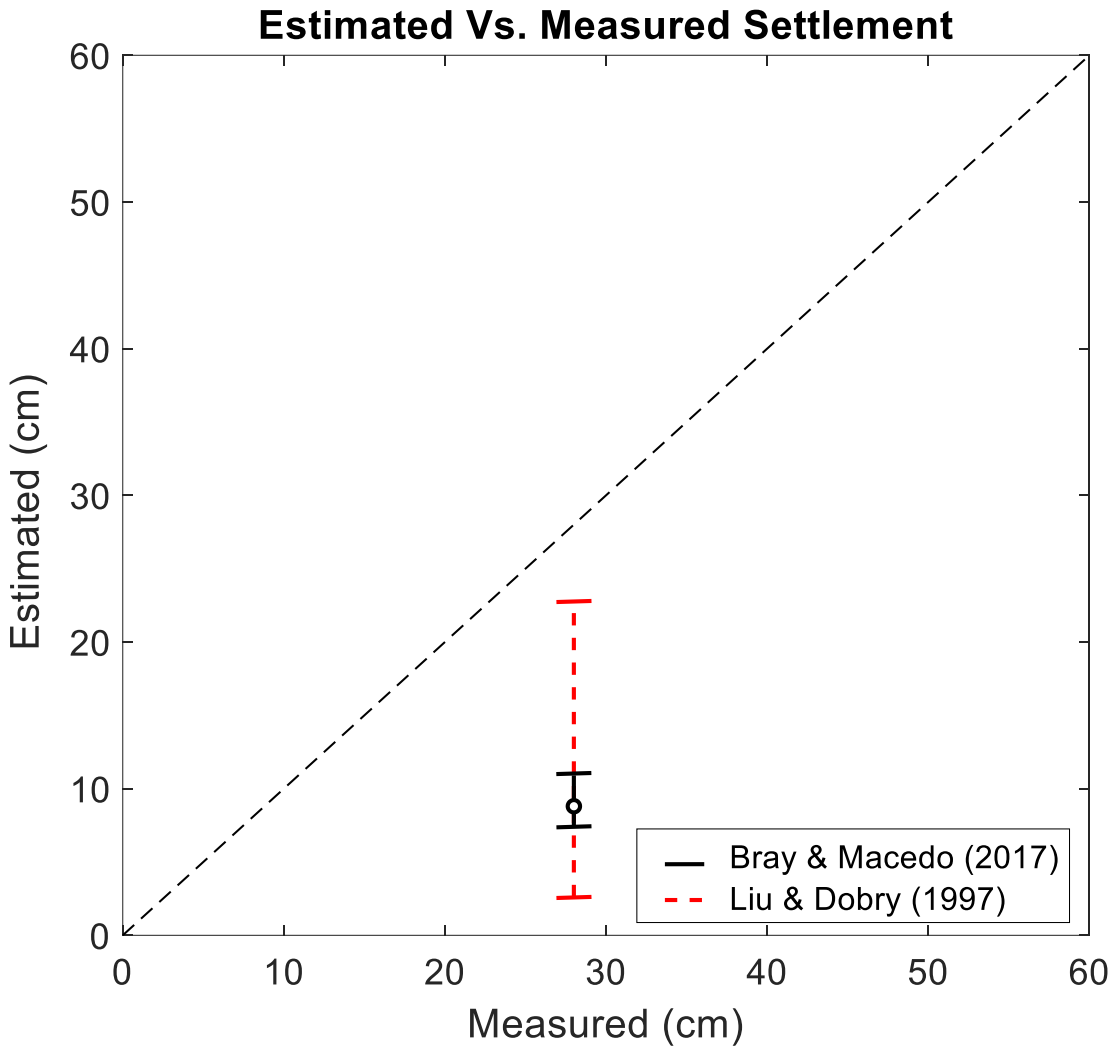

Figure 2.23. Estimated versus measured total settlement of the foundation for Shake 1-1.

2.5. Conclusions

A series of large-scale shake table tests were conducted to evaluate the liquefaction-induced settlement of a shallow foundation. A shallow rigid foundation was placed atop a three-layer model ground, including a shallow surficial liquefiable medium representing typical soil profiles observed in past earthquakes.

The following is a summary of the main findings of this experimental study:

- This series of shake table tests on a shallow foundation on liquefiable soil is the first set of experimental data at this scale exploring the response of a soil-foundation system to liquefaction-induced ground movement effects featuring a realistic reproduction of sand ejecta. The produced experimental data provides researchers and practicing engineers a baseline dataset to validate numerical simulations focused on liquefaction-induced settlement of buildings as well as future evaluation of effective mitigation strategies.
- A dense array of high-resolution accelerometers was used for system identification, capturing the fundamental frequency of the model ground (around 5 Hz) by establishing transfer functions. This set of data was further used to characterize the shear wave velocity profile of the model ground.
- The EPWP generation at different depths indicated extensive liquefaction and pore-water pressure buildup even after the end of shaking in the middle of the dense layer. The EPWP isochrones after Shake 1-1 became relatively uniform along the depth of the model in both the free-field and below the foundation arrays. This emphasizes that the transient hydraulic gradients vanishes after ground shaking ceases. The calculation of flow velocity based on Darcy's law and assuming 1D flow inside the ground indicated the direction of flow on top of the dense and on the boundary of the dense/loose layers was toward the dense layer (downward flow), whereas inside the loose layer, the direction of flow was upward. This, especially the downward direction of flow, further explains why EPWP dissipation at the middle of the dense layer did not occur even after the shaking ended. The

upward flow direction in the loose layer was confirmed by the observed sand ejecta after the shaking ceased.

- The calculated CAV_{dp} in different depths indicated maximum CAV_{dp} occurred at the middle of the dense layer in the case of free-field array, where the corresponding maximum value for the array located below the foundation was at the bottom of the liquefiable layer. This indicates higher acceleration at similar depths in each array, which is in line with the acceleration time histories presented. The CAV_{dp} values were also used for calculating shear-induced settlement of the foundation based on Bray and Macedo's (2017) simplified procedure. The IMs (including CAV_{dp}) were also estimated based on DEEPSOIL version 7.0 analysis assuming free-field no liquefaction condition for shear-induced settlement of the foundation as suggested by Bray and Macedo (2017). The use of CAV_{dp} at different depths and location resulted in lower consistency of the estimated values compared with the observed settlement, whereas utilizing IM parameters (i.e. in this case CAV_{dp} and S_{a1}) at the free-field no liquefaction condition yielded to a better estimate from shear-induced foundation settlement calculations.
- Measured free-field and foundation settlement trends indicated a local shear failure mechanism in the model, supported by observed heave in the surrounding ground and excessive punching settlement of the foundation. Post-shaking settlements were carefully quantified carefully and attributed to ground loss due to sand ejecta as well as to post-liquefaction consolidation of the liquefiable layer.
- Two simplified procedures were used to estimate the liquefaction-induced settlement of the foundation, those of Liu and Dobry (1997) and Bray and Macedo

(2017). The normalized settlement versus normalized width of the foundation presented by Liu and Dobry (1997) indicated settlement values in the range of 2.6-22.7 cm, which is lower than the 28 cm measured settlement of the foundation in the case of Shake 1-1. Using Bray and Macedo's (2017) simplified procedure resulted in total settlement of the foundation ranging from 7.5 cm to 10.9 cm (excluding ejecta-induced settlement), which also is lower than the measured total settlement value (i.e. 28 cm). Both methods underestimated the measured total settlement obtained through this shake table study.

Overall, this study demonstrated that 1g shake table tests can provide valuable insight into the liquefaction-induced building settlement phenomenon by reproducing all the controlling mechanisms. However, similar to any other experimental methods, it has limitations, specifically the inability to reproduce higher confining pressures observed at deeper depths. This series of large-scale tests were focused on evaluating the effects of a shallow liquefiable layer on the response of a shallow foundation, consistent with the observed damage during past earthquakes, and care should be taken when using the results of this study in cases where deep liquefiable layers are present.

2.6. Notation

The following symbols are used in this paper:

B = width of foundation (m);

CAV_{dp} = cumulative absolute velocity for no-liquefaction free-field condition (g.s);

$c1$ = -7.48 for LBS > 16 and -8.35 for LBS ≤ 16;

$c2$ = 0.014 for LBS > 16 and 0.072 for LBS ≤ 16;

D_s = shear-induced settlement (mm);

H_L = cumulative thickness of layers with $FS_L \leq 1.0$ (m);

LBS = liquefaction building settlement index [Eq. (3)];

Q = foundation contact pressure (kPa);

S_{a1} = spectral acceleration at T = 1 s (g) and

ε = uncertainty parameter (normal random variable with zero mean and 0.50 standard deviation).

2.7. References

Abdoun, T., Dobry, R., O'Rourke, T. D., & Goh, S. H. (2003). "Pile response to lateral spreads: centrifuge modeling." Journal of Geotechnical and Geoenvironmental engineering, 129(10), 869-878.

Adachi, T., Iwai, S., Yasui, M., and Sato, Y. (1992). "Settlement and inclination of reinforced concrete buildings in Dagupan City due to liquefaction during 1990 Philippine earthquake" Proc. 10th World Conference on Earthquake Engineering, Vol. 2, A.A. Balkema Rotterdam, The Netherlands, 147-152.

Bastidas, A. M. P. (2016). "Ottawa F-65 sand characterization." Ph.D. Dissertation, Dept. of Civil and Environmental Engineering, Univ. of California, Davis.

Badanagki, M., Dashti, S., & Kirkwood, P. (2018). "Influence of dense granular columns on the performance of level and gently sloping liquefiable sites." Journal of Geotechnical and Geoenvironmental Engineering, 144(9), 04018065.

Bahmanpour, A., Towhata, I., Sakr, M., Mahmoud, M., Yamamoto, Y., & Yamada, S. (2019). "The effect of underground columns on the mitigation of liquefaction in shaking table model experiments." Soil Dynamics and Earthquake Engineering, 116, 15-30.

Borghei, A., Ghayoomi, M., & Turner, M. (2020). "Centrifuge tests to evaluate seismic settlement of shallow foundations on unsaturated silty sand." In Geo-Congress 2020: Geotechnical Earthquake Engineering and Special Topics (pp. 198-207). Reston, VA: American Society of Civil Engineers.

Boulanger, R. W., Kutter, B. L., Brandenberg, S. J., Singh, P., Chang, D., & University of California, Davis. Center for Geotechnical Modeling. (2003). "Pile foundations in

liquefied and laterally spreading ground during earthquakes: centrifuge experiments & analyses" (No. UCD/CGM-03/01). Center for Geotechnical Modeling, Department of Civil and Environmental Engineering, University of California, Davis, California.

Bray, J. D., R. B. Sancio, H.T. Durgunoglu, A. Onalp, T. L. Youd, J. P. Stewart, R. B. Seed, O.K. Cetin, E. Bol, M. B. Baturay, C. Christensen, and T. Karadayilar (2004). "Subsurface characterization at ground failure sites in Adapazari, Turkey," Journal of Geotechnical and Geoenvironmental Engineering, ASCE, Vol. 130, No. 7, pp. 673-685.

Bray, J.D., Frost, J.D. (Eds) (2010). "Geo-engineering reconnaissance of the 2010 Maule, Chile earthquake." Accessed May 25, 2010. http://learningfromearthquakes.org/2010-02-27-chile/images/2010_02_27_chile/pdfs/prel_report/GEER_Report_Chile_2010_Final.pdf.

Bray, J. D. and Dashti, S. (2014). "Liquefaction-induced building movements." Bulletin Earthquake Engineering, 12, 1129-1156.

Bray, J. D., Cubrinovski, M., Zupan, J., & Taylor, M. (2014). "Liquefaction effects on buildings in the central business district of Christchurch." Earthquake Spectra, 30(1), 85-109.

Bray, J. D. & Macedo, J. (2017). "6th Ishihara lecture: Simplified Procedure for estimating liquefaction-induced building settlement." Soil Dyn. Earthquake Eng., (102) 215-231 http://dx.doi.org/10.1016/j.soildyn.2017.08.026.

Bray, J. D., & Luque, R. (2017). “Seismic performance of a building affected by moderate liquefaction during the Christchurch earthquake.” Soil Dynamics and Earthquake Engineering, 102, 99-111.

Bullock, Z., Karimi, Z., Dashti, S., Porter, K., Liel, A. B., & Franke, K. W. (2018). “A physics-informed semi-empirical probabilistic model for the settlement of shallow-founded structures on liquefiable ground.” Géotechnique, 69(5), 406-419.

Bullock, Z., Dashti, S., Liel, A. B., Porter, K. A., & Karimi, Z. (2019). “Assessment Supporting the Use of Outcropping Rock Evolutionary Intensity Measures for Prediction of Liquefaction Consequences.” Earthquake Spectra, 35(4), 1899-1926.

Campbell, K.W., Bozorgnia, Y. (2011). “Predictive equations for the horizontal component of standardized cumulative absolute velocity as adapted for use in the shutdown of U.S. nuclear power plants.” Nucl Eng Des 2011; 241 (7): 2558–2569 https://doi.org/10.1016/j.nucengdes 933.2011.04.020.

Cetin, K. O., Bilge, H. T., Wu, J., Kammerer, A. M., & Seed, R. B. (2009). “Probabilistic model for the assessment of cyclically induced reconsolidation (volumetric) settlements.” Journal of Geotechnical and Geoenvironmental Engineering, 135(3), 387-398.

Cubrinovski, M., Green, R. A., Allen, J., Ashford, S., Bowman, E., Bradley, B., Cox, B., Hutchinson, T., Kavazanjian, E., Orense, R., Pender, M., Quigley, M., and Wotherspoon, L., (2010). “Geotechnical reconnaissance of the 2010 Darfield (Canterbury) earthquake.” Bulletin of the New Zealand Society for Earthquake Engineering 43 (4), 243–320.

Cubrinovski, M., Bray, J.D., Taylor, M., Giorgini, S., Bradley, B., Wotherspoon, L., Zupan, J., (2011). “Soil liquefaction effects in the central business district during the February 2011 Christchurch earthquake.” Seismol Res Lett 82(6):893–904.

Cubrinovski, M., (2013). ‘‘Liquefaction-induced damage in the 2010–2011 Christchurch (New Zealand) earthquakes.’’ Proceedings of the International Conference on Case Histories in Geotechnical Engineering. Missouri University of Science and Technology, Missouri.

Dashti, S. (2009). “Toward evaluating building performance on softened ground.” Ph.D. Dissertation, Dept. of Civil and Environmental Engineering, Univ. of California, Berkeley.

Dashti, S., Bray, J. D., Pestana, J. M., Riemer, M. R., and Wilson, D. (2010a). “Mechanisms of the seismically-induced settlement of buildings with shallow foundations on liquefiable soil.” J. Geotech. Geoenviron. Eng., 136(1), 151–164.

Dashti, S., Bray, J. D., Pestana, J. M., Riemer, M. R., and Wilson, D. (2010b). “Centrifuge testing to evaluate and mitigate liquefaction-induced building settlement mechanisms” J. Geotech. Geoenviron. Eng., 136(7), 918–929.

Dashti, S. and Bray, J.D., (2013). “Numerical simulation of building response on liquefiable sand.” J Geotech Geoenviron Eng., 139(8):1235–49.

Dobry, R., O'Rourke, T. D., & Abdoun, T. (2001). Centrifuge-Based Evaluation of Pile Foundation Response to Lateral Spreading and Mitigation Strategies: Research Progress and Accomplishments Report. In Report MCEER-01-SP01, Multidisciplinary Center for Earthquake Engineering Research (MCEER) (Vol. 2000-2001, pp. 87-101).

Ebeido, A., Elgamal A., Tokimatsu K., Akio A., (2019a). “Pile and pile group response to liquefaction-induced lateral spreading in four large-scale shake table experiments”. Journal of Geotechnical & Geoenvironmental Engineering 145(10) https://doi.org/10.1061/(ASCE)GT.1943-5606.0002142.

Ebeido, A., Elgamal, A., & Zayed, M. (2019b). "Large Scale Liquefaction-Induced Lateral Spreading Shake Table Testing at the University of California San Diego." In Geo-Congress 2019: Earthquake Engineering and Soil Dynamics (pp. 22-30). Reston, VA: American Society of Civil Engineers.

Hashash, Y.M.A., Musgrove, M.I., Harmon, J.A., Ilhan, O., Xing, G., Groholski, D.R., Phillips, C.A., and Park, D. (2020) “DEEPSOIL 7.0, User Manual”. Urbana, IL, Board of Trustees of University of Illinois at Urbana-Champaign.

Hausler, E.A. (2002) “Influence of ground improvement on settlement and liquefaction: a study based on field case history evidence and dynamic geotechnical centrifuge tests” Ph.D. Dissertation, Dept. of Civil and Natural Resources Engineering, Univ. of California Berkeley.

Henderson, D. (2013). “The Performance of House Foundations in the Canterbury earthquakes.” (Master’s thesis). University of Canterbury, August 2013, 1-448 http://ir.canterbury.ac.nz/handle/10092/8741.

Honnette, T. R. (2018). “Measuring Liquefied Residual Strength Using Full-Scale Shake Table Cyclic Simple Shear Tests.” Thesis in partial fulfillment of MS degree in Civil and Environmental Engineering, California Polytechnic State University, November.

Ishihara, K. (1985). "Stability of natural deposits during earthquakes." In Proceedings of the 11th International Conference on Soil Mechanics and Foundation Engineering, San Francisco, 12-16 AUGUST 1985. vol. 1; p. 321–376. Publication of: Balkema (AA).

Ishihara, K. and Yoshimine, M. (1992). "Evaluation of settlement in deposits following liquefaction during earthquakes." Soils and Foundations, 32(1), 173-188.

Jacobs, J.S. (2016). Full-Scale Shake Table Cyclic Simple Shear Testing of Liquefiable Soil. Thesis in partial fulfillment of MS degree in Civil and Environmental Engineering, California Polytechnic State University, January: http://digitalcommons.calpoly.edu/theses/1527/.

Jafarian, Y., Mehrzad, B., Lee, C.J., Haddad, A.H. (2017). "Centrifuge modeling of seismic foundation-soil-foundation interaction on liquefiable sand." Soil Dyn. Earthquake Eng., (97) 184-204 http://dx.doi.org/10.1016/j.soildyn.2017.03.019.

Jahed Orang, M., Bruketta, S., & Motamed, R. (2019). "Experimental Evaluation of Spatial Variability Effects on Liquefaction-Induced Settlements." Geo-Congress 2019: Earthquake Engineering and Soil Dynamics (pp. 294-303). Reston, VA: American Society of Civil Engineers.

Jahed Orang, M., Bousheri, R., Motamed, R., Prabhakaran, A., and Elgamal, A. (2020) "Large-scale Shake Table Experiment on the Performance of Helical Piles in Liquefiable Soils" In Proc, *DFI 45th Annual Conference on Deep Foundations*, Hawthorne, NJ: Deep Foundation Institute.

Karamitros, D. K., Bouckovalas, G. D., Chaloulos, Y. K., & Andrianopoulos, K. I. (2013). "Numerical analysis of liquefaction-induced bearing capacity degradation of

shallow foundations on a two-layered soil profile." Soil Dynamics and Earthquake Engineering, 44, 90-101.

Karimi, Z. and Dashti, S. (2016). "Numerical and centrifuge modeling of seismic soil-foundation-structure interaction on liquefiable ground." J Geotech Geoenviron Eng., 142(1):04015061.

Karimi, Z., & Dashti, S. (2017). "Ground motion intensity measures to evaluate II: the performance of shallow-founded structures on liquefiable ground." Earthquake spectra, 33(1), 277-298.

Karimi, Z., Dashti, S., Bullock, Z., Porter, K., & Liel, A. (2018). "Key predictors of structure settlement on liquefiable ground: a numerical parametric study." Soil Dynamics and Earthquake Engineering, 113, 286-308.

Kirkwood, P., & Dashti, S. (2018). "A centrifuge study of seismic structure-soil-structure interaction on liquefiable ground and implications for design in dense urban areas." Earthquake Spectra, 34(3), 1113-1134.

Kirkwood, P., & Dashti, S. (2019). "Influence of prefabricated vertical drains on the seismic performance of similar neighboring structures founded on liquefiable deposits.' Géotechnique, 1-15.

Liu, L., and Dobry, R. (1997). "Seismic response of shallow foundation on liquefiable sand." J. Geotech. Geoenviron. Eng., 123(6), 557–567.

Lu, C. W. (2017). "A simplified calculation method for liquefaction-induced settlement of shallow foundation." Journal of Earthquake Engineering, 21(8), 1385-1405.

Luque, R., & Bray, J. D. (2017). "Dynamic analyses of two buildings founded on liquefiable soils during the Canterbury earthquake sequence." Journal of Geotechnical and Geoenvironmental Engineering, 143(9), 04017067.

Macedo, J. and Bray J.D. (2018). "Key trends in liquefaction-induced building settlement.' J. Geotech. Geoenviron. Eng., 144(11): 04018076.

Mehrzad, b., Jafarian, Y., Lee, C.J., Haddad, A.H. (2018). "Centrifuge study into the effect of liquefaction extent on permanent settlement and seismic response of shallow foundations." Soils & Foundation, (58) 228–240.

Mirshekari, M., & Ghayoomi, M. (2017). "Centrifuge tests to assess seismic site response of partially saturated sand layers." *Soil Dynamics and Earthquake Engineering*, *94*, 254-265.

Moss, R. E., Seed, R. B., Kayen, R. E., Stewart, J. P., Der Kiureghian, A., & Cetin, K. O. (2006). "CPT-based probabilistic and deterministic assessment of in situ seismic soil liquefaction potential." Journal of Geotechnical and Geoenvironmental Engineering, 132(8), 1032-1051.

Motamed, R., Orang, M. J., Parayancode, A., & Elgamal, A. (2020). "Results of a Class C Blind Prediction Competition on the Numerical Simulation of a Large-Scale Liquefaction Shaking Table Test." In *Geo-Congress 2020: Foundations, Soil Improvement, and Erosion* (pp. 334-342). Reston, VA: American Society of Civil Engineers.

Motamed, R., & Towhata, I. (2009). “Shaking table model tests on pile groups behind quay walls subjected to lateral spreading.” Journal of Geotechnical and Geoenvironmental Engineering, 136(3), 477-489.

Motamed, R., Towhata, I., Honda, T., Tabata, K., & Abe, A. (2013). “Pile group response to liquefaction-induced lateral spreading: E-Defense large shake table test.” Soil Dyn and Earthquake Eng., 51, 35-46 http://dx.doi.org/10.1016/j.soildyn.2013.04.007.

Paramasivam, B., Dashti, S., & Liel, A. (2018). “Influence of prefabricated vertical drains on the seismic performance of structures founded on liquefiable soils.” Journal of Geotechnical and Geoenvironmental Engineering, 144(10), 04018070.

Tokimatsu, K., and Seed, H. B. (1987). “Evaluation of settlements in sands due to earthquake shaking.” J. Geotech. Eng., 10.1061/(ASCE)0733-9410(1987)113:8(861), 861–878.

Tokimatsu, K., et al., (2011). “Quick report on geotechnical problems in the 2011 Tohoku Pacific Ocean earthquake.” Research reports on earthquake engineering, CUEE, Tokyo Institute of Technology, #118, pp 21–47 (in Japanese)

Tokimatsu, K., Hino, K., Suzuki, H., Ohno, K., Tamura, S., & Suzuki, Y. (2019). “Liquefaction-induced settlement and tilting of buildings with shallow foundations based on field and laboratory observation.” Soil Dynamics and Earthquake Engineering, 124, 268-279. https://doi.org/10.1016/j.soildyn.2018.04.054.

Toth, J. A. W., and R. Motamed. (2017). “Parametric study on liquefaction-induced building settlements using 1-g shake table experiments.” In Proc., 3rd Int. Conf. on

Performance Based Design in Earthquake Geotechnical Engineering. London: International Society for Soil Mechanics and Geotechnical Engineering.

Vesic, A. S. 1973. “Analysis of ultimate loads of shallow foundations.” J. Soil Mech. Found. Div. 99 (1): 45–73.

Yasuda, S., Harada, K., Ishikawa, K., and Kanemaru, Y. (2012). “Characteristics of liquefaction in Tokyo Bay area by the 2011 Great East Japan Earthquake” Soils and Foundations, 52(5): 793-810.

Yoshimi, Y., and Tokimatsu, K. (1977). “Settlement of buildings on saturated sand during earthquakes.” Soils & Foundation, 17(1), 23–38.

Zeghal, M., & Elgamal, A. W. (1994). “Analysis of site liquefaction using earthquake records.” Journal of geotechnical engineering, 120(6), 996-1017.

Zeghal, M., Elgamal, A. W., Zeng, X., & Arulmoli, K. (1999). “Mechanism of liquefaction response in sand–silt dynamic centrifuge tests.” Soil Dynamics and Earthquake Engineering, 18(1), 71-85.

3. An Experimental Evaluation of Helical Piles as a Liquefaction-Induced Building Settlement Mitigation Measure

ABSTRACT

This study evaluates the application of helical piles to reduce liquefaction-induced foundation settlement and investigates their seismic performance in liquefiable grounds. Two large-scale shake table test series, one without mitigation and one using helical piles, were conducted using the shake table facility at the University of California, San Diego. Each model was extensively instrumented and subjected to two consistently applied shaking sequences. The experimental results indicated reduced excess pore-water pressure generation around the helical pile group, attributed mainly to the densification around the piles during installation. The foundation supported on helical piles underwent almost no foundation differential settlement and tilt. The post-shaking liquefaction-induced settlement mechanisms did not affect the helical pile foundation settlement. Although this study introduced helical piles as a reliable and highly-efficient measure to mitigate liquefaction-induced foundation tilt and settlement, the proper design and application of helical piles still needs thorough investigation due to possible amplified superstructure response.

3.1. Background

Recent examples of foundation settlement due to liquefaction illustrated widespread damage to buildings, such as in the 2011 Tohoku earthquake (Tokimatsu and Katsumata 2011) and Canterbury Earthquake Sequence (CES) in 2010 and 2011 (Bray et al. 2014). In many cases, the foundations' differential settlement and tilt even resulted in the demolition

of buildings after earthquake events (Bray et al. 2014). The cost associated with the destructive nature of liquefaction-induced effects, such as settlement and lateral spreading of the loose saturated deposits, guide the researchers to scrutinize the physics of the liquefaction phenomenon and its ground movement effects. In this regard, the liquefaction-induced foundation settlement has been categorized into three main features: volumetric-induced, shear-induced, and ejecta-induced. Each category was further sub-divided into the contributing mechanisms (Dashti et al. 2010a, b; Bray and Dashti 2014), which are briefly discussed below. The mechanisms contributing to the volumetric-induced settlement are partial drainage, sedimentation or solidification, and post-liquefaction reconsolidation. The shear-induced settlement is attributed to the partial bearing capacity failure of the foundation and soil-structure-interaction (SSI) induced ratcheting displacement near the edges of the foundation (Bray and Dashti 2014). The ejecta-induced settlement is manifested by the sand boils on the ground surface. The ground failure indices, along with the correlations between ejecta volume and foundation settlement, can be used to further quantify ejecta-induced settlement (Bray and Macedo 2017; Jahed Orang et al. 2019a). Researchers have observed that much of the foundation settlement takes place during shaking, indicating a higher contribution of shear-induced mechanisms and partial drainage due to high hydraulic transient gradients (Dashti et al. 2010a, b; Bray and Dashti 2014).

The performance of shallow foundations on top of liquefied soils has been studied through field case histories (Yoshimi and Tokimatsu 1977; Adachi et al. 1992; Cubrinovski et al. 2010, 2011; Tokimatsu and Katsumata 2011; Bray et al. 2014), shake table experiments (Kokusho 1999; Rasouli et al. 2016; Toth and Motamed 2017; Jahed Orang et al. 2019; Prabhakaran et al. 2020; Bahadori et al. 2020; Jahed Orang et al. 2021), centrifuge

tests (Lambe and Whitman 1985; Liu and Dobry 1997; Dashti et al. 2010a,b; Hayden et al. 2015; Kirkwood and Dashti 2018), and numerical simulations (Dashti and Bray 2013; Karamitros et al. 2013; Karimi and Dashti 2016; Karimi et al. 2018; Macedo and Bray 2018). These studies have investigated the controlling mechanisms of liquefaction-induced building settlement and the effects of key parameters on the overall response. Each provided insight into this complex phenomenon and contributed to current knowledge. Here, we review the current state-of-knowledge and highlight the remaining knowledge gaps.

One of the major steps in dealing with liquefaction-induced foundation damages is to provide ground improvement techniques to minimize the liquefaction-induced foundation tilt and settlement. Several studies examined various ground improvement techniques, taking into account the contributing mechanisms of liquefaction-induced settlement. Among these liquefaction mitigation measures are the use of ground densification methods (Liu and Dobry 1997; Yegian et al. 2007; Dashti et al. 2010a, b; Olarte et al. 2017; Rasouli et al. 2018); drainage methods such as using underground columns (Ashford et al. 2000; Adalier et al. 2003; Badanagki et al. 2018; Bahmanpour et al. 2019), Prefabricated Vertical Drains (PVD) (Howell et al. 2012; Olarte et al. 2017; Paramasivam et al. 2018; Kirkwood and Dashti 2019), and diagonal drains (Rasouli et al. 2018); ground bracing methods such as gravel drains (Hayden and Baez 1994; Iai et al. 1994; Adalier et al. 2003), in-ground structural walls (i.e. sheet pile walls) (Olarte et al. 2017; Rasouli et al. 2018), and soil-cement walls (Khosravi et al. 2016; Boulanger et al. 2018); microbial induced calcite precipitation (MICP) (Montoya et al. 2013; Darby et al. 2019); induced partial saturation (Eseller-Bayat et al. 2013; Mousavi and Ghayoomi 2019;

Mousavi and Ghayoomi 2021); and the use of geocomposite and geogrid reinforcement (Bahadori et al. 2020). The listed ground improvement techniques address some of the liquefaction-induced settlement mechanisms, providing varying mitigation efficiencies depending on different ground conditions and shaking intensities. In a recent study, the use of polymer injection was studied to minimize liquefaction-induced foundation settlement using large-scale shake table tests, and the results indicated the salient performance of shallow foundation in a shallow liquefiable stratum rehabilitated with synthetic polymer (Prabhakaran et al. 2020a, b). Although various methods provide some extent of efficiency in reducing foundation tilt and settlement, the cost-effectiveness and higher-order efficiencies in mitigating liquefaction-induced settlement still need further investigation.

The behavior of pile foundations in liquefied and lateral spreading grounds has been investigated through 1g shake table experiments (Motamed and Towhata 2009; Motamed et al. 2013; Ebeido et al. 2019) and centrifuge testing (Zeghal et al. 1999; Dobry et al. 2001; Abdoun et al. 2003; Boulanger et al. 2003). Amongst several types of deep foundations studied by the researchers, there is a lack of knowledge regarding the response of helical piles in the liquefiable grounds. Helical piles are one of the deep foundation elements, comprised of a number of helical plates welded to their slender steel shaft. The helical piles are mainly used to underpin shallow foundations due to their ease of installation in low headroom areas with limited access (Perko 2009). Helical piles have been reported to perform well during past earthquakes; nonetheless, the U.S. design codes do not provide details on the application of these deep foundations in high seismic areas (Cerato et al. 2017). The dynamic response of different helical piles and helical pile groups in dense dry sand has been recently examined using shake table experiments. These shake table studies

included the evaluation of several parameters, such as the effects of loading frequency and intensity, installation methods, the number of helices, pile shaft shape, and pile group damping characteristics (Elsawy et al. 2019; Jahed Orang et al. 2019b; Shahbazi et al. 2020a, b). Yet, the seismic performance of helical piles in liquefiable ground conditions and their efficiency in improved soil-pile-foundation response to liquefaction-induced settlement and tilt has not been well understood.

This study evaluates the use of helical piles as a mitigation measure against liquefaction-induced shallow foundation settlement using a series of large-scale shake table tests. The main objective is to achieve high efficiencies in reducing liquefaction-induced foundation settlement and tilt while keeping costs at a minimum. The presence of shallow liquefiable soil deposits further encouraged the use of a large-scale 1g shake table to precisely replicate ground conditions observed in recent earthquakes in Japan, New Zealand, Turkey, and the United States (Bray et al. 2004; Bray et al. 2014; Luque and Bray 2017).

3.2. Shake Table Experimental Program

Two series of shake table tests were conducted at the University of California, San Diego (UCSD) Powell Laboratory for this study. The first series of tests is referred to as the "Baseline test", and the second series is referred to as the "Helical Pile test". In the Baseline test series, no mitigation measure was applied to focus on the mechanisms controlling the response of shallow foundations on liquefiable soils. In contrast, four single-helix helical piles were used to underpin the shallow foundation against liquefaction-induced settlement in the Helical Pile test series. Each test series comprised of two shakings, "Shake 1" and "Shake 2." The main characteristics of the table motion during each shaking are

summarized in Table 3.1. Both test series featured fairly comparable table motion characteristics, although there were minor differences observed in some of the parameters. The acceleration time histories of the table motions in both shakings are presented in Figure 3.1. The test series were performed in a displacement-controlled setup, with a target input displacement history provided to the shake table controller. The achieved input acceleration time histories for Shake 1 and Shake 2 were obtained through unfiltered recordings from double integration of displacement time histories recorded by a string potentiometer connected to base of the laminar container. In the figures presented throughout this paper, dashed lines are used to represent the Baseline test results, and solid lines are used for the Helical Pile test results. As shown in Figure 3.1, the shaking scheme for both tests included 6 seconds of ramp up followed by 6 seconds of uniform motion with a constant amplitude that ceased through 3 seconds of motion tapering down (total of 15 seconds). The input motions for both Shake 1 and Shake 2 were applied at a constant frequency of 2 Hz, with the peak acceleration ranging from 0.53 *g* to 0.66 *g*. Details about ground motion selection and soil box specifications can be found in Jahed Orang et al. (2021).

Table 3.1. Ground motion parameters for the Baseline and Helical Pile test series.

Parameters	Baseline		Helical Pile	
	Shake 1	Shake 2	Shake 1	Shake 2
Achieved peak acceleration (g)	0.53	0.66	0.57	0.55
Arias intensity, I_a (m/s)	3.42	9.21	4.47	9.19
Significant duration, $D_{5\text{-}95}$ (s)	10.10	9.74	10.08	11.31
Peak Ground Velocity, PGV (cm/s)*	121.05	121.43	42.91	52.21
Cumulative Absolute Velocity, CAV (g.s)*	1.35	2.36	1.51	2.38

*For 25 seconds of recorded data

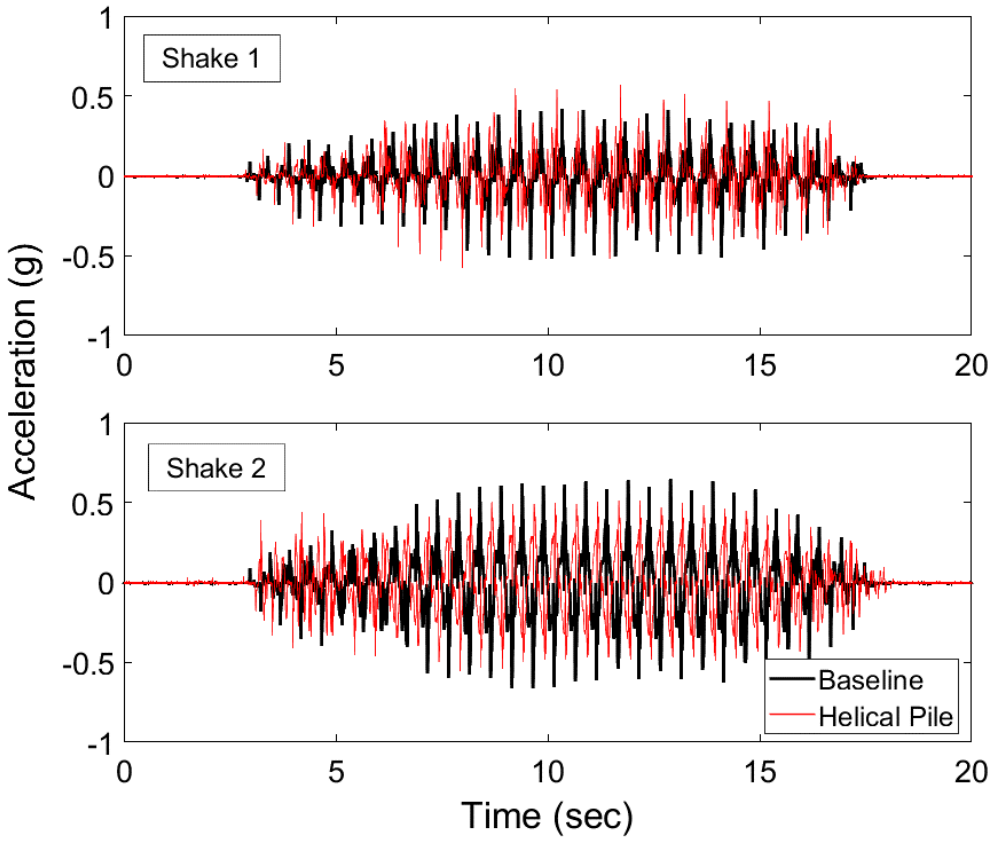

Figure 3.1. Acceleration time histories for both shakes during the Baseline and Helical Pile tests.

Figure 3.2 presents the isometric view of the Helical Pile test before Shake 1. The 2.9-m-tall laminar box was used to contain the sand and structural components inside and on top of the sandy soil medium. A total of six cameras were used to videotape all the shakings from different angles to capture the soil-foundation response. More details about ground model preparation and instrumentation, helical pile specification, protection and instrumentation, and further ground model identification were provided in the following sections. It is worth noting that the details of the Baseline test series and discussions on the controlling mechanisms of shallow foundation response on top of a liquefiable soil layer is presented in Jahed Orang et al. (2021), and this paper presents the Helical Pile test series mainly focusing on the response of helical piles and their performance in liquefied soils.

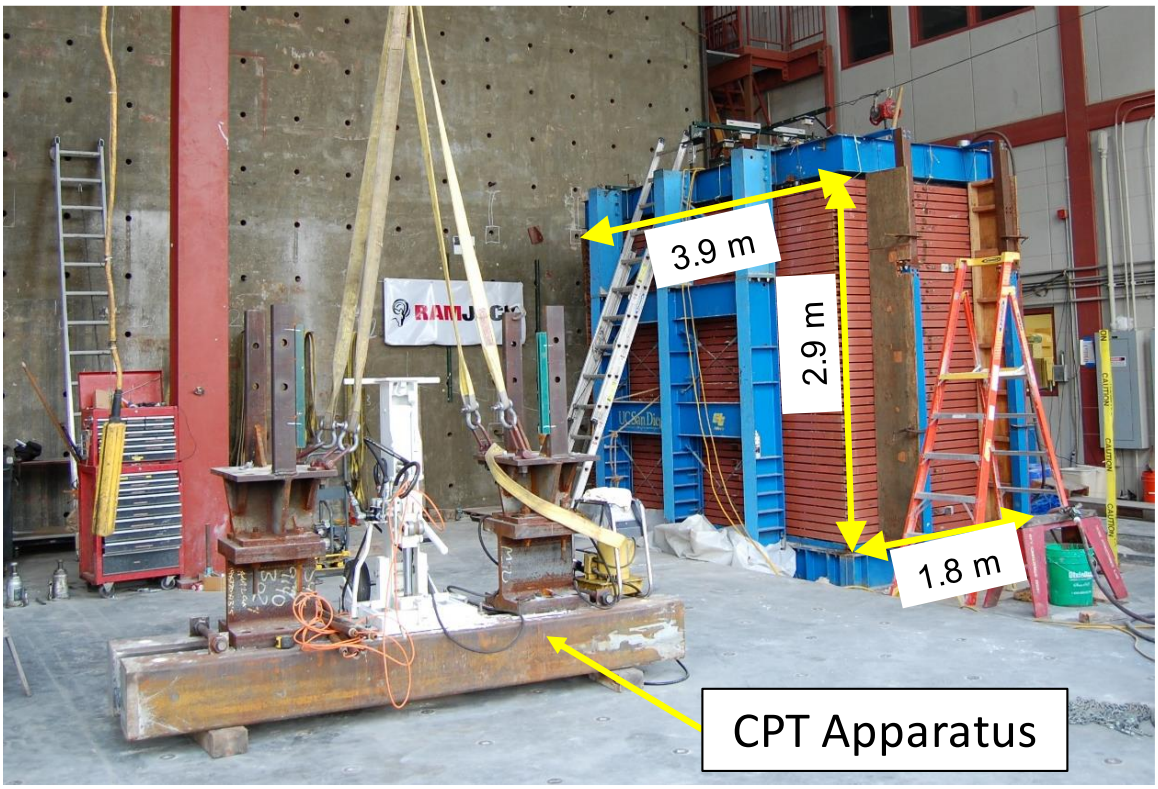

Figure 3.2. Isometric view of the Helical Pile test before Shake 1.

3.2.1. Model Ground Preparation and Instrumentation

Ottawa F-65 sand was used to build a three-layer ground model including dense, loose, and crust layers in both test series (i.e. the Baseline and Helical Pile tests). The geotechnical properties of Ottawa F-65 sand can be found in Bastidas (2016). The thickness of dense, loose, and crust layers were 1.0, 1.3, and 0.6 m, respectively. The bottom layer was constructed as a dense sand medium, overlain by loose sand deposit. Finally, a top crust layer was constructed to place the shallow foundation. The ground water level was located at the top of the liquefiable layer (i.e. 0.6 m below ground level). The achieved relative densities for dense, loose, and crust layers were in the range of 85-90%, 40-45%, and 50-55%, respectively. Details regarding the construction method and achieved relative densities for each layer can be found in Jahed Orang et al. (2021). The model ground for both Baseline and Helical Pile test series was constructed in similar conditions. Four instrumented single-helix helical piles were tied to the shallow foundation in the Helical Pile test to examine the efficiency of these deep foundation elements to mitigate liquefaction-induced settlements in shallow foundations. Details of instrumentation, strain gauge protection, and helical pile installation will be discussed in Section 3.2.2.

The shallow foundation embedded in the crust layer was 1.3 m in length, 0.6 m in width, and 0.4 m in depth. The 23 kg single weights stacked in six rows added a 3280 kg load on top of the shallow foundation (see Figure 3.3). The final foundation contact pressure was about 41.6 kPa, which replicated the contact pressure of a two-to-four story building.

Figure 3.3. Model shallow foundation and superstructure weights in the Helical Pile test.

3.2.1.1. Ground Model Instrumentation

Various instruments were utilized to capture the seismic response of the soil-pile-foundation-superstructure system. A breakdown of the instrumentation used in the Baseline and Helical Pile test series are provided in Table 3.2. A total of 150 sensors were used in the Helical Pile test series. The instrumentation layout for the Helical Pile tests is presented in Figure 3.4. A similar instrumentation plan was used in both test series, except the strain gauges, which were only used on four helical piles to examine their dynamic response in the Helical Pile tests. As illustrated in Figure 3.4, three arrays of pore-water pressure sensors and accelerometers were installed to capture the ground model response. A total of 14 string potentiometers were used to capture the lateral displacement of the laminar box. The foundation and near-foundation settlements were measured using four string and four linear potentiometers located at four corners of the foundation and the

ground model, respectively. Seven pairs of strain gauges were attached to each helical pile. Two pairs of these strain gauges were located in the dense medium, where the rest were located within the liquefiable layer. The location and spacing of the strain gauges (Figure 3.4) were designated based on pile length, type and dimensions of strain gauge protective measures, length of the helical pile guide sleeve, and depth of the loose-dense layer interface.

Table 3.2. Types and number of instrumentation used in the Baseline and Helical Pile tests.

Test / Type	Baseline	Helical Pile
Accelerometer	35	14
PCB accelerometer	28	24
Pore-water pressure sensor	47	33
String potentiometer	18	19
Linear potentiometer	6	4
Strain gauge	-	56
Total	134	150

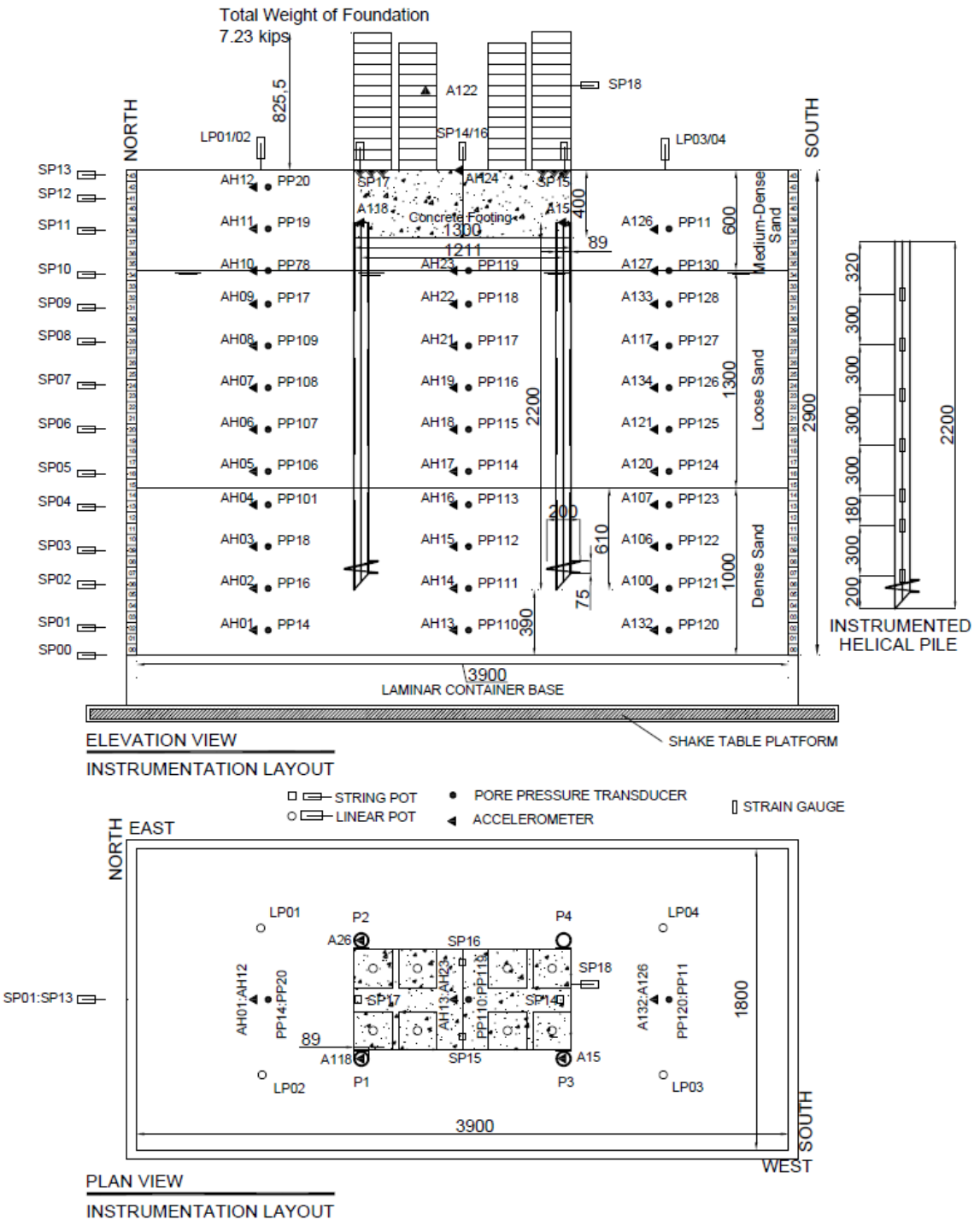

Figure 3.4. Elevation and plan view of instrumentation layout for the Helical Pile test (all dimensions are in millimeters). Helical Piles Specifications and Instrumentation

A total of four single-helix helical piles were used in the second test series (Figure 3.5a). Each of the helical piles was connected to the shallow foundation using 4021.1 side brackets (Figure 3.5c). Each side bracket was pinned to the foundation using two 1.6-cm anchor bolts (Figure 3.5b). A total of four 4021.1 side brackets with the allowable compression capacity of 162.5 kN and eight 1.6-cm anchor bolts were used in the Helical Pile tests to connect the piles to the shallow foundation. Details and specifications regarding the helical pile properties are provided in Table 3.3. More information regarding the mechanical properties of the helical piles and side brackets can be found in the ICC-ES evaluation report (ESR-1854 Ram Jack, 2017). It is also worth mentioning that there were no specific seismic design guidelines for using side brackets in the International Building Code (IBC). However, the designated side brackets performed reasonably well under specific ground motion applied in these shake table tests.

Figure 3.5. Photo of (a) single-helix helical piles (b) bolts and nuts and (c) side bracket used in the Helical Pile tests.

Table 3.3. Helical pile properties and specifications.

Property	Value (cm)
Helix pitch	7.5
Helix level below ground	240.0
Penetration into dense layer	61.0
Longitudinal pile to pile spacing	121.0 (13.50D)
Transverse pile to pile spacing	69.0 (7.75D)
Outside diameter	8.9
Wall thickness	0.5
Shaft length	220.0
Helix diameter	20.0

In the Baseline test series, the allowable static bearing capacity of the shallow foundation was calculated, yielding a factor of safety greater than three; however, the foundation underwent excessive settlement (during and after first shake), constituting an unsatisfactory performance (Jahed Orang et al. 2021). Underpinning the shallow foundation with four helical piles is expected to increase the bearing capacity and decrease the settlement, achieving an acceptable foundation performance under static and dynamic loading.

The bearing capacity of the helical piles was calculated using the individual bearing capacity method (Perko 2009):

$$Q_H = \sum A(cN_c + q'N_q + \frac{1}{2}\gamma N_\gamma) \quad (3.\ 1)$$

where N_c, N_q and N_γ are bearing capacity factors, c is soil cohesion, q' is effective overburden pressure at the bearing depth, γ is the soil unit weight, and A is the area of the helical bearing plate. The following assumptions were made in the allowable bearing capacity calculation of the helical piles:

- N_q was obtained from Hansen and Vesic bearing capacity factors (Vesic 1973).
- The friction angle of the dense sand was assumed to be 35 degrees ($\varphi = 35^\circ$).
- The effect of liquefiable layer weight was neglected in effective overburden pressure calculation.
- The factor of safety was assumed to be two ($F.S. = 2$) for each helical pile.

Based on Equation 1, the allowable capacity of each helical pile was calculated to be 16.7 kN. The pile group capacity, assuming a group efficiency of 1, was 66.8 kN. The calculated group capacity is almost twice the load exerted on the ground model through both shakes (the total load exerted to the ground model was 32.5 kN). The bearing capacity of the helical piles can be verified through torque measurements during helical pile installation, as the measured torque is correlated to the ultimate bearing capacity of the helical pile. During the helical pile installation in this study, the measured torque was affected due to the presence of a shallow liquefiable layer and relatively low thickness of the ground model compared to real site conditions. The maximum measured torque was about 0.68 kN.m, resulting in the 15.5 kN ultimate bearing capacity of a single helical pile, which was close to the estimated theoretical capacity. The calculated bearing capacity of the helical piles was further justified after both shakings, where there was no observed foundation bearing capacity failure due to the dynamic loading.

A total of 56 strain gauges (FLA 5-11-5LJC, Tokyo Sokki Kenyujo Co., Ltd) were attached to the helical piles to measure bending strain at different depths. Seven pairs of strain gauges were bonded on each helical pile at the designated depths, as illustrated in Figure 3.4. All strain gauges were connected in full-bridge configuration into the Data Acquisition system (DAQ). Various measures were adopted to protect the strain gauges from any damage during the helical pile installation. Figure 3.6 illustrates the protective measures taken to avoid damage in strain gauges during installation. First, the area around each strain gauge location was welded in a U shape (Figure 3.6a). This measure can reduce the abrasion of the strain gauges during installation. Second, all the strain gauges were guided through the 2-cm holes (Figure 3.6b) drilled on the side of each helical pile at designated depths. These holes were used to guide strain gauge wires through the inner hollow part of the helical piles. All the strain gauges were set in place before applying the adhesive material (Figure 3.6c). Third, acrylic glue was applied on top of each strain gauge, followed by a mastic tape cover for further protection (Figures 3.6d and 3.6e). Finally, wide aluminum wraps were rolled around the periphery of the designated area to further protect the strain gauges (Figure 3.6f). These protective measures ensured that a high percentage of strain gauges functioned during the Helical Pile tests, with 22 out of 28 pairs measuring quality data. The protection procedure was based on information provided by Professor Amy Cerato (University of Oklahoma), who used similar precaution procedures during a series of large-scale shake table tests on helical piles in 2015 (Cerato 2019).

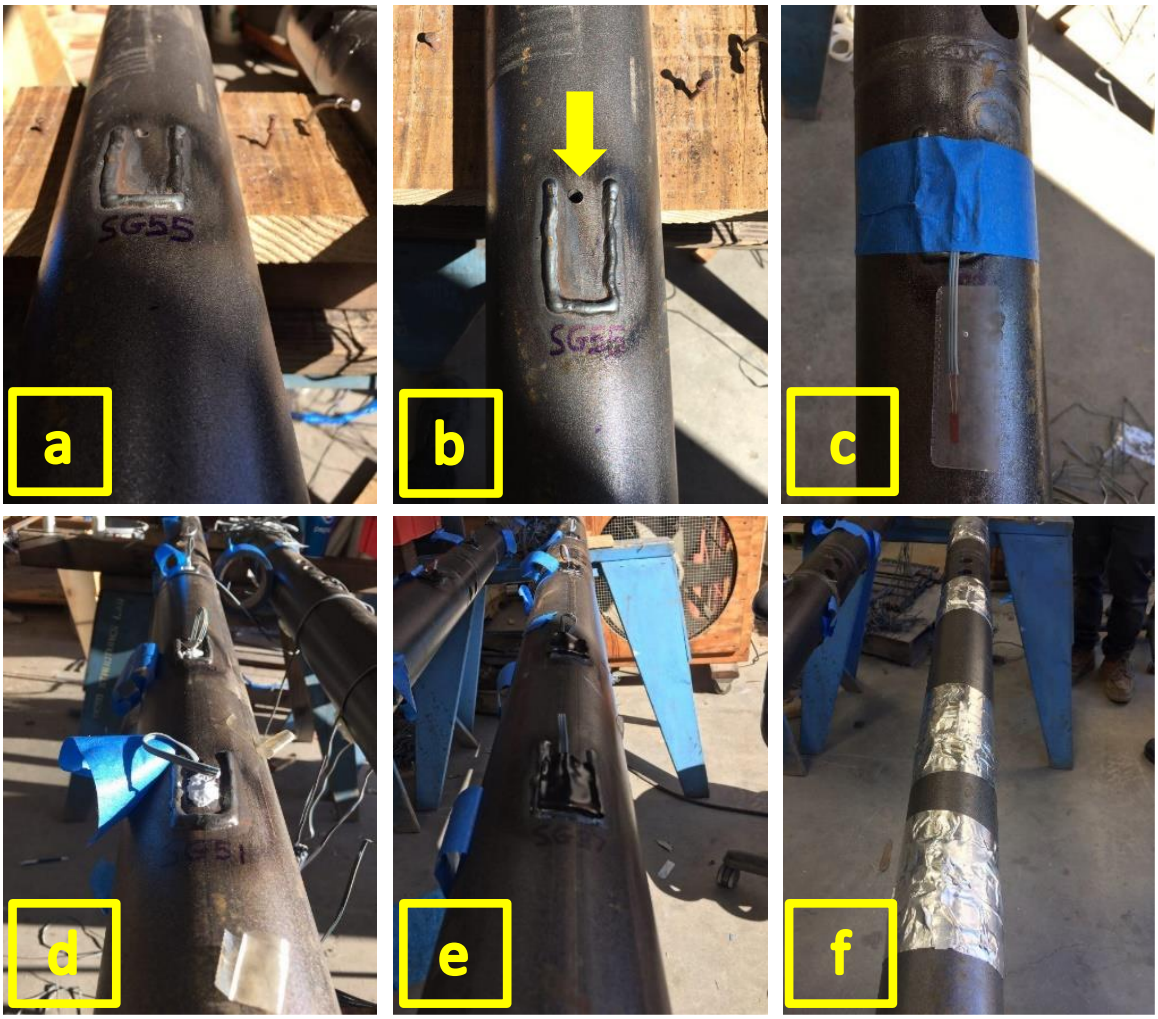

Figure 3.6. Strain gauge installation and protection measures.

3.2.2. CPT and Shear Wave Velocity Measurements

The Cone Penetration Test (CPT) was used to characterize the model soil profile before and after Shake 1 during the Helical Pile tests. Figure 3.2 illustrates the CPT apparatus used for this purpose. Two CPT soundings were obtained at each stage on the northern and southern sections of the soil box. The CPT test provided better realization of the variations in relative density of different layers, which helped to evaluate the ground model before and after each shake.

Figure 3.7 presents the measured tip resistance (q_c) along the depth of the ground model for the Helical Pile test series, along with the measured shear wave velocity (V_s) profile for the Baseline test series. PCB accelerometers were used to screen the peak-to-peak wave arrival time between two consecutive PCB accelerometers. Further details regarding the shear wave velocity measurements are provided in Jahed Orang et al. (2021). Both the tip resistance and shear wave velocity measurements before Shake 1 show an increasing trend with the increase in depth. The measured tip resistance along depth both in the northern and southern section of the ground model display increased resistance after Shake 1, especially at the dense-liquefiable layer interface (i.e. the bottom half of liquefiable and top one-third of the dense layer), indicative of increased relative density (D_r) after Shake 1 (Figure 3.7b).

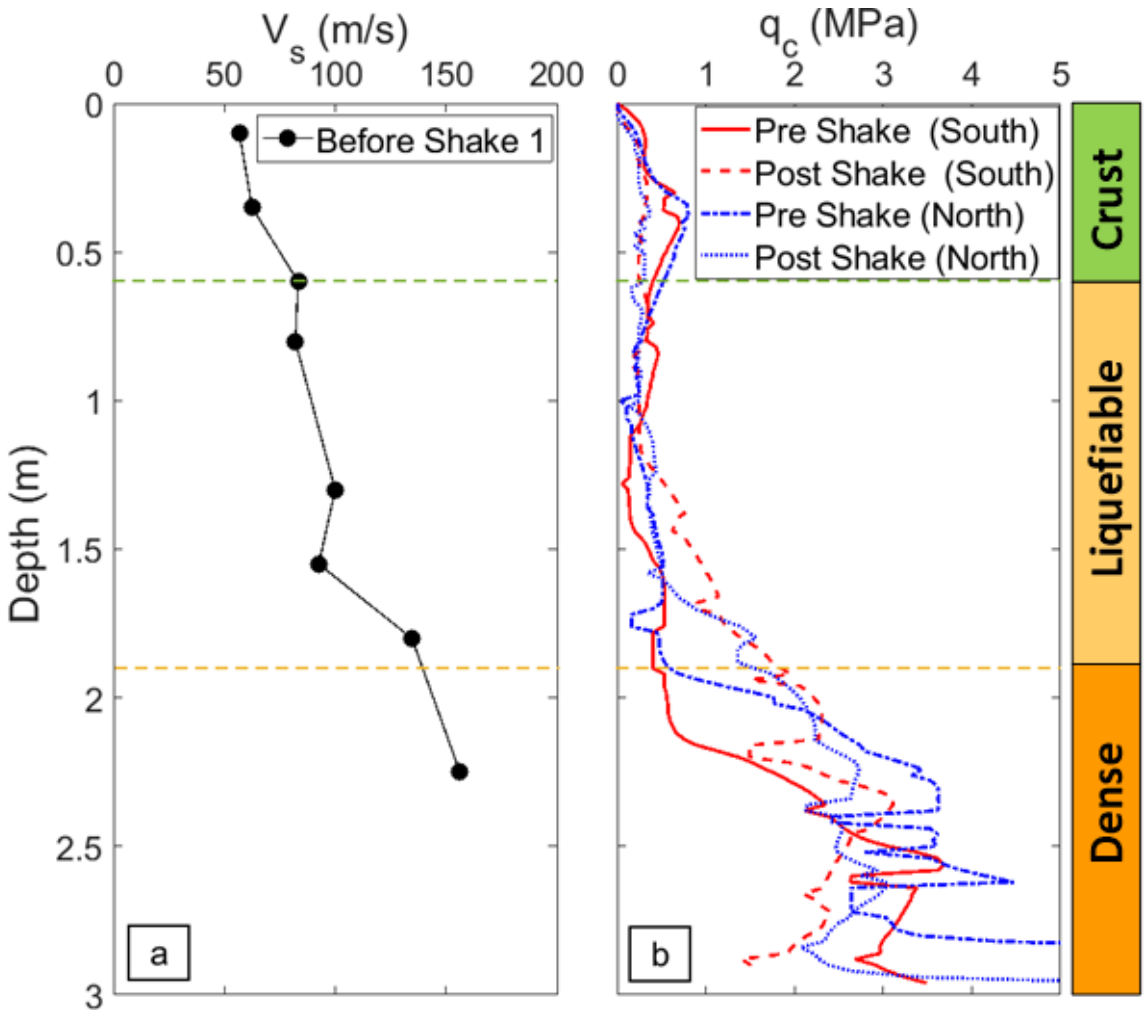

Figure 3.7. (a) Shear wave velocity (V_s) profile before Shake 1 and (b) cone penetration resistance (q_c) along depth before and after Shake 1.

3.3. Experimental Results

Measured data from two large-scale shake table test series were utilized to better understand the dynamic behavior of helical piles in liquefied soils and their efficiency in reducing liquefaction-induced shallow foundation settlement. Both test series featured similar model ground conditions and shallow foundations, with the ground model and structural components were subjected to similar input motions described earlier. The acceleration time histories measured at various locations inside the ground model within

different layers are presented in Figure 3.8. A comparison between these records illustrates a comparable response in acceleration time histories at the North and South arrays, indicating the reproduction of reasonable near-foundation conditions in both tests. Recorded accelerations at the surface exhibit two key features of liquefaction response: reductions in amplitude and period elongation. In addition, the observed higher frequency response in the below-foundation array compared to the near-foundation arrays for the Helical Pile test could be attributed to higher confinement around helical piles as a result of helical pile installation.

The extent of mitigation efficiency can be seen in Figure 3.9. Both photos were taken after Shake 1, indicating a smaller settlement and tilt of the foundation during the Helical Pile test (Figure 3.9b). Extensive cracks and near-foundation heaves, along with the punching settlement of the foundation, occurred in the Baseline test (Figure 3.9a). Detailed discussions regarding Excess Pore-water Pressure (EPWP) generation, dynamic response of the helical piles, liquefaction-induced foundation and near-foundation settlements, foundation tilt and differential settlement, and the contribution of liquefaction-induced settlement mechanisms in both the Baseline and Helical Pile tests are provided hereafter.

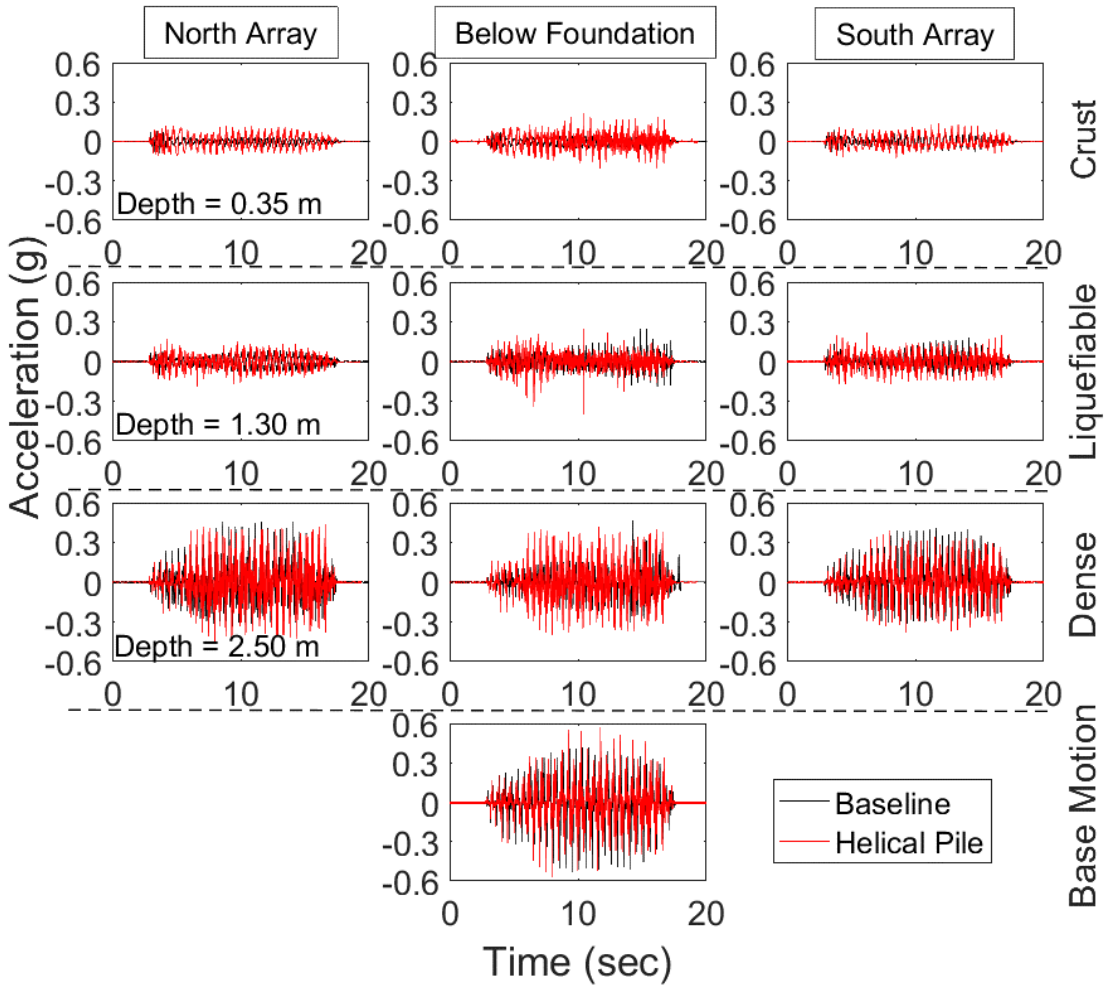

Figure 3.8. Acceleration time histories at various depths within each layer during Shake 1.

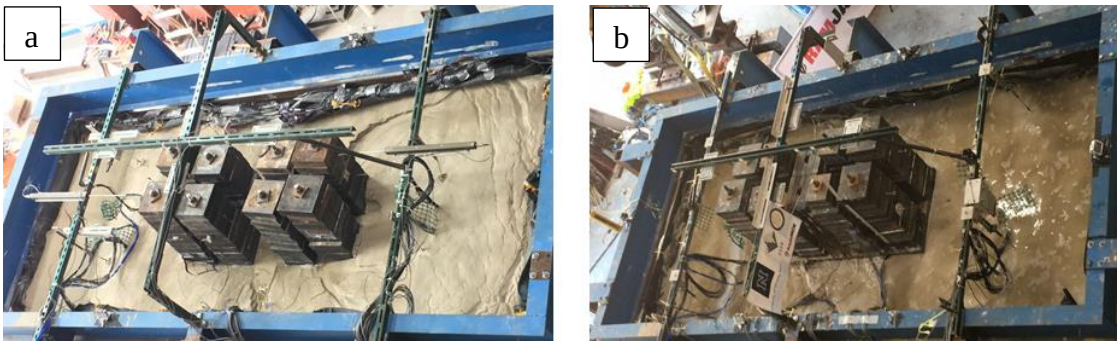

Figure 3.9. Ground model and shallow foundation after Shake 1 in (a) Baseline and (b) Helical Pile tests.

3.3.1. Excess Pore-Water Pressure Generation

The generated Excess Pore-Water Pressure (EPWP) isochrones in the near-foundation and below-foundation arrays are presented in Figure 3.10. These EPWP isochrones present time steps before, during, and after shaking for the Helical Pile test during Shake 1. As can be seen, the increase in EPWP within the dense layer continued even after shaking ceased. Moreover, the EPWP values were stabilized long after shaking (i.e. starting after t = 50 seconds) along the depth of the ground model for both the near- and below-foundation arrays. In addition to the EPWP data, Figure 3.10 includes an estimate for the initial effective vertical stresses at the two locations, illustrating the significance of the shallow foundation presence in the increased stresses at the below-foundation array (Figure 3.10b). The EPWP generation pattern within the liquefiable layer showed rapid buildup at the bottom half, which reached to a steady state as the shaking proceeded. The patterns of the pore-water pressure generation/dissipation behavior were similar in both test series. Detailed discussions regarding EPWP response in the Baseline test series can be found in Jahed Orang et al. (2021).

The EPWP contours along the depth and length of the ground model are also generated using three arrays of pore-water pressure sensors located at different depths, and are presented in Figure 3.11. The internal MATLAB interpolation function was used to determine the EPWPs around three measured arrays. The contour plots represent the Baseline and Helical Pile tests during Shake 1 and the EPWP difference between these two tests. Three different time steps were selected to present the measured EPWP at different depths. The selected time steps were the time of maximum generated EPWP, middle of shaking (i.e. t = 10.5 seconds), and long after shaking ceased (i.e. t = 80 seconds).

The observed EPWPs during the Helical Pile test were generally lower than in the corresponding Baseline test, especially inside the zone of pile group influence at the bottom of the liquefiable and top of the dense layer. This zone further extended around each pile to some extent. The EPWP difference in Figure 3.11 also illustrates higher variation around the group of helical piles. This effect is mainly attributed to the stress bulb generated around helical piles, which subsequently increased the relative density of the liquefiable layer at their zone of influence. Densification around each pile as a result of installation also could have contributed to this observation. The transferred foundation pressure through the helical piles into a more competent layer (i.e. dense layer) resulted in a higher surcharge carried through the dense layer during the Helical Pile test (this negates the reduced relative density of the dense layer due to soil disturbance around a group of helical piles), which further substantiates the observed maximum EPWP difference around the helical piles.

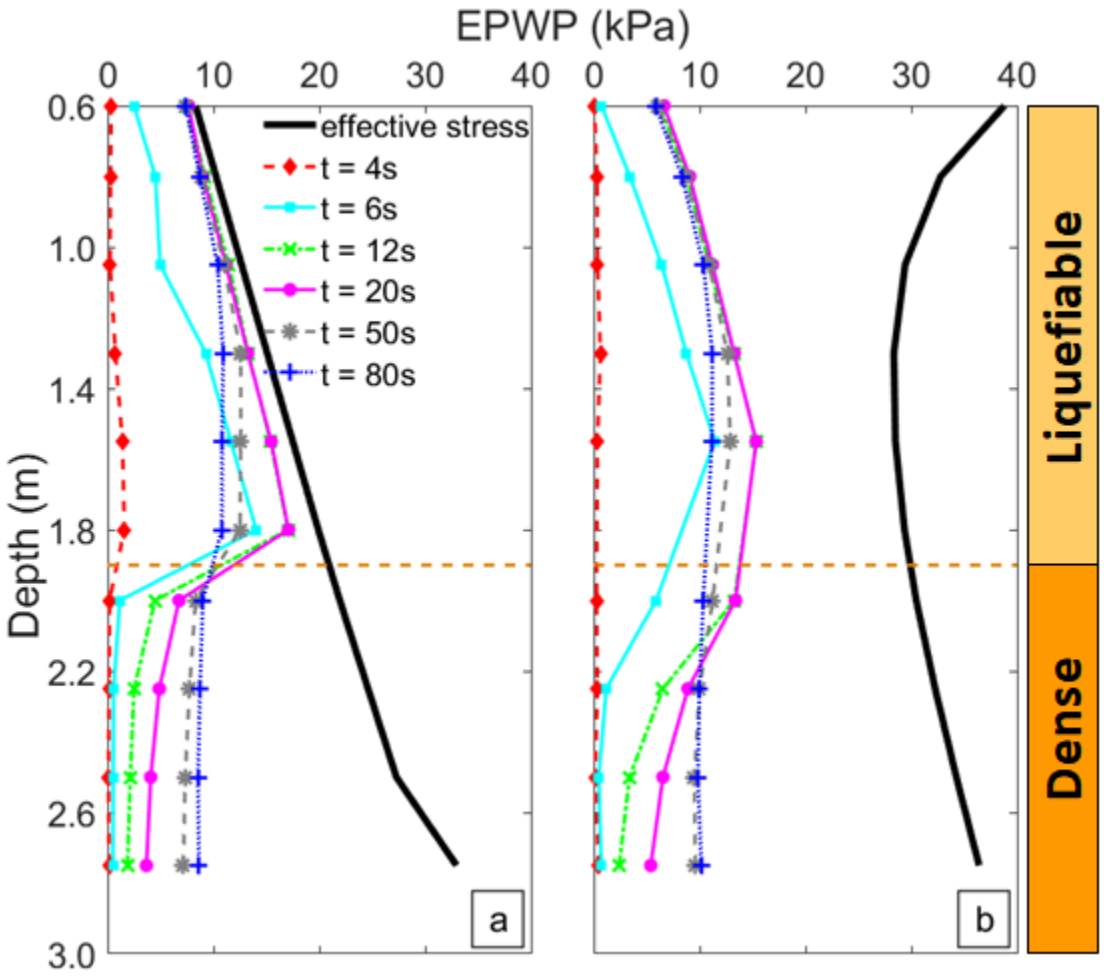

Figure 3.10. EPWP isochrones for (a) near-foundation and (b) below-foundation arrays in the Helical Pile test (Shake 1).

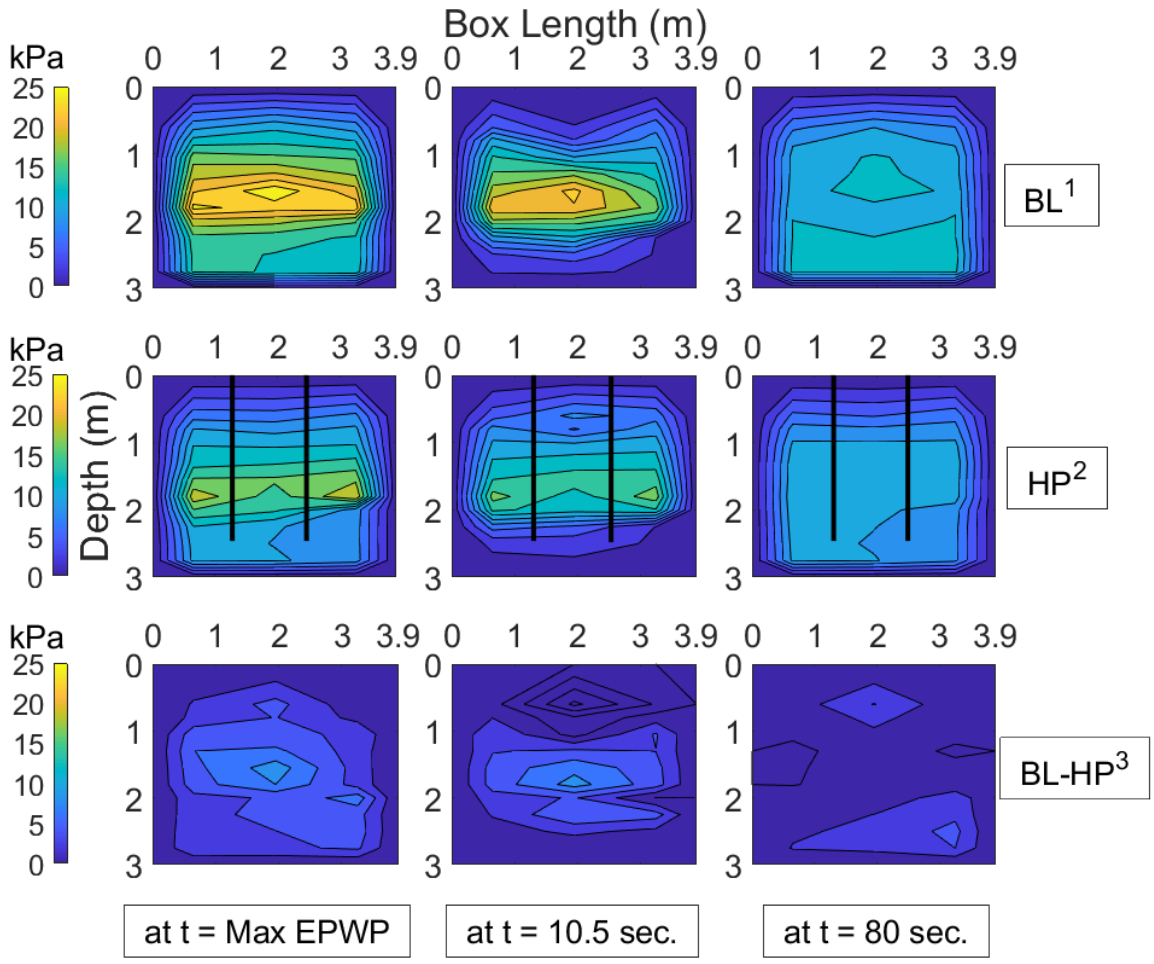

[1]Baseline test. [2]Helical Pile test. [3]EPWP difference.

Figure 3.11. EPWP difference between the Baseline and Helical Pile tests at time of maximum generated PWP, *t* = 10.5 seconds (i.e. middle of shaking) and *t* = 80 seconds (long after shaking ceased) during Shake 1.

3.3.2. Dynamic Response of Helical Piles

The bending moment along the depth of each pile was measured using the attached strain gauges and used to evaluate the dynamic response of the helical piles in this study, further discussed hereafter. The bending moment time histories were obtained using Equation 3.2,

and the bending strain data measured by strain gauges attached on the piles at different depths:

$$M = \frac{(EI)_p\,(\varepsilon_1 - \varepsilon_2)}{D} \tag{3. 2}$$

where D is the pile outer diameter, $(EI)_p$ is the bending stiffness of helical pile, and ε_1 & ε_2 are strain gauge readings at opposite sides of each pile section at their corresponding depth.

The maximum bending moments of piles at each depth were derived using the absolute maximum bending moment observed in the time histories. Figure 3.12 presents the bending moment time histories at different depths in selected helical piles during Shake 1, and Figure 3.13 exhibits the calculated maximum bending moments along depth for all the piles. Several researchers have studied the response of piles in layered soil profiles involving liquefiable soils. For example, Abdoun et al. (2003) used model steel-driven piles in a series of centrifuge tests to study their dynamic behavior in layered soil deposits. A critical observation from Abdoun et al. (2003)'s study was the maximum bending moment at the loose-dense layer interface, which is attributed to the shear discontinuity effect. This effect is mainly due to the difference in the shear stiffness of the loose and dense layers, where both layers undergo the same shear stresses, which ultimately results in the maximum bending moment at the interface of loose and dense layers (Abdoun et al. 2003). A similar response was also observed in this series of tests, where the maximum bending moments along the helical piles occurred at the interface of the liquefiable-dense layers for all the single-helix helical piles during both shaking sequences (Figure 3.13). As can be seen in Figure 3.13, all the helical piles exhibited similar responses during both shakings, which is also expected due to the similarity in the size, shape, and number of helices in all

the helical piles. Overall, the bending moments along depth during Shake 2 were generally higher, especially within the dense and lower half of the liquefiable layer compared to the measured bending moments at corresponding depths during Shake 1. This is also expected due to densification of the ground layers due to post-liquefaction consolidation discussed using the CPT tip resistance data presented in Figure 3.7b.

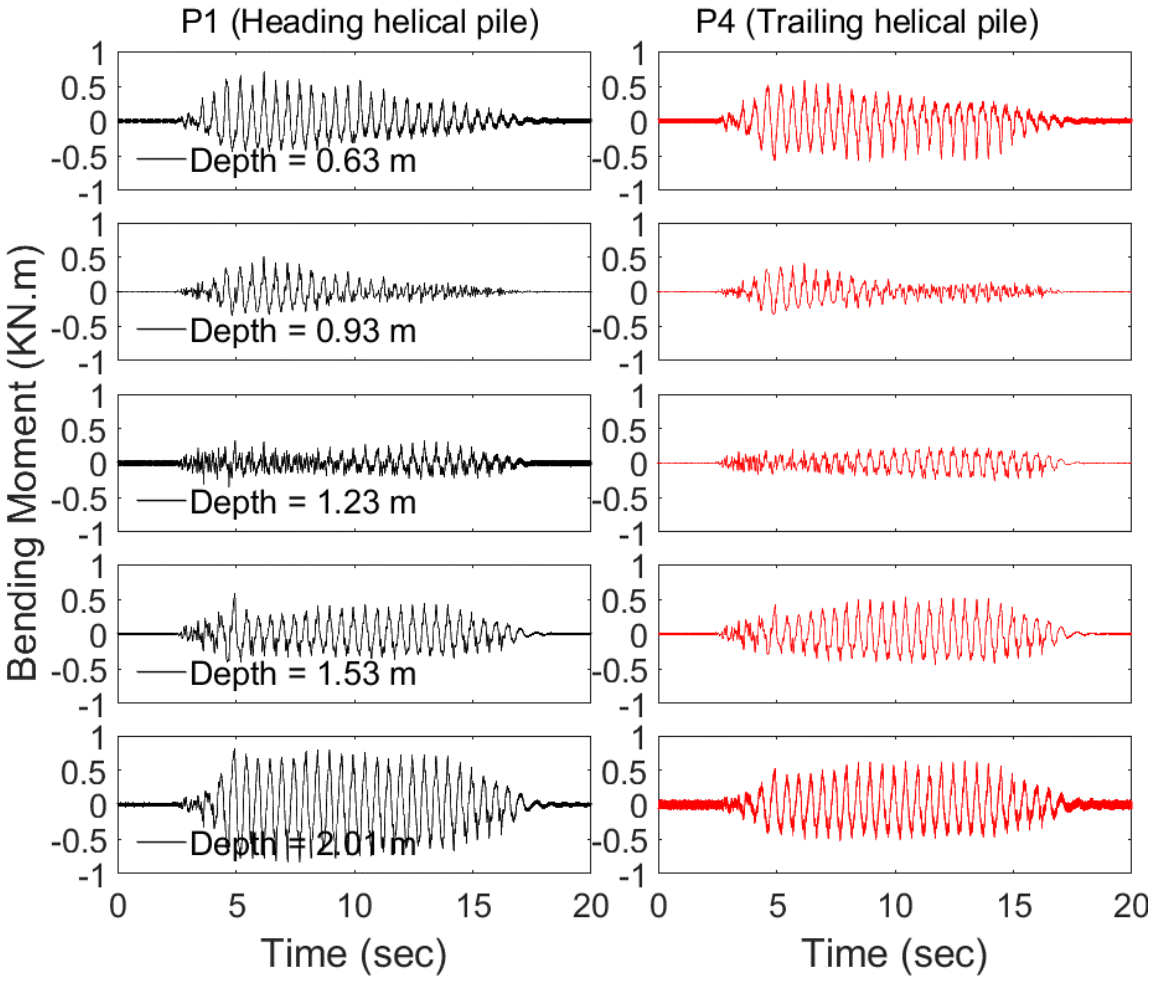

Figure 3.12. Bending moment time histories at different depths in heading (P1) and trailing (P4) helical pile.

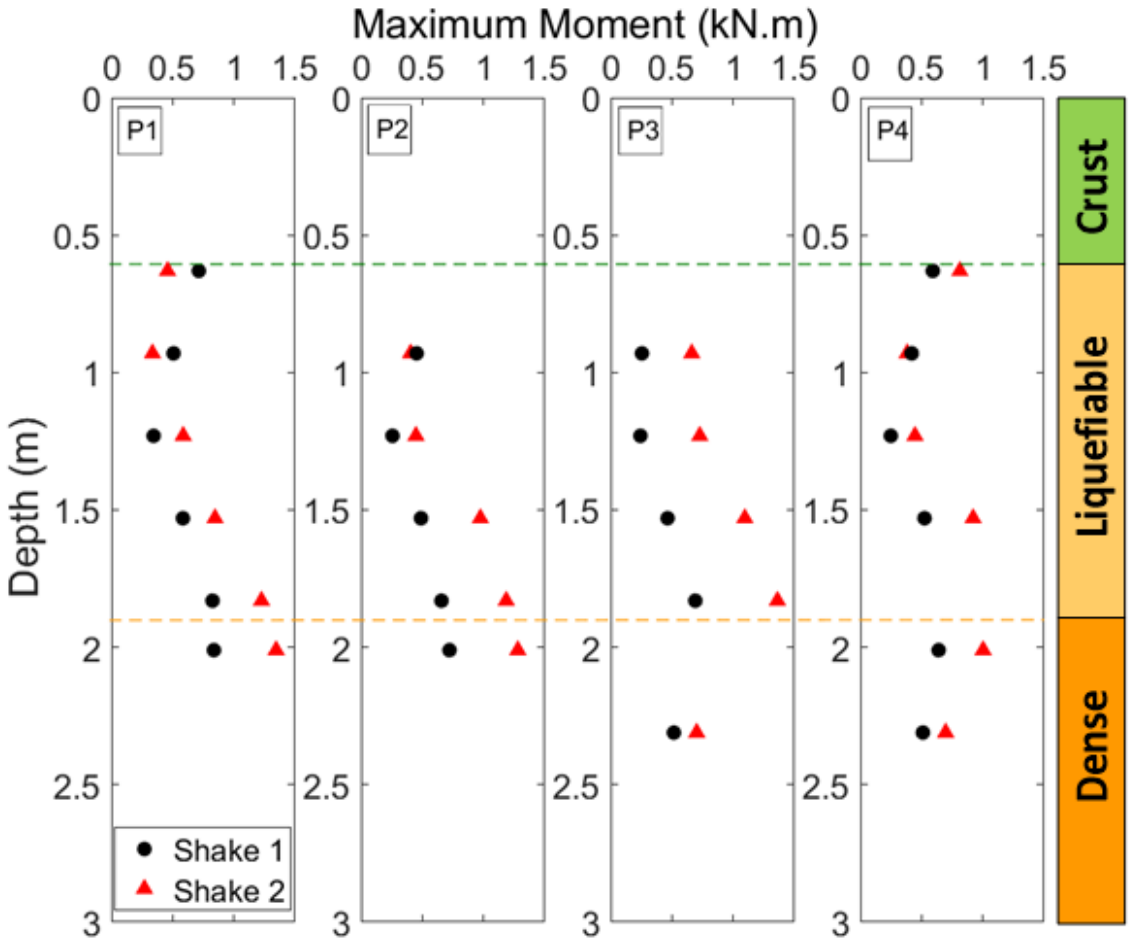

Figure 3.13. Maximum bending moment along depth for both Shake 1 and Shake 2 for all the helical piles.

3.3.3. Liquefaction-Induced Foundation and Near-Foundation Settlements

The foundation and near-foundation settlements were measured using string and linear potentiometers during both test series. Four string potentiometers were used to measure foundation settlement at four different locations shown in Figure 3.4, while four linear potentiometers were utilized to record settlement of the near-foundation ground indicated in Figure 3.4. Figure 3.14 presents the foundation settlement for both test series during Shake 1. At four different locations during the Helical Pile test, the measured foundation

settlement was almost twenty times lower than the corresponding foundation settlement in the Baseline test. Please note the different scales for the y-axes in Figure 3.14. As can be seen, there was no observed foundation settlement after the shaking ceased during the Helical Pile test, whereas there was a visible and continuous post-shaking component of liquefaction-induced foundation settlement in the Baseline test. Details of foundation and near-foundation settlements and contribution of different liquefaction-induced foundation settlement mechanisms during the Baseline test series are thoroughly discussed in Jahed Orang et al. (2021).

The measured near-foundation and foundation settlements during both shakes are summarized in Tables 3.4 and 3.5, respectively. These measured values are also illustrated in Figures 3.15a and 3.15b. The total measured settlements are divided into two categories, depending on their occurrence time (during or after shaking), and are labeled as “settlement during shaking” and “post-shaking settlement” in this study.

The total near-foundation settlements measured at four different locations presented in Table 3.4 and Figure 3.15(a) were fairly comparable for the Baseline and Helical Pile tests during Shake 2. However, higher post-shaking settlements were observed in the Baseline test compared to the Helical Pile test due to the continuous settlement even when the shaking ceased. The substantial post-shaking settlement in the Baseline test is attributed to observed sand ejecta and post-shaking consolidation of the liquefied soil layer. The latter component was absent in the Helical Pile test. The observed sand ejecta near the shallow foundation after Shake 1 in the Helical Pile test can be seen in Figure 3.16. Negative near-foundation settlement values, indicating the observed heave during the Baseline test for Shake 1 as a result of the local shear bearing capacity failure of the shallow

foundation, were caused by reduced shear strength and stiffness of the liquefiable soil during shaking and manifested as near-foundation heave at all four measuring locations (Motamed et al. 2020; Jahed Orang et al. 2021). Nonetheless, the positive near-foundation settlement values indicated settled ground conditions in the Helical Pile test, where no bearing capacity failure of the shallow foundation was observed during either shake test. The average near-foundation settlements are also tabulated in Table 3.4.

Figure 3.15b compares the foundation settlements measured during and after shaking in both test series. There was no measured post-shaking settlement of the foundation during the Helical Pile test series, since the foundation load was transferred to the bottom dense layer by the helical piles. The significant extent of foundation settlement mitigation is also illustrated in Figure 3.15b, in which the foundation settlements were reduced drastically in both shakes where helical piles were used as a countermeasure. Different liquefaction-induced settlement mechanisms contributed to the foundation and near-foundation settlements during each shake. Further discussion on the controlling mechanisms is provided in Section 3.3.5.

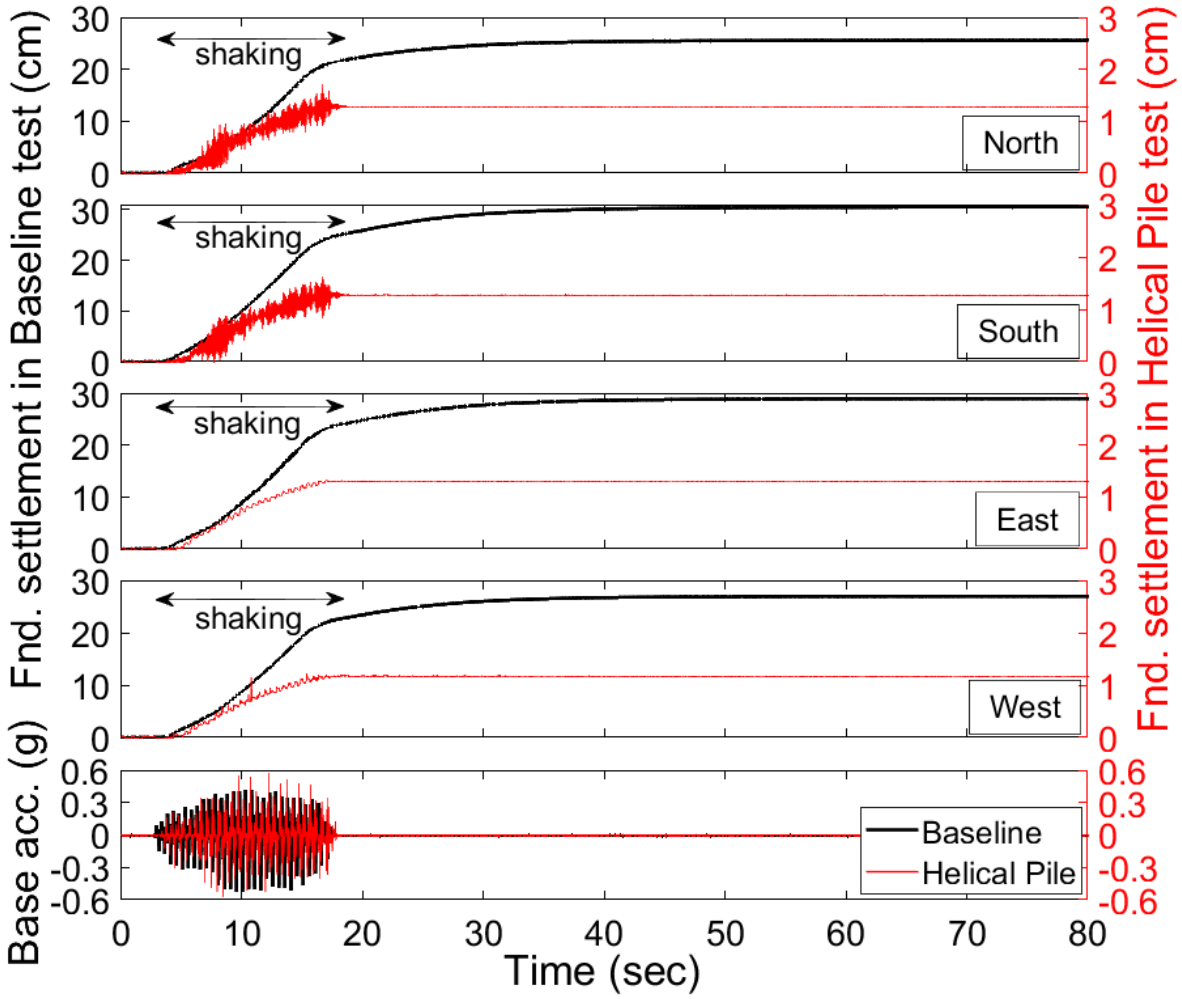

Figure 3.14. Foundation settlement at four different locations during Shake 1.

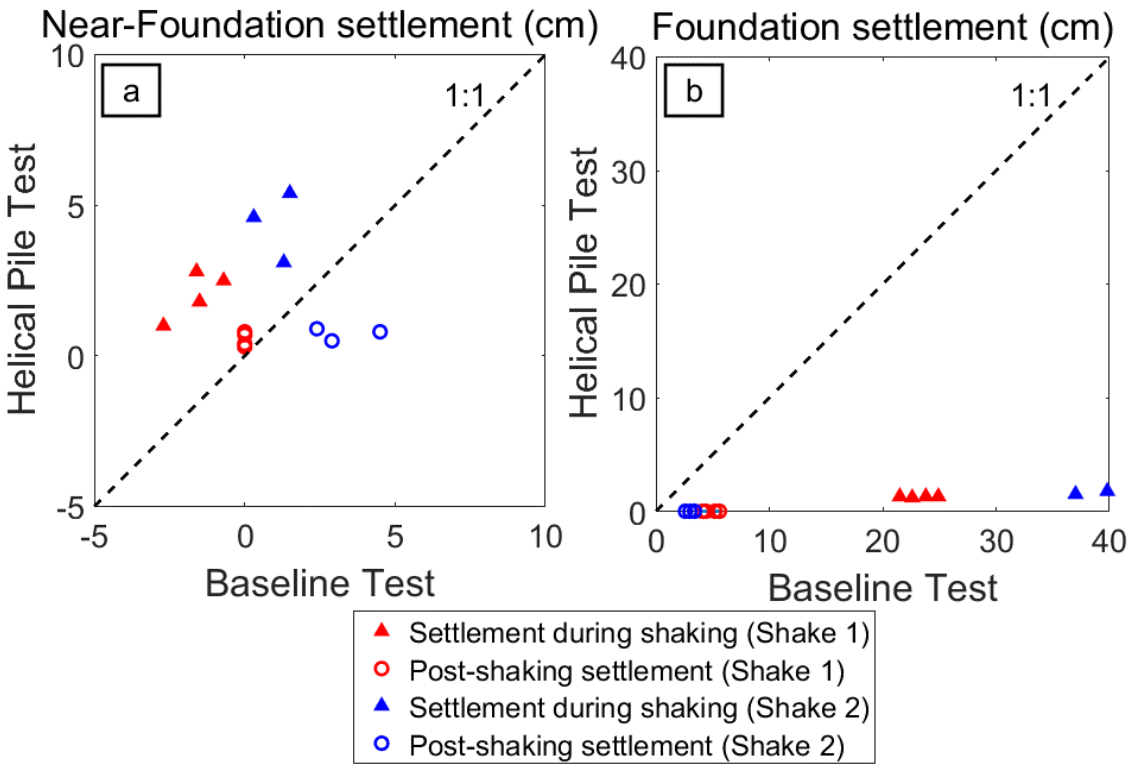

Figure 3.15. (a) Near-Foundation and (b) foundation settlement during the Baseline and Helical Pile tests for both Shakes 1 & 2.

Figure 3.16. Observed sand ejecta in both (a) eastern and (b) western side of the soil box in the Helical Pile test after Shake 1.

Table 3.4. Near-foundation settlements in the Baseline and Helical Pile tests for both Shakes 1 & 2.

	Total settlement (cm)				Settlement during shaking (cm)				Post-shaking settlement (cm)			
Test	Baseline*		Helical Pile		Baseline		Helical Pile		Baseline		Helical Pile	
Shake No.	1	2	1	2	1	2	1	2	1	2	1	2
Northeast	-1.6	6.0	3.6	6.2	-1.6	1.5	2.8	5.4	0.0	4.5	0.8	0.8
Northwest	-2.7	4.2	1.3	-	-2.7	1.3	1	-	0.0	2.9	0.3	-
Southeast	-1.5	2.7	2.2	3.6	-1.5	0.3	1.8	3.1	0.0	2.4	0.4	0.5
Southwest	-0.7	-	3.2	5.5	-0.7	-	2.5	4.6	0.0	-	0.7	0.9
Average	-1.6	4.3	2.6	5.1	-1.6	1.0	2.0	4.4	0.0	3.3	0.6	0.7

*negative values indicate heave

Table 3.5. Foundation settlements in the Baseline and Helical Pile tests for both Shakes 1 & 2.

	Total settlement (cm)				Settlement during shaking (cm)				Post-shaking settlement (cm)			
Test	Baseline		Helical Pile		Baseline		Helical Pile		Baseline		Helical Pile	
Shake No.	1	2	1	2	1	2	1	2	1	2	1	2
North	25.6	42.8	1.3	1.8	21.5	39.8	1.3	1.76	4.1	3.0	0.0	0.0
South	30.5	45.7	1.3	-	24.9	42.3	1.3	-	5.6	3.4	0.0	0.0
East	29.0	-	1.3	1.7	23.8	-	1.3	1.7	5.2	-	0.0	0.0
West	27.0	39.6	1.2	1.5	22.6	37.0	1.2	1.5	4.4	2.6	0.0	0.0
Avg	28.0	42.7	1.26	1.67	23.2	39.7	1.26	1.67	4.8	3.0	0.0	0.0

3.3.4. Foundation Tilt and Differential Settlement

In this study, the performance of helical piles was assessed to examine their efficiency in minimizing the adverse effects on superstructures as a result of liquefaction-induced foundation movements. As a result, the settlement-rotation response of the foundation during the Baseline and Helical pile tests were evaluated and are presented in Figure 3.17. As can be seen, the tilt of the foundation in the Helical Pile test was measured to be very small during both shakes, with the residual value of almost zero. However, the measured residual foundation rotation in the Baseline tests were 0.038 radians (2.2 degrees) and 0.022 radians (1.3 degrees), respectively. The maximum foundation rotation during the

second shake in the Baseline test was 0.026 radians (1.5 degrees), as shown in Figure 3.17. In addition, the rate of tilt accumulation was higher during Shake 1 compared to Shake 2 in the Baseline tests, as illustrated in Figure 3.17, with a steeper response in Shake 1. Overall, the use of helical piles provided a robust integrity to the shallow foundation and impeded foundation movements including settlement and tilt during the liquefaction phenomenon.

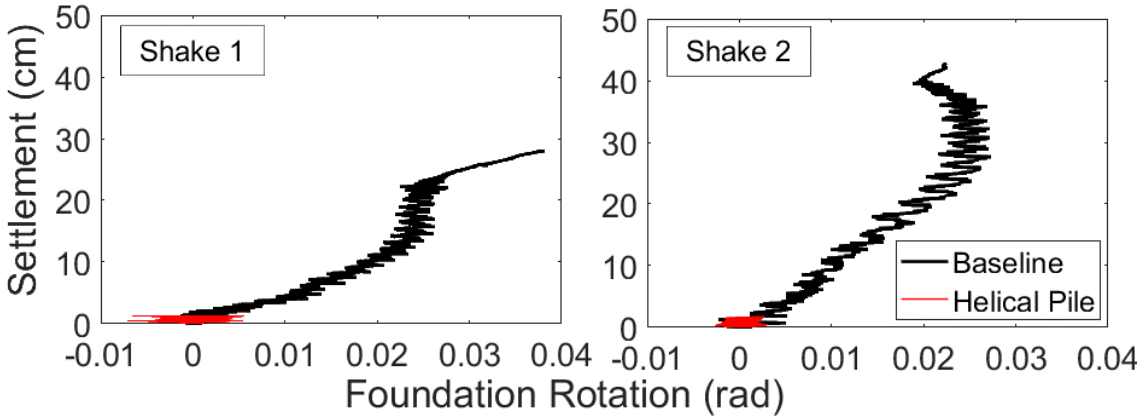

Figure 3.17. Settlement-rotation of the shallow foundation during the Baseline and Helical Pile tests.

In-plane and out-of-plane differential settlements of the foundation are illustrated in Figure 3.18. The ground motion was applied in the North-South direction along the laminar soil box during both test series. The amount of in-plane and out-of-plane differential settlements in the Baseline tests were 4.9 and 2.0 cm, respectively; however, the use of helical piles merely compensated the foundation differential settlement in both directions. These observations, along with the negligible measured foundation tilt, verified the improved performance of the shallow foundation underpinned with helical piles in liquefiable ground conditions.

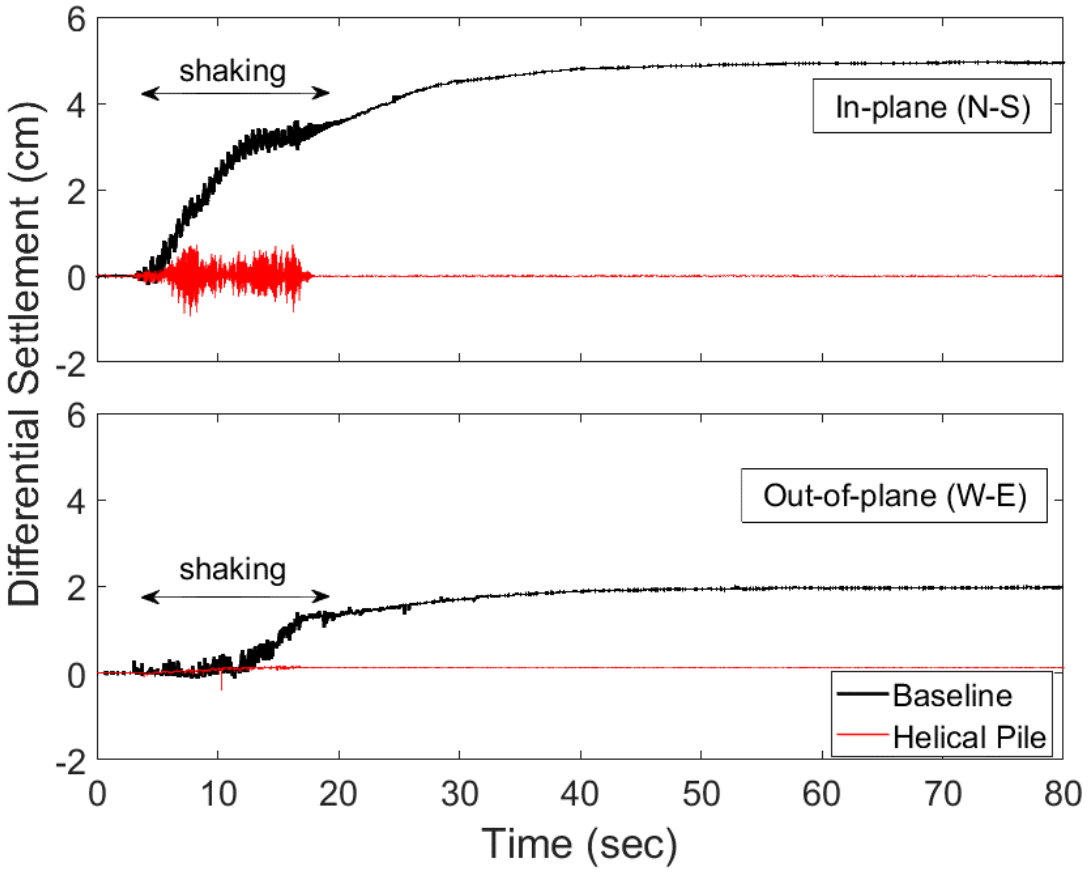

Figure 3.18. In-plane and out-of-plane differential settlement during the Baseline and Helical Pile tests (Shake 1).

3.3.5. Discussion on the Contributing Settlement Mechanisms

As presented in the Background Section, liquefaction-induced foundation settlement mechanisms are categorized as (1) volumetric-induced, (2) shear-induced, and (3) ejecta-induced. Each of these mechanisms contributes to the foundation settlement during and after shaking. Figure 3.19 demonstrates the average foundation settlement during both shakes in the Baseline and Helical Pile tests. These average settlements were obtained from four string potentiometer measurements presented earlier in Table 3.5. The improved performance of the shallow foundation during the Helical Pile test during both shakes can

be seen in Figure 3.19: a significant reduction in the foundation settlement (96% on average) was achieved, demonstrating the efficiency of using helical piles to mitigate liquefaction-induced shallow foundation settlements.

The contribution of liquefaction-induced settlement mechanisms was evaluated during both test series using the presented time histories in Figure 3.19. All the listed settlement mechanisms contributed to the foundation settlement during the Baseline tests, as discussed hereafter. The settlement of the foundation during shaking is attributed to the shear-induced mechanism (including SSI ratcheting and partial bearing capacity failure), as well as the high hydraulic transient gradients. Although this mechanism existed in both the Baseline and Helical Pile tests, its magnitude was significantly higher in the Baseline tests, resulting in 23.2 cm and 39.7 cm of settlement during Shake 1 and 2, respectively. The corresponding numbers in the Helical Pile tests were 1.3 cm and 1.7 cm, illustrating 95% reduction on average. The observed mitigation in the foundation settlement during the Helical Pile tests (Figure 3.19, solid lines) indicated a significant reduction in the contribution of these two mechanisms, coupled with the exclusion of foundation bearing capacity failure as a result of helical piles. Comparison between the rates of settlement accumulation between the two tests (i.e. the average rate of settlement during Shake1 in the Baseline and Helical Pile tests were 1.5 cm/s and 0.08 cm/s, respectively) further substantiates the effectiveness of helical piles to mitigate liquefaction-induced damage.

The post-shaking settlement mechanisms included ejecta-induced and volumetric-induced settlement (excluding the high hydraulic transient gradients), where the contribution of these mechanisms after shaking ceased is illustrated in Figure 3.19. During the Baseline tests, the shallow foundation continued to settle up to 4.8 cm and 3.0 cm after

Shake 1 and 2, respectively. These numbers indicate a smaller post-shaking settlement accumulation compared to the shaking phase in the Baseline tests. In contrast, the use of helical piles resulted in practically no observed foundation settlement after both shakings ceased. This observation indicates that the post-shaking settlement mechanisms were eliminated in the Helical Pile tests.

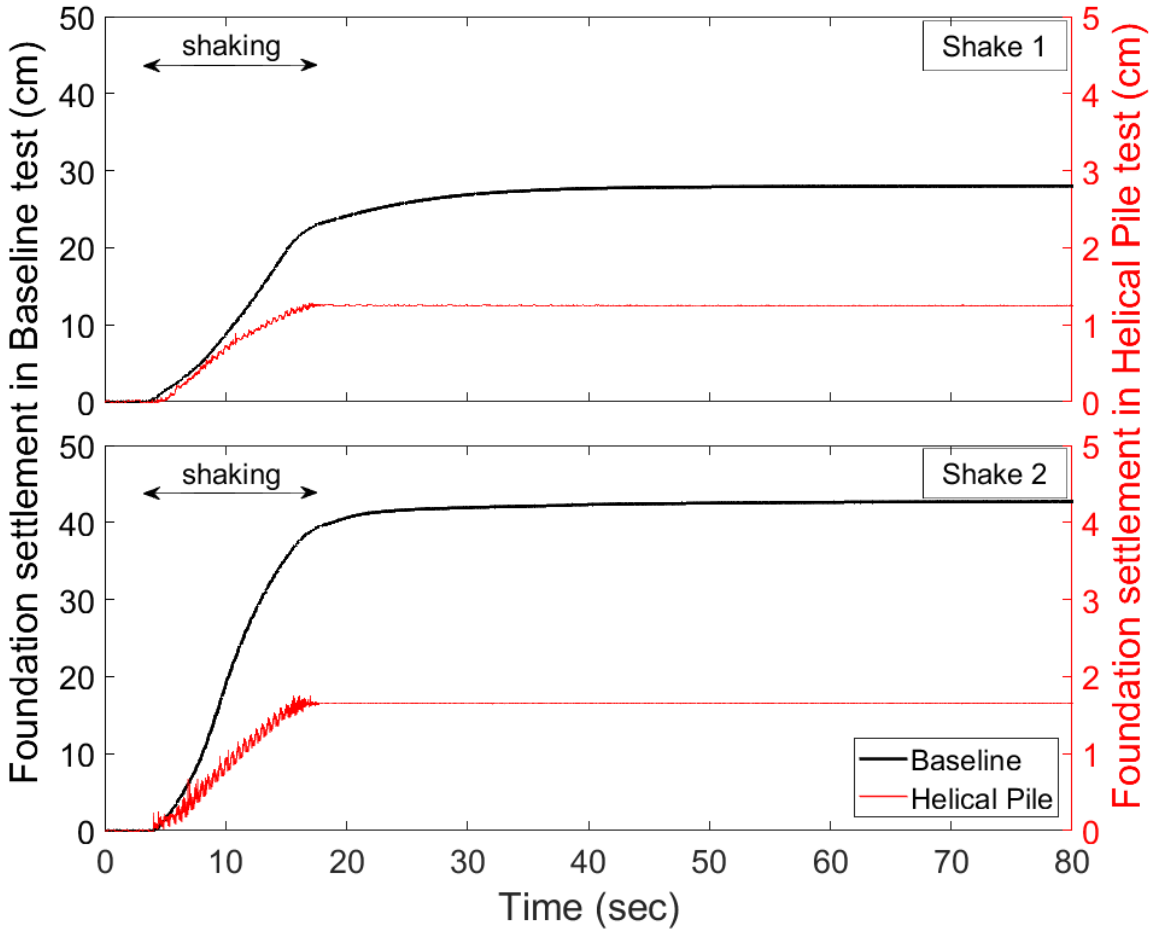

Figure 3.19. Average foundation settlement in the Baseline and Helical Pile tests.

3.4. Efficiency Evaluation of Different Mitigation Measures

3.4.1. Settlement Mitigation Efficiency (SME)

The application of various liquefaction mitigation techniques was already discussed in Section 3.1. Figure 3.20 illustrates the Settlement Mitigation Efficiency (SME) of different ground improvement methods including stone columns (Adalier et al. 2003), densification (Olarte et al. 2017; Rasouli et al. 2018), Prefabricated Vertical Drains (PVD) (Olarte et al. 2017), structural walls (Olarte et al. 2017; Rasouli et al. 2018), along with the use of helical piles (this study) to mitigate liquefaction-induced foundation settlement. The measured foundation settlements (S_f) were normalized with respect to the liquefiable layer thickness (H_L) for all the provided data sets in Figure 3.20. The SME is defined as the foundation settlement difference between the baseline and mitigated test divided by the baseline foundation settlement. As presented in Figure 3.20, the previous liquefaction mitigation methods resulted in lower efficiency as the S_f / H_L increased; however, the use of helical piles provided high efficiency regardless of the S_f / H_L calculation. The largest SME achieved in the previous research reached 67%, whereas the application of helical piles yielded 96% SME on average, which was substantially higher than other methods.

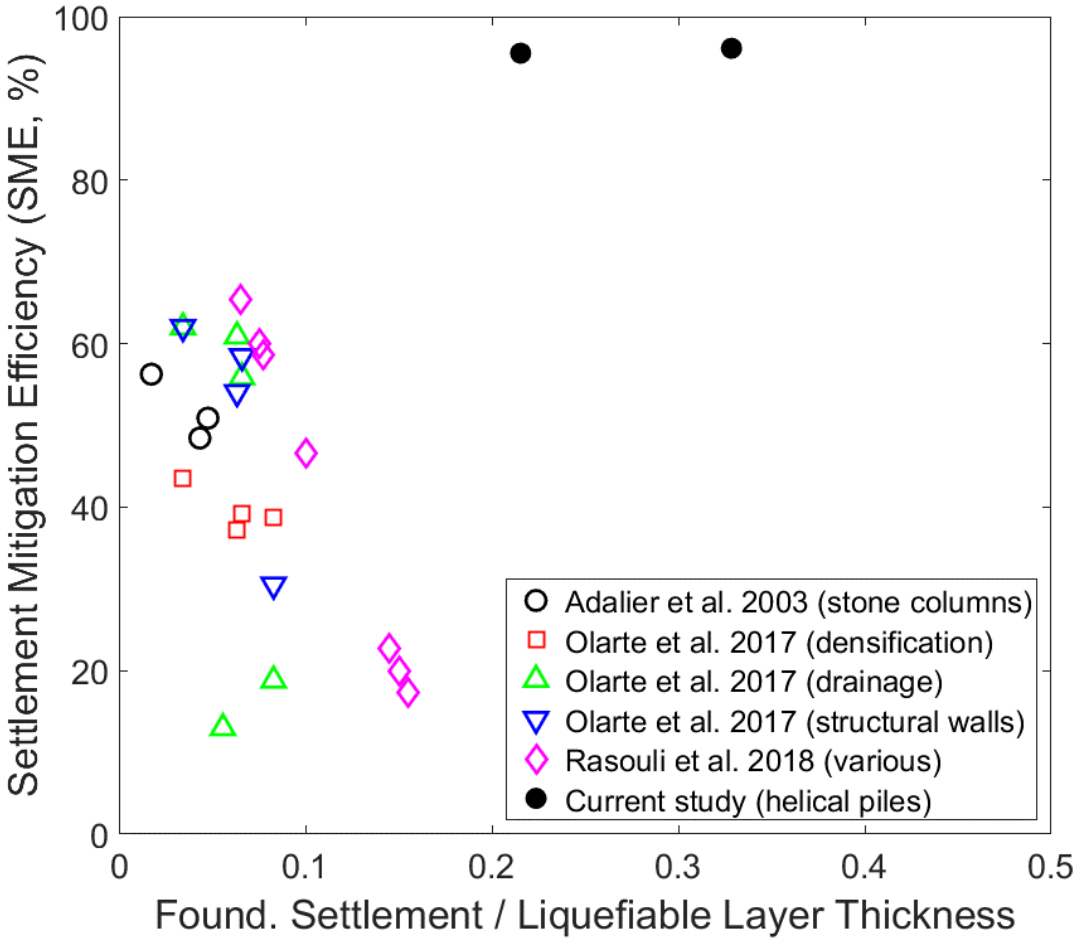

Figure 3.20. Settlement mitigation efficiency versus normalized foundation settlement for different mitigation measures in liquefaction-induced foundation settlement.

3.4.2. Tilting Mitigation Efficiency (TME)

Tilting of the foundations as a result of liquefaction is one of the important aspects to be considered when evaluating the efficiency of a selected liquefaction mitigation methodology. Figure 3.21 presents the Tilting Mitigation Efficiency (TME) of these ground improvement approaches. The higher embedment depth will result in higher restraint against foundation rocking and tilting. Thus, the rotation of the foundation due to liquefaction normalized with the ratio of embedment depth to foundation width (i.e. Arctan

(D_f / B)). The use of various methods under different test conditions can also result in negative TMEs, which indicates an increase in the foundation tilt compared to the baseline test and an insufficient performance (Figure 3.21). The use of helical piles resulted in 99% TME on average, exhibiting a satisfactory efficiency amongst all other methods. The significantly improved performance of the shallow foundation was observed consistently during both shakes. This series of large-scale shake table experiments substantiated the state-of-the-practice information on the salient performance of helical piles in the liquefiable ground by providing high settlement and rotation mitigation efficiencies.

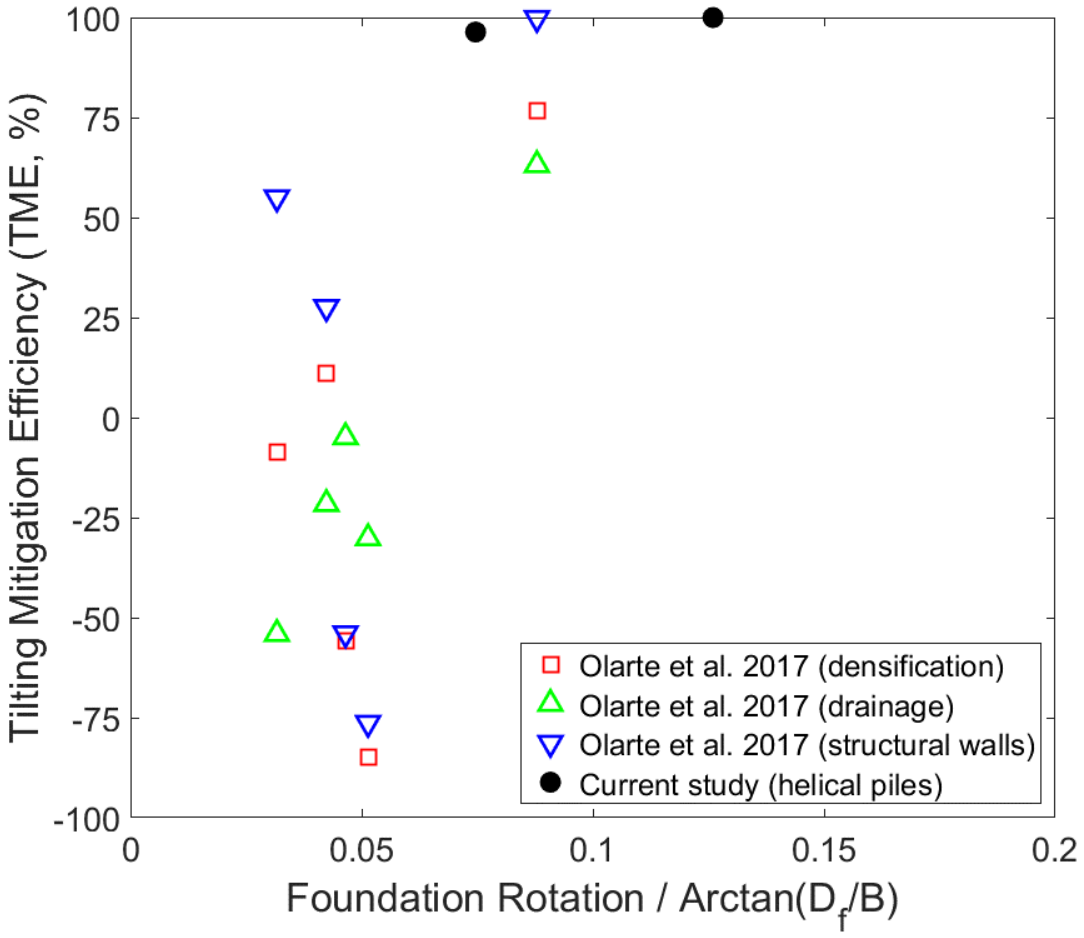

Figure 3.21. Tilting mitigation efficiency versus normalized foundation rotation for different mitigation measures in liquefaction-induced foundation rotation.

3.4.3. Influence of Helical Piles on the Superstructure Response

The implementation of different ground improvement techniques can increase the structural demand due to the amplified superstructure response. The tradeoff between liquefaction mitigation measures and the corresponding increase in structural demand should be considered when exploring different mitigation strategies (Olarte et al. 2017). In this series of shake table tests, the target foundation contact pressure was replicated using several steel plates on top of the foundation to simulate the superstructure response. The measured acceleration and lateral displacement of the shallow foundation can provide insight into the superstructure response, considering the rigid nature of the model superstructure used in the experiments. The response acceleration time histories on top of the foundation were measured during Shake 1 for both tests (Figure 3.22). According to Figure 3.22, the comparison between the recorded foundation motions in the Baseline and Helical pile tests shows an increased amplitude in the acceleration time history in the Helical Pile test, which is further manifested at short periods in the transfer function and amplification factor plots as well. This increase in the structural response at short periods in the Helical Pile test implies the subsequent increase in the structural demand due to the use of helical piles. The increased response intensity in the Helical Pile test was mainly evident at short periods (i.e. T = 0.1- 0.3 sec).

Figure 3.22 further illustrates the calculated transfer functions for the Baseline and Helical Pile tests, along with the code-based recommended transfer function (ASCE 41-17), which has been developed for buildings with shallow embedded foundations. The transfer functions for both tests are fairly consistent with the code-based transfer function from the comparison plots. Moreover, the higher variability within the transfer function

in the Helical Pile test confirms the increase in the structural demand, especially in shorter periods (i.e. around T = 0.1 sec). This can be attributed to a stiffer response of the soil-pile-foundation system in the Helical Pile test. This observation further highlights the importance of short period structural response when helical piles were used to mitigate liquefaction-induced settlement. Thus, care should be taken considering the use of any liquefaction mitigation measures that can alter the soil-foundation system's stiffness due to higher superstructure demand, along with their settlement and tilting mitigation efficiencies.

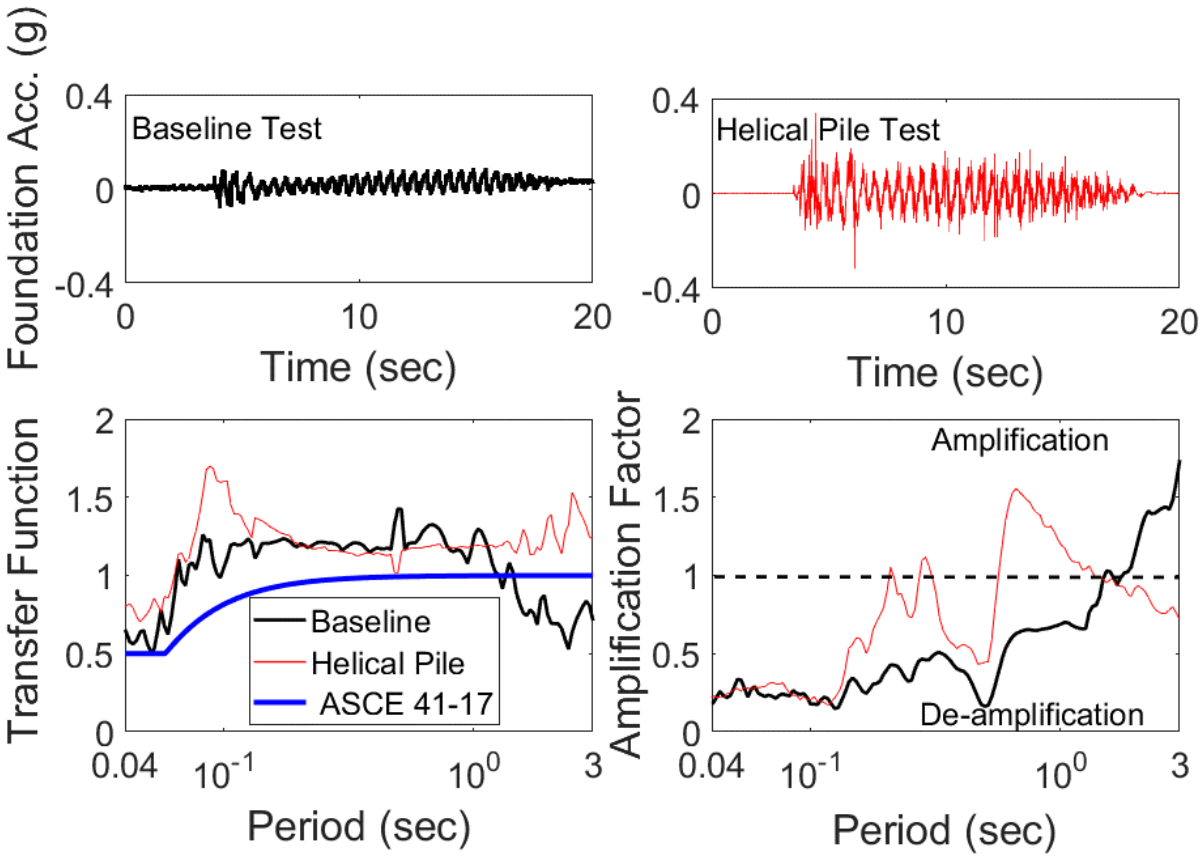

Figure 3.22. Comparison between foundation acceleration time histories, transfer functions, and amplification factors in the Baseline and Helical Pile tests during Shake 1.

3.5. Concluding Remarks

In this study, the performance of a group of helical piles in liquefied ground was evaluated in a series of large-scale shake table tests. Two test series (one without any mitigation and one using helical piles as a mitigation measure) with similar ground conditions and input motions, but with different soil-foundation response characteristics, were designed to examine the dynamic behavior of helical piles and the effectiveness of using these deep foundation elements in reducing liquefaction-induced foundation settlement and tilt.

The EPWP isochrones indicated a uniform pore-water pressure pattern along the depth of the ground model long after shaking terminated. The EPWP contour plots at different time steps indicated reduced EPWP generation in the Helical Pile test. The extent of EPWP reduction was more significant in the zone of helical pile influence at the top of the dense layer and the bottom of the liquefiable layer. The densification of the area around helical piles, with the changes in the load-carrying patterns of the coupled pile-foundation-ground model system in the Helical Pile test, explains the observed EPWP difference between the two test series.

The high functionality of strain gauges was achieved by implementing various protective measures on the strain gauges. The bending moments obtained through the measured bending strains along the depth of the ground model were used further to investigate the dynamic response of the single-helix helical piles. All the helical piles showed a similar trend in their bending moment response in both shakings. The higher bending moment difference between the two shakes was observed at the bottom half of the liquefiable layer. The highest bending moment at all of the helical piles observed at the

loose-dense layer interface was similar to the observation in the steel- driven piles in layered deposits (i.e. shear discontinuity effect).

The measured near-foundation settlements were comparable in both test series during Shake 2, whereas excessive heave was observed in the near-foundation ground due to bearing capacity failure of the unsupported shallow foundation in the Baseline test during Shake 1. A higher portion of the foundation settlement took place during shakings in both the Baseline and Helical Pile tests; however, the foundation supported by helical piles did not experience any settlement after both shakings. The use of helical piles resulted in almost no measured differential settlement and tilt of the foundation.

The observed foundation settlement accumulation in both test series shed light on the contribution of different liquefaction-induced settlement mechanisms. The only contributing mechanisms of the foundation settlement during the Helical Pile tests were transient high-hydraulic gradients and SSI ratcheting during shakings. During each shake, the settlement accumulation rate was significantly reduced using a group of helical piles to support the shallow foundation. The contribution of ejecta-induced and volumetric-induced (except high hydraulic transient gradients) components of foundation settlement were substantially reduced during the Helical Pile tests.

Comparing different mitigation techniques indicated the salient performance of helical piles in reducing settlement and tilt of the shallow foundation. Considering the differences in testing conditions, including the type of physical model test, simulated ground model, structural model characteristics, and input motions, the highest settlement and tilting mitigation efficiencies (i.e. SME and TME) were achieved using the four single-helix helical piles in shallow liquefiable deposits. Nonetheless, measured acceleration time

histories, along with the calculated transfer functions in both tests, indicated amplified response due to increased stiffness of the soil-pile-foundation system in the Helical Pile test. This study, combined with previous research, suggests a holistic approach in examining the efficiency of different liquefaction-mitigation measures considering the increased demand for the superstructure.

This series of large-scale shake table tests provided valuable insight into the efficiency of helical piles as a reliable countermeasure in liquefaction-induced foundation settlement and rotation. The results of this study were obtained using large-scale shake table tests on a specific ground condition, foundation contact pressure, and input motion characteristics. Caution should be taken in a real built-environment, since any change or combined variation of these factors can ultimately affect the performance of helical piles in liquefiable grounds.

3.6. References

Abdoun, T., Dobry, R., O'Rourke, T. D., & Goh, S. H. (2003). "Pile response to lateral spreads: centrifuge modeling." Journal of Geotechnical and Geoenvironmental engineering, 129(10), 869-878.

Adachi, T., Iwai, S., Yasui, M., and Sato, Y. (1992). "Settlement and inclination of reinforced concrete buildings in Dagupan City due to liquefaction during 1990 Philippine earthquake" Proc. 10th World Conference on Earthquake Engineering, Vol. 2, A.A. Balkema Rotterdam, The Netherlands, 147-152.

Adalier, K., Elgamal, A., Meneses, J., & Baez, J. I. (2003). "Stone columns as liquefaction countermeasure in non-plastic silty soils." Soil Dynamics and Earthquake Engineering, 23(7), 571-584.

American Society of Civil Engineers, & Structural Engineering Institute. (2017). Seismic evaluation and retrofit of existing buildings: ASCE/SEI, 41-17.

Ashford, S. A., Rollins, K. M., Bradford, S. C., Weaver, T. J., and Baez, J. I. (2000). "Liquefaction mitigation using stone columns around deep foundations: Full scale test results." Transp. Res. Rec., 1736, 110–118.

Badanagki, M., Dashti, S., & Kirkwood, P. (2018). "Influence of dense granular columns on the performance of level and gently sloping liquefiable sites." Journal of Geotechnical and Geoenvironmental Engineering, 144(9), 04018065.

Bahadori, H., Motamedi, H., Hasheminezhad, A., Motamed, R. (2020). "Shaking table tests on shallow foundations over geocomposite and geogrid-reinforced liquefiable soils." Soil Dyn Earthq Eng 2020; 128:105896. https://doi.org/10.1016/j.soildyn.2019.105896.

Bahmanpour, A., Towhata, I., Sakr, M., Mahmoud, M., Yamamoto, Y., & Yamada, S. (2019). “The effect of underground columns on the mitigation of liquefaction in shaking table model experiments.” Soil Dynamics and Earthquake Engineering, 116, 15-30.

Bastidas, A. M. P. (2016). "Ottawa F-65 Sand Characterization," PhD Dissertation, University of California Davis.

Boulanger, R. W., Khosravi, M., Khosravi, A., and Wilson, D. W. (2018). “Remediation of liquefaction effects for an embankment using soil-cement walls: Centrifuge and numerical modeling.” Soil Dynamics and Earthquake Engineering, 114(2018), 38-50, 10.1016/j.soildyn.2018.07.001.

Boulanger, R. W., Kutter, B. L., Brandenberg, S. J., Singh, P., & Chang, D. (2003). “Pile foundations in liquefied and laterally spreading ground during earthquakes: centrifuge experiments & analyses.” (No. UCD/CGM-03/01). Center for Geotechnical Modeling, Department of Civil and Environmental Engineering, University of California, Davis, California.

Bray, J. D., R. B. Sancio, H.T. Durgunoglu, A. Onalp, T. L. Youd, J. P. Stewart, R. B. Seed, O.K. Cetin, E. Bol, M. B. Baturay, C. Christensen, and T. Karadayilar. (2004). “Subsurface characterization at ground failure sites in Adapazari, Turkey,” Journal of Geotechnical and Geoenvironmental Engineering, ASCE, Vol. 130, No. 7, pp. 673-685.

Bray, J. D., Cubrinovski, M., Zupan, J., & Taylor, M. (2014). “Liquefaction effects on buildings in the central business district of Christchurch.” Earthquake Spectra, 30(1), 85-109.

Bray, J. D. and Dashti, S. (2014). “Liquefaction-induced building movements.” Bulletin Earthquake Engineering, 12, 1129-1156.

Bray, J. D. & Macedo, J. (2017). “6th Ishihara lecture: Simplified Procedure for estimating liquefaction-induced building settlement.” Soil Dyn. Earthquake Eng., (102) 215-231 http://dx.doi.org/10.1016/j.soildyn.2017.08.026.

Cerato, A.B., Vargas, T.M. & Allred S.M. (2017). “A critical review: state of knowledge in seismic behavior of helical piles.” The Journal of the Deep Foundation Institute 11(1): 39-87.

Cerato, A. (2019). “discussions on how to instrument helical piles in large-scale testing” personal communication.

Cubrinovski, M., Green, R. A., Allen, J., Ashford, S., Bowman, E., Bradley, B., Cox, B., Hutchinson, T., Kavazanjian, E., Orense, R., Pender, M., Quigley, M., and Wotherspoon, L. (2010). “Geotechnical reconnaissance of the 2010 Darfield (Canterbury) earthquake.” Bulletin of the New Zealand Society for Earthquake Engineering 43 (4), 243–320.

Cubrinovski, M., Bray, J.D., Taylor, M., Giorgini, S., Bradley, B., Wotherspoon, L., Zupan, J. (2011). “Soil liquefaction effects in the central business district during the February 2011 Christchurch earthquake.” Seismol Res Lett 82(6):893–904.

Darby, K. M., Hernandez, G. L., DeJong, J. T., Boulanger, R. W., Gomez, M. G., & Wilson, D. W. (2019). “Centrifuge model testing of liquefaction mitigation via microbially induced calcite precipitation.” *Journal of Geotechnical and Geoenvironmental Engineering*, *145*(10), 04019084.

Dashti, S., Bray, J. D., Pestana, J. M., Riemer, M. R., and Wilson, D. (2010a). "Mechanisms of the seismically-induced settlement of buildings with shallow foundations on liquefiable soil." J. Geotech. Geoenviron. Eng., 136(1), 151–164.

Dashti, S., Bray, J. D., Pestana, J. M., Riemer, M. R., and Wilson, D. (2010b). "Centrifuge testing to evaluate and mitigate liquefaction-induced building settlement mechanisms." J. Geotech. Geoenviron. Eng., 136(7), 918–929.

Dashti, S. and Bray, J.D. (2013). "Numerical simulation of building response on liquefiable sand." J Geotech Geoenviron Eng., 139(8):1235–49.

Dobry, R., O'Rourke, T. D., & Abdoun, T. (2001). "Centrifuge-Based Evaluation of Pile Foundation Response to Lateral Spreading and Mitigation Strategies: Research Progress and Accomplishments Report." In Report MCEER-01-SP01, Multidisciplinary Center for Earthquake Engineering Research (MCEER) (Vol. 2000-2001, pp. 87-101).

Ebeido, A., Elgamal A., Tokimatsu K., Akio A. (2019). "Pile and Pile Group Response to Liquefaction -Induced Lateral Spreading in Four Large-Scale Shake Table Experiments." Journal of Geotechnical & Geoenvironmental Engineering 145(10) https://doi.org/10.1061/(ASCE)GT.1943-5606.0002142.

Elsawy, M.K., El Naggar, M.H., Cerato, A., & Elgamal, A. (2019). "Seismic performance of helical piles in dry sand from large-scale shaking table tests." Géotechnique, 69(12), 1071-1085.

Eseller-Bayat, E., Gokyer, S., Yegian, M.K., Alshawabkeh., A. (2013). "Liquefaction Response of Partially Saturated Sands: An Empirical Model." ASCE Journal of Geotechnical and Geoenvironmental Engineering, 139(6), 2013, 872-879

Hayden RF, Baez JI. (1994). “State of practice for liquefaction mitigation in North America.” In: Proceedings of international workshop on remedial treatment of liquefiable soils. Tsukuba City, Japan: Public Works Research Institute.

Hayden, C. P., Zupan, J. D., Bray, J. D., Allmond, J. D., & Kutter, B. L. (2015). “Centrifuge tests of adjacent mat-supported buildings affected by liquefaction.” *Journal of Geotechnical and Geoenvironmental Engineering*, *141*(3), 04014118.

Howell R, Rathje EM, Kamai R, Boulanger R. (2012). “Centrifuge modeling of prefabricated vertical drains for liquefaction remediation.” J Geotech Geoenviron Eng 138(3):262‑71.

Iai S, Matsunaga Y, Morita T, Miyata M, Sakurai, H, Oishi, H, et al. (1994). “Effects of remedial measures against liquefaction at 1993 Kushiro-Oki earthquake.” In: Proceedings of 5th U.S-Japan workshop on earthquake resistant design of lifeline facilities and countermeasures against soil liquefaction. Technical Rep. NCEER-94-0026.

ICC-ES report, (2017). RAM JACK foundation and driven foundation systems. ICC Evaluation Service, LLC, ESR-1854.

Jahed Orang, M., Bruketta, S., & Motamed, R. (2019a). “Experimental Evaluation of Spatial Variability Effects on Liquefaction-Induced Settlements.” Geo-Congress 2019: Earthquake Engineering and Soil Dynamics (pp. 294-303). Reston, VA: American Society of Civil Engineers.

Jahed Orang, M., Toth, J., and Motamed, R. (2019b). “Experimental evaluation of dynamic response of helical piles in dry sand using 1g shaking table tests.” VII International

Conference on Earthquake Geotechnical Engineering (7ICEGE), Roma, Italy, 17-20 June 2019, pp 4226-4234.

Jahed Orang, M., Bousheri, R., Motamed, R., Prabhakaran, A., and Elgamal, A. (2020). "Large-scale Shake Table Experiment on the Performance of Helical Piles in Liquefiable Soils" In Proc, *DFI 45th Annual Conference on Deep Foundations*, Hawthorne, NJ: Deep Foundation Institute.

Jahed Orang, M., Motamed, R., Prabhakaran, A., & Elgamal, A. (2021). "Large-Scale Shake Table Tests on a Shallow Foundation in Liquefiable Soils." Journal of Geotechnical and Geoenvironmental Engineering, 147(1), 04020152.

Karamitros, D. K., Bouckovalas, G. D., Chaloulos, Y. K., & Andrianopoulos, K. I. (2013). "Numerical analysis of liquefaction-induced bearing capacity degradation of shallow foundations on a two-layered soil profile." Soil Dynamics and Earthquake Engineering, 44, 90-101.

Karimi, Z. and Dashti, S. (2016). "Numerical and centrifuge modeling of seismic soil-foundation-structure interaction on liquefiable ground." J Geotech Geoenviron Eng., 142(1):04015061.

Karimi, Z., Dashti, S., Bullock, Z., Porter, K., & Liel, A. (2018). "Key predictors of structure settlement on liquefiable ground: a numerical parametric study." Soil Dynamics and Earthquake Engineering, 113, 286-308.

Khosravi, M., Boulanger, R. W., Tamura, S., Wilson, D. W., Olgun, G., and Wang, Y. (2016). "Dynamic centrifuge tests of soft clay reinforced by soil-cement grids." Journal of Geotechnical and Geoenvironmental Engineering, ASCE, 04016027, 10.1061/ (ASCE) GT.1943-5606.0001487.

Kirkwood, P., & Dashti, S. (2018). “A centrifuge study of seismic structure-soil-structure interaction on liquefiable ground and implications for design in dense urban areas.” Earthquake Spectra, 34(3), 1113-1134.

Kirkwood, P., & Dashti, S. (2019). “Influence of prefabricated vertical drains on the seismic performance of similar neighboring structures founded on liquefiable deposits.” Géotechnique, 1-15.

Kokusho, T. (1999). “Water film in liquefied sand and its effect on lateral spread.” *Journal of Geotechnical and Geoenvironmental Engineering, 125*(10), 817-826.

Lambe, P. C., & Whitman, R. V. (1985). “Dynamic centrifugal modeling of a horizontal dry sand layer.” *Journal of geotechnical engineering, 111*(3), 265-287.

Liu, L., and Dobry, R. (1997). “Seismic response of shallow foundation on liquefiable sand.” J. Geotech. Geoenviron. Eng., 123(6), 557–567.

Luque, R., & Bray, J. D. (2017). “Dynamic analyses of two buildings founded on liquefiable soils during the Canterbury earthquake sequence.” Journal of Geotechnical and Geoenvironmental Engineering, 143(9), 04017067.

Macedo, J. and Bray J.D. (2018). “Key trends in liquefaction-induced building settlement.’ J. Geotech. Geoenviron. Eng., 144(11): 04018076.

Montoya, B. M., DeJong, J. T., and Boulanger, R. W. (2013). “Dynamic response of liquefiable sand improved by microbial induced calcite precipitation.” Geotechnique, 63(4), 302-312

Motamed, R., & Towhata, I. (2009). “Shaking Table Model Tests on Pie Groups behind Quay Walls Subjected to Lateral Spreading.” Journal of Geotechnical and Geoenvironmental Engineering, 136(3), 477-489.

Motamed, R., Towhata, I., Honda, T., Tabata, K., & Abe, A. (2013). "Pile group response to liquefaction-induced lateral spreading: E-Defense large shake table test." Soil Dyn and Earthquake Eng., 51, 35-46 http://dx.doi.org/10.1016/j.soildyn.2013.04.007.

Motamed, R., Orang, M. J., Parayancode, A., & Elgamal, A. (2020). "Results of a Class C Blind Prediction Competition on the Numerical Simulation of a Large-Scale Liquefaction Shaking Table Test." In *Geo-Congress 2020: Foundations, Soil Improvement, and Erosion* (pp. 334-342). Reston, VA: American Society of Civil Engineers.

Mousavi, S., & Ghayoomi, M. (2019). "Liquefaction mitigation of silty sands via microbial induced partial saturation." In *Geo-Congress 2019: Earthquake Engineering and Soil Dynamics* (pp. 304-312). Reston, VA: American Society of Civil Engineers.

Mousavi, S., & Ghayoomi, M. (2021). "Liquefaction mitigation of sands with nonplastic fines via microbial-induced partial saturation." *Journal of Geotechnical and Geoenvironmental Engineering*, *147*(2), 04020156.

Olarte, J., Paramasivam, B., Dashti, S., Liel, A., & Zannin, J. (2017). "Centrifuge modeling of mitigation-soil-foundation-structure interaction on liquefiable ground." Soil Dynamics and Earthquake Engineering, 97, 304-323.

Paramasivam, B., Dashti, S., & Liel, A. (2018). "Influence of prefabricated vertical drains on the seismic performance of structures founded on liquefiable soils." Journal of Geotechnical and Geoenvironmental Engineering, 144(10), 04018070.

Perko, H.A. (2009). "Helical piles: a practical guide to design and installation." New York, NY, USA: John Wiley & Sons.

Prabhakaran, A., Kyungtae, K., Ebeido, A., Jahed Orang, M., Motamed, R., Elgamal, A., and Frazao, C. (2020a). "Polymer injection and associated site liquefaction remediation mechanisms." 17th World Conference on Earthquake Engineering, 17WCEE, Sendai, Japan – September 13-18., Paper no: 4b-0024

Prabhakaran, A., Kyungtae, K., Jahed Orang, M., Qiu, Z., Ebeido, A., Zayed, M., Boushehri, R., Motamed, R., Elgamal, A., and Frazao, C. (2020b). "Polymer injection and liquefaction-induced foundation settlement: a shake table test investigation." In *Geo-Congress 2020: Geotechnical Earthquake Engineering and Special Topics* (pp. 1-9). Reston, VA: American Society of Civil Engineers.

Rasouli, R., I. Towhata, and T. Akima. (2016). "Experimental evaluation of drainage pipes as a mitigation against liquefaction-induced settlement of structures." J. Geotech. Geoenviron. Eng. 142 (9): 04016041. https://doi.org/10.1061/ (ASCE) GT.1943-5606.0001509.

Rasouli, R., Towhata, I., Rattez, H., & Vonaesch, R. (2018). "Mitigation of nonuniform settlement of structures due to seismic liquefaction." Journal of Geotechnical and Geoenvironmental Engineering, 144(11), 04018079.

Shahbazi, M., Cerato, A. B., Allred, S., El Naggar, M. H., & Elgamal, A. (2020a). "Damping characteristics of full-scale grouped helical piles in dense sands subjected to small and large shaking events." Canadian Geotechnical Journal, 57(6), 801-814.

Shahbazi, M., Cerato, A. B., El Naggar, H. M., and Elgamal, A. (2020b) "Evaluation of Seismic Soil–Structure Interaction of Full-Scale Grouped Helical Piles in Dense Sand." International Journal of Geomechanics, 20(12), 04020228.

Tokimatsu, K., & Katsumata, K. (2011). “Liquefaction-induced damage to buildings in Urayasu city during the 2011 Tohoku Pacific earthquake.” In proceedings of the international symposium on engineering lessons learned from the (pp. 665-674).

Toth, J. A. W., and R. Motamed. (2017). “Parametric study on liquefaction-induced building settlements using 1-g shake table experiments.” In Proc., 3rd Int. Conf. on Performance Based Design in Earthquake Geotechnical Engineering. London: International Society for Soil Mechanics and Geotechnical Engineering.

Vesic, A. S. (1973). “Analysis of ultimate loads of shallow foundations.” J. Soil Mech. Found. Div. 99 (1): 45–73.

Yegian, M. K., Eseller-Bayat, E., Alshawabkeh, A., Ali, S. (2007). “Induced Partial Saturation for Liquefaction Mitigation: Experimental Investigation.” Journal of Geotechnical and Geoenvironmental Engineering, ASCE, 133 (4).

Yoshimi, Y., and Tokimatsu, K. (1977). “Settlement of buildings on saturated sand during earthquakes.” Soils & Foundation, 17(1), 23–38.

Zeghal, M., Elgamal, A. W., Zeng, X., & Arulmoli, K. (1999). “Mechanism of liquefaction response in sand–silt dynamic centrifuge tests.” Soil Dynamics and Earthquake Engineering, 18(1), 71-85.

4. Dynamic Behavior of Helical Piles in Dry and Liquefiable Soils using Scaled Shake Table Tests

Abstract

The dynamic behavior of helical piles with different numbers of helices as well as a single slender shaft was examined through a series of scaled shake table tests. Multiple shakings were applied during each test series to evaluate the seismic behavior of the helical piles and the slender shaft considering different response parameters. Considerable ground settlement was observed during the first shaking in each test series, whereas negligible helical pile and slender shaft settlements were measured during all tests. The dynamic response of the helical piles was evaluated based on their bending moment variation along the depth and various measured response parameters at the model superstructure level. The bending moment variation indicated a similar trend along the depth for the helical piles and the slender shaft: the maximum moment was consistently observed at the boundary between dense and liquefiable layers. The observed bending moments along the depth increased with increases in input motion amplitude and superstructure weight. Densification of the liquefiable layer during different test series reduced the maximum bending moment along the depth for each pile due to increased relative density. Increasing the number of helices enhanced the dynamic performance of the helical piles compared to the slender shaft in terms of maximum bending moment, maximum horizontal displacement, residual horizontal displacement, and superstructure acceleration in different ground conditions.

4.1. Background

The dynamic behavior of deep foundations has been studied through past research and considerable progress has been made to explore the seismic behavior of different types of deep foundations at various ground conditions. Experimental studies including centrifuge tests (Boulanger *et al.*, 1999; Wilson *et al.*, 2000; Ghayoomi *et al.*, 2018) and shake table experiments (Makris *et al.*, 1997; Tokimatsu *et al.*, 2005; Mashhoud *et al.*, 2018; Lim and Jeong, 2018) were used to investigate the dynamic response of single steel piles, single micropiles, and pile groups mainly in dry and unsaturated sandy, silty, and cohesive soils. The effect of multi-layer soil deposits on the seismic response of driven steel piles was studied in Wilson *et al.* (2000) and Abdoun *et al.* (2003). Additionally, field test results garnered useful insight on soil-pile-structure interaction under dynamic loading (Novak and Grigg, 1976; El-Marsafawi *et al.*, 1992; Nikolaou *et al.*, 2001; Abd Elaziz and El Naggar, 2014; Capatti *et al.*, 2018; Farhangi *et al.*, 2020).

Liquefaction can cause significant damage to buildings and lifeline systems. The effects of liquefaction, including lateral ground spread and settlement of shallow foundations, have a significant impact on the seismic response of different foundation types. There has been much focus on the dynamic response of various deep foundations to lateral ground displacement using 1*g* shake table tests (Motamed and Towhata, 2009; Motamed *et al.*, 2009; Motamed *et al.*, 2013; Ebeido *et al.*, 2019) and centrifuge experiments (Zeghal *et al.*, 1999; Dobry *et al.*, 2001; Abdoun *et al.*, 2003; Boulanger *et al.*, 2003; Dobry *et al.*, 2003). A recent study elaborated on the efficiency of using a group of single-helix helical piles in liquefiable ground along with the dynamic response of a helical pile group to liquefaction-induced foundation tilt and settlement (Jahed Orang *et al.*, 2020;

Jahed Orang *et al.*, 2021a). Yet, there is a lack of knowledge on the response of single helical piles with different characteristics in liquefiable grounds.

Among other deep foundations elements, helical piles are categorized as small-diameter piles composed of a number of helices welded to a hollow steel shaft. The ease of installation of helical piles makes them a popular solution to buttress shallow foundations in new and existing structures, primarily in limited-access areas and low-overhead spaces (Perko, 2009). The typical shaft and helix diameters vary from 5 - 60cm and 15 – 120 cm, respectively, based on the required capacity (Ridgley, 2015). Reconnaissance reports shed light on the satisfactory performance of shallow foundations underpinned by helical piles during past earthquakes (Cerato *et al.*, 2017). However, the application of these deep foundation elements in earthquake-prone areas was not included in U.S. design codes (Cerato *et al.*, 2017). Additionally, the growing demand for helical pile utilization in dense urban areas motivates practitioners and researchers to further scrutinize the dynamic behavior of helical piles. Recent state-of-practice examples of seismic helical pile evaluation include field investigations of helical piles (Elkasabgy and El Naggar, 2018; Elkasabgy and El Naggar, 2019) and 1*g* large-scale shake table physical model tests (Elsawy *et al.* 2019a, b; Jahed Orang *et al.*, 2019a; Shahbazi *et al.*, 2020a, b). These observations were obtained at different ground conditions, applied input motions, helical pile specifications, and dynamic load applications. Overall, these experimental studies shed light on the satisfactory performance of helical piles under dynamic loading.

The experimental program presented in this paper aims to provide broader insight on the seismic behavior of multi-helix helical piles in liquefiable grounds considering

variable ground conditions, peak input acceleration, superstructure weight, and multiple shaking event scenarios.

4.2. Shake Table Experimental Setup

The 1*g* shake table facility at the University of Nevada, Reno was used to carry out scaled tests on helical piles in dry and liquefiable ground conditions. One of the advantages of using scaled shake table tests is the ability to conduct parametric studies on different factors that influence the dynamic performance of the soil-pile-structure system. In these tests, a medium-size soil box resided on top of a shake table that was excited with controlled frequency and amplitude by a rotary motor. Two 7.5cm-thick high-density foam paddings were used on each side of the rigid soil box to minimize the boundary effects. The inner dimensions of the box were 204cm (length) by 64cm (width) by 82cm (height) (Jahed Orang *et al*., 2019b).

Figure 4.1 illustrates the soil box with the scaled ground model, helical piles, and top weights on piles representing superstructure inertia, along with the instrumentation used to capture the soil-pile system response to the input motions. In this study, the shake table tests were divided into two types namely Dry and Liquefaction Tests (see Table 4.1). The Dry Tests were conducted on dry sand and included a single test (Test #15) with six shaking sequences. The Dry Tests aimed to replicate the ground conditions, helical pile dimensions, and top weights used in a full-scale shake table experiment at the UC San Diego Large High-Performance Outdoor Shake Table (LHPOST). Details of this full-scale experiment can be found in Elsawy *et al.* (2019a, b). The Liquefaction Tests focused on the response of helical piles in liquefied soils during various shakings and included a total

of four tests with various shaking scenarios. Table 4.1 summarizes these tests and the number of shakings during each test.

Table 4.1. Test series and number of shakings during each test

Test series	Test number	Peak input acceleration (g)[a]	Number of shakings
Dry	Test #15	0.15	LWS[b]: 3
			HWS[c]: 3
Liquefaction	Test #16	0.3	LWS: 3
			HWS: 3
	Test #17	0.3	LWS: 2
			HWS: 2
	Test #18	0.2	LWS: 4
			HWS: 4
	Test #19	0.2	LWS: 4
			HWS: 4

[a]For first shaking in each test
[b]LWS = Light Weight Series
[c]HWS = Heavy Weight Series

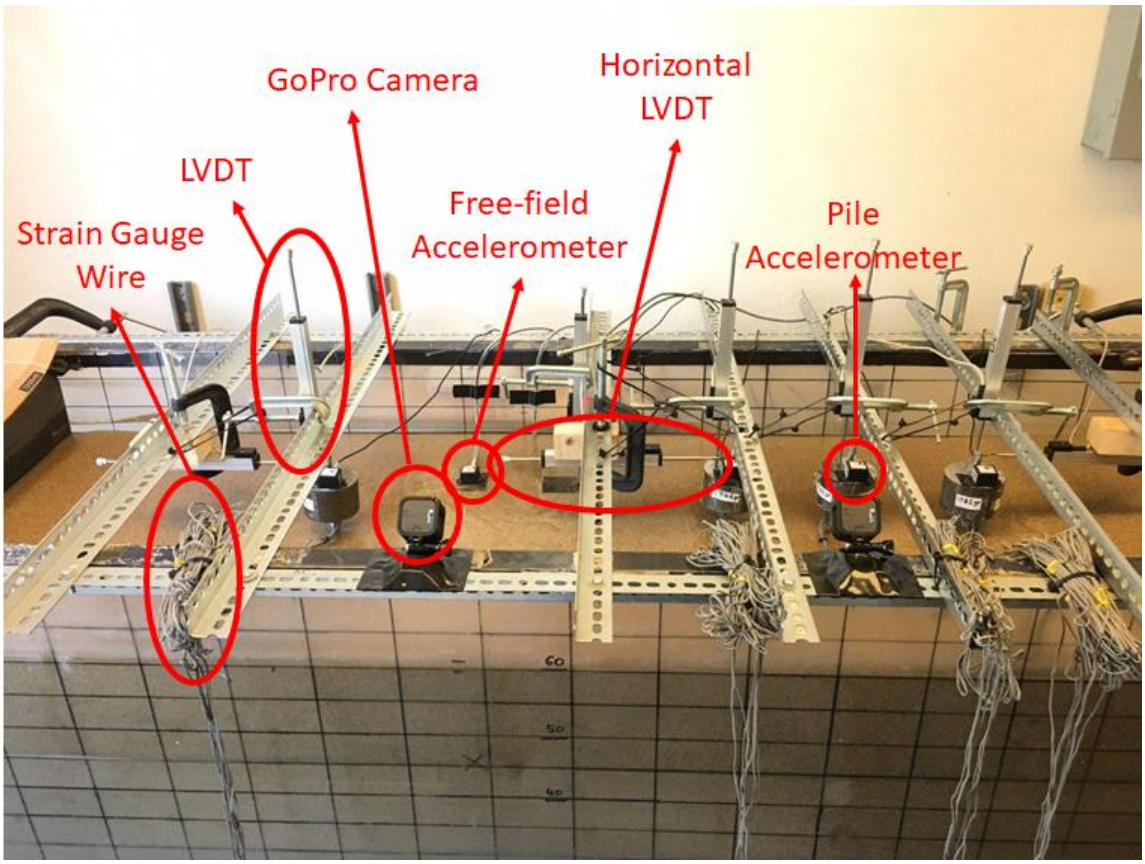

Figure 4.1. Instrumented ground and helical pile setup used for scaled shake table tests

4.2.1. Scaling Procedure

Iai *et al.*'s (2005) similitude law was used to scale down the prototype properties of the soil, pile, and superstructure. The scaling factor was assumed to be 7.5 based on overall consideration of box dimensions, ground model thickness, and helical pile material properties. The prototype properties were obtained based on large-scale shake table experiments conducted on helical piles in dense sandy ground (Elsawy *et al.*, 2019a). The model and prototype properties of the soil, pile, and superstructure are summarized in Table 4.2. All of the results in this paper are presented in scaled level.

Table 4.2. Soil, pile, and superstructure properties in model and prototype scale

Property	Ratio (Prototype/Model)	Model (N = 7.5)	Prototype (Elsawy *et al*., 2019a)
Soil layer thickness (cm)	N	60.0	450.0
Pile length (cm)	N	41.0	366.0
Pile diameter (cm)	N	1.0	8.8
Pile's young modulus (GPa)	$N^{0.5}$	68.9	200.0
Pile's cross section area (cm^2)	N^2	0.64	13.2
Helix diameter (cm)	N	3.0	25.4
Helix spacing (cm)	N	9.0	60.0
Pile to pile distance (cm)	N	15.0	100.0
Top mass (LWS) (kg)	N^3	1.8	750.0
Top mass (HWS) (kg)	N^3	2.95	1245.0
Flexural rigidity (per unit length)	$N^{3.5}$	638.2	0.58

4.2.2. Model Preparation and Instrumentation

Two different ground models were built for the dry and liquefiable test series. A dense 0.6m-thick dry sand layer was constructed in the dry test series, and the top 0.2m dense sandy layer was replaced with a loose sand layer in the liquefaction test series. As presented earlier, the ground model configuration was selected based on a scaling factor of 7.5 and designated depth of fixity for the helical piles. Poorly graded #60 Monterey sand was used to build the model ground. The properties of #60 Monterey sand are summarized in Table 4.3 and its grain size distribution is illustrated in Figure 4.2.

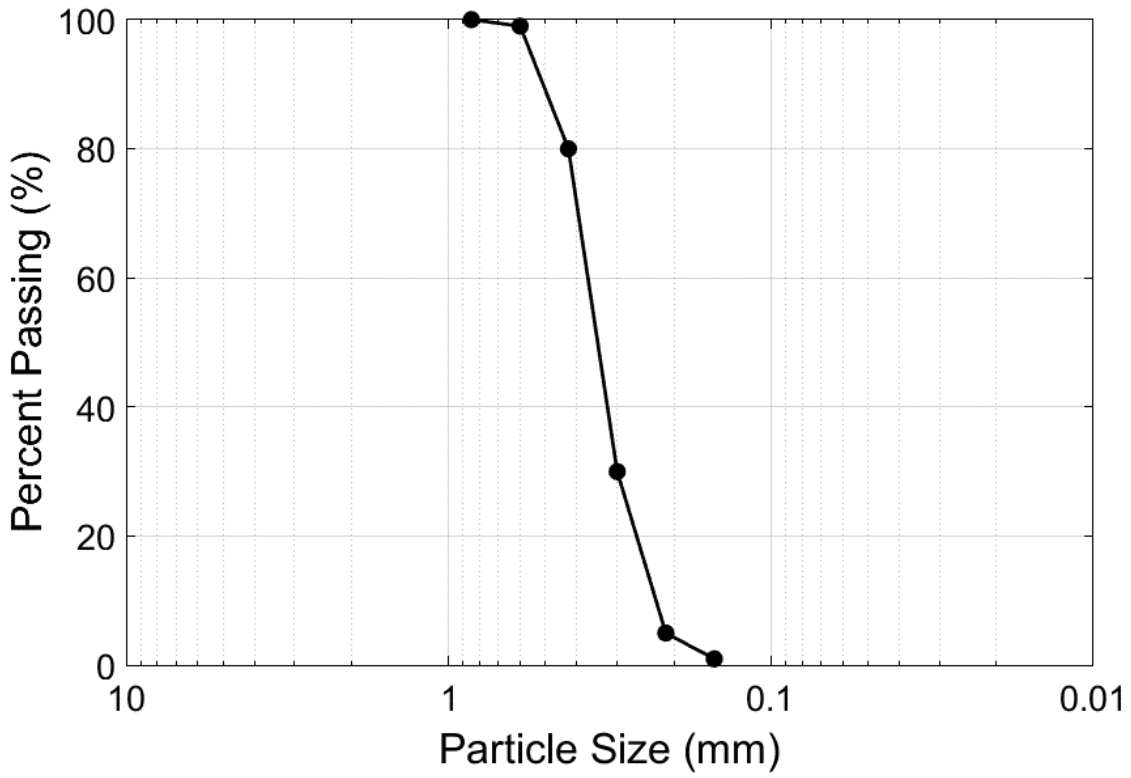

Figure 4.2. Grain size distribution of #60 Monterey sand

Table 4.3.Geotechnical properties of #60 Monterey sand

Property	#60 Monterey sand
Specific gravity, G_s	2.65
Maximum void ratio, e_{max}	0.78
Minimum void ratio, e_{min}	0.54
Coefficient of curvature, C_c	1.03
Coefficient of uniformity, C_u	1.65
Grain size, D_{50} (mm)	0.34

The dense layer was constructed using the wet compaction method with a manual compactor. The achieved relative density for the dense layer was 70%. After the dense layer was constructed, the model was saturated through a single inlet below the container, where water was slowly infiltrated into the soil through porous glass sheets at the bottom of the box. The water level continued to rise to the mid-height of the liquefiable layer. The

air pluviation method was used to sediment the loose layer inside the water. The achieved relative density of the loose layer was 30%. All of the relative density values were calculated based on weight-volume relationships.

As shown in Figure 4.3, the model ground was densely instrumented to capture the dynamic behavior of the dense and liquefiable layers during various shakings. A total of 20 sensors including accelerometers, pore water pressure sensors, linear variable displacement transducers (LVDTs), and GoPro cameras were used during all test series. In order to model inertial effects of superstructure, two different weight configurations were used in each test: in the Light Weight Series (LWS) configuration, 1.80kg steel weights were placed on top of each pile, and in the Heavy Weight Series (HWS) configuration, 2.95kg steel weights were used. A lateral LVDT along with an accelerometer was also connected to the top of each helical pile to investigate their dynamic behavior. The pore water pressure sensors also captured the excess pore water pressures at mid-depth of each layer. An accelerometer array including three accelerometers located at the mid-depth of each layer and on the free-field ground surface was used to capture the ground response. The model ground and pile settlements were measured using five LVDTs (one on top of each pile and one in the free-field ground). The whole model including all the piles and ground was also videotaped by two GoPro cameras located at different angles during and after each shaking. The helical pile instrumentation will be discussed in the following section.

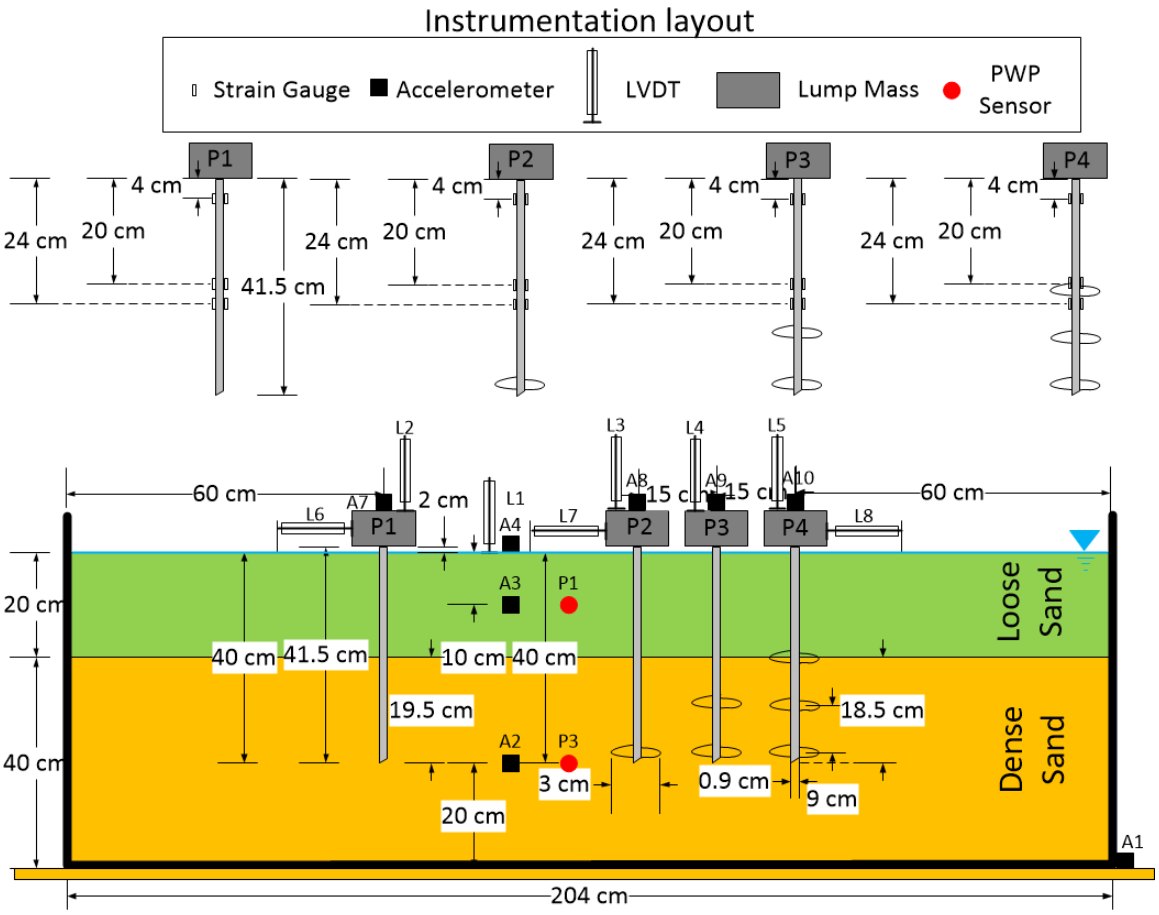

Figure 4.3. Instrumentation layout used for model ground, slender shaft, and helical piles

4.2.3. Helical Pile Specifications and Instrumentation

One slender shaft and three helical piles with different numbers of helices were used during these shake table experiments. As shown in Figure 4.3, P1 represented the slender shaft and P2, P3, and P4 were helical piles with one, two, and three helices, respectively. The shaft of each pile was made from aluminum. The specifications of the slender shaft and helical piles are provided in Table 4.4. Each pile was instrumented with six strain gauges to measure bending strains along the piles (locations depicted in Figure 4.3). Two pairs of strain gauges were installed at the interface of the loose and dense layers in every pile to

evaluate the shear discontinuity effect reported in previous studies using centrifuge tests, such as Abdoun *et al*. (2003).

All the strain gauges along the length of the helical piles and the single slender shaft were protected using multiple measures including mastic tape, aluminum wrap, and zip ties around strain gauge locations. The instrumented piles with protected strain gauges are presented in Figure 4.4.

The piles were installed in the model ground in two stages: First, the instrumented piles were drilled gently into the soil by hand until they reached a competent stratum. Then, each pile was torqued by a mechanical drill with a constant push to finalize the pile installation. The applied torque was low enough to minimize the soil disturbance during helical pile installation in both stages.

Table 4.4. Geometric and mechanical properties of the model helical piles and the slender shaft

Model pile properties	Value
Pile length (cm)	41.0
Pile diameter (cm)	1.0
Helix pitch (cm)	0.5
Helix diameter (cm)	3.0
Elastic modulus (GPa)	68.9
Helical pile’s spacing (cm)	15.0
Spacing between helices (cm)	9.0
Penetration depth into the dense layer (cm)	19.0
Top mass weight (Light Weight series) (kg)	1.8
Top mass weight (Heavy Weight series) (kg)	2.95

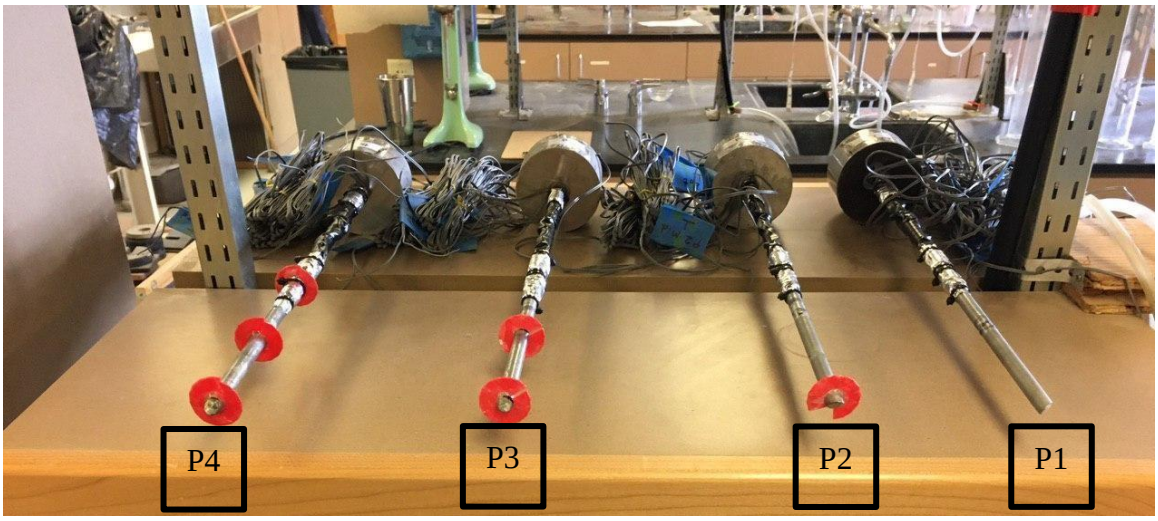

Figure 4.4. Photo of protected strain gauges on each pile before tests

4.2.4. Shaking Sequences

A total of five scaled shake table tests with multiple shakings (a total of 36 shakings) were conducted to assess the dynamic behavior of the helical piles in dry and liquefiable grounds. Each test included several shakings with varying peak input accelerations. The peak input accelerations during the test series ranged from 0.15 - 0.42*g* as observed in recent earthquakes, such as the 1999 Adapazari earthquake in Turkey and the 2010-2011 Canterbury Earthquake Sequence (CES) in New Zealand. The variation of motion amplitudes in each shaking event is depicted in Figure 4.5. As mentioned earlier, each test was conducted with two different top weights; in Figure 4.5, solid lines indicate the LWS and dashed lines indicate the HWS for each test. The number of shakings varied from four to eight depending on the designated shaking sequence for each test.

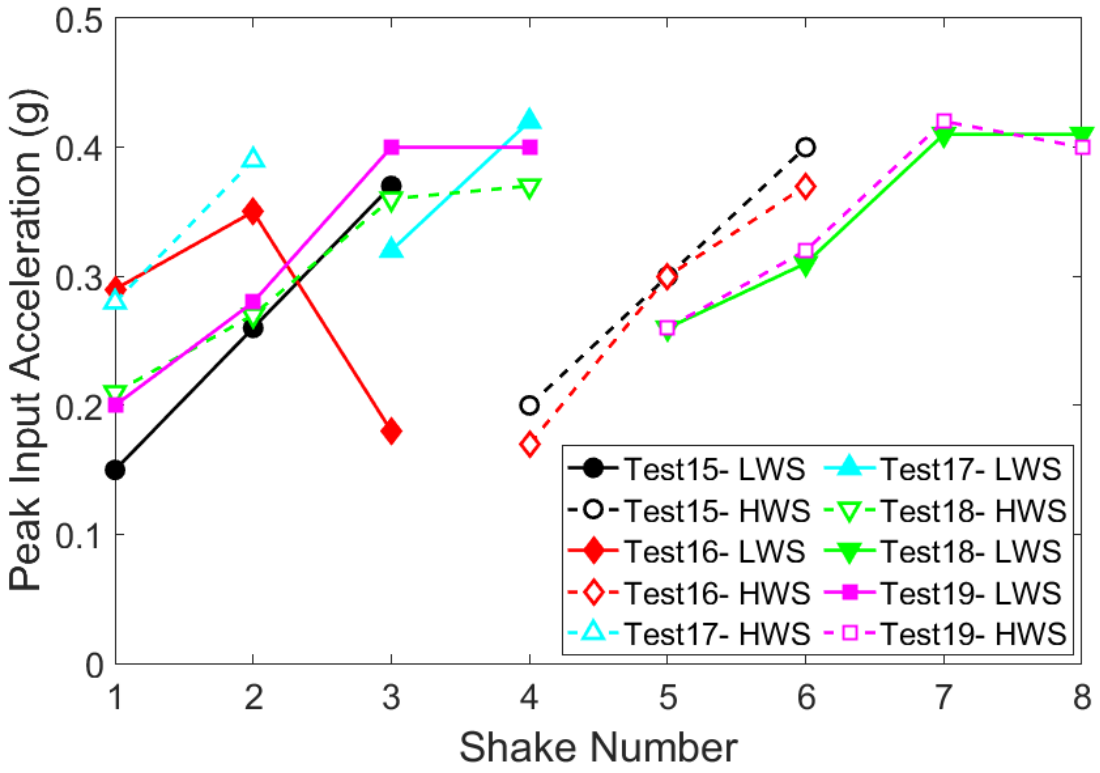

Figure 4.5. Shake table test series with different peak input accelerations during multiple shaking sequences

4.3. Shake Table Experimental Results

This section presents the observed performance of helical piles in dry and liquefiable soils and the model ground response. Figure 4.6 illustrates the ground condition along with the helical piles after liquefaction in Test #18 and highlights the relative amount of ground settlement compared to helical pile settlement. The structural weights supported by the helical piles (and the slender shaft), which were meant to model superstructure, experienced insignificant settlements. A detailed discussion about ground and helical pile settlements will be provided in this section.

Example acceleration time histories at various depths inside the model ground, horizontal displacement time histories at the top of each pile, and generated excess pore

water pressure (EPWP) at mid-depth of the liquefiable layer are summarized in Figure 4.7. These test results were obtained from the first shaking in Test #17 (LWS). The acceleration time histories at different depths are presented in Figures 7 (a) - (d). Observed reductions in acceleration amplitudes after 8 seconds and the elongated frequency content at the mid-liquefiable and free-field surface ground are attributed to liquefaction occurrence and pore water pressure buildup. The recorded EPWP time history at mid-depth of the liquefiable layer is illustrated in Figure 4.7 (h), which is also indicative of liquefaction occurrence (i.e., r_u = 1.0). Time histories of horizontal displacement at pile heads are presented in Figures 7 (e) - (g). As can be seen, the important observation was the amount of residual horizontal displacement obtained through the LVDT time histories at the top of each pile. The amount of top residual horizontal displacement was higher in P1 (slender shaft) compared to P2 (single-helix helical pile) and P4 (triple-helix helical pile). The correlation between number of helices and residual horizontal displacement on top of each pile along with other pile response parameters will be further elaborated in the "Effects of Number of Helices" section. Detailed discussions on the effect of different parameters on helical pile behavior including the effects of multiple shaking events on the relative density of the liquefiable layer ($D_{r,\,L}$), ground motion intensity, and superstructure weight in dry and liquefiable grounds are presented in subsequent sections.

Figure 4.6. Model ground and pile configuration after first shaking in Test #18

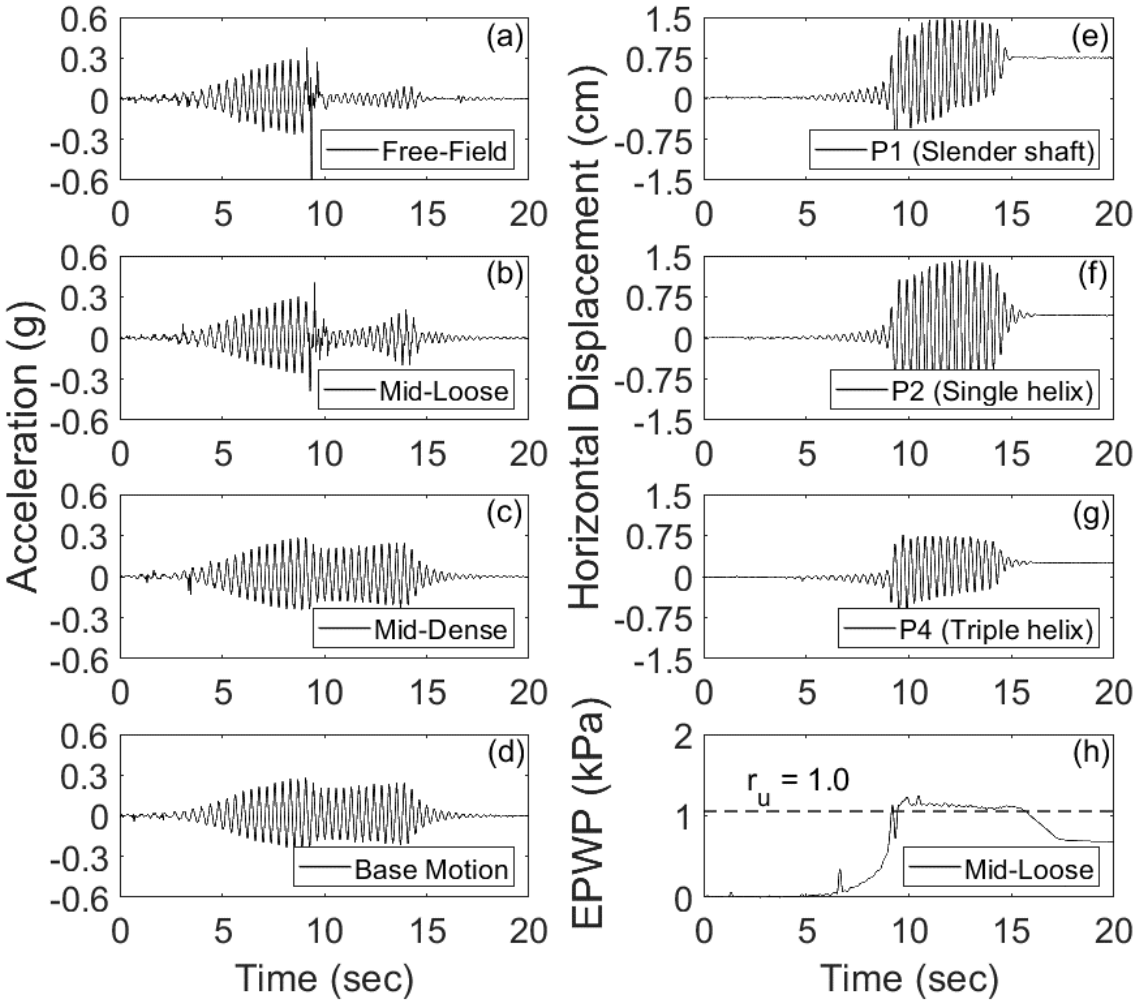

Figure 4.7. (a)-(d) Acceleration, (e)-(g) horizontal displacement, and (h) EPWP time histories in Test #17 (Shake 1, LWS)

4.3.1. Effects of Multiple Shakings

The variation in the relative density of the liquefiable layer ($D_{r,L}$) during multiple shakings in each test is shown in Figure 4.8. The variation in $D_{r,L}$ was calculated based on measured ground surface settlements after each shaking. Test #15 was conducted under the dry dense ground condition with a relative density of 70%, where no densification occurred after each shaking sequence. The maximum measured $D_{r,L}$ reached as high as 80% depending on the shaking scenario of the corresponding test. As mentioned earlier, a total of 36 shakings

with various ground conditions and relative densities were conducted during this experimental program.

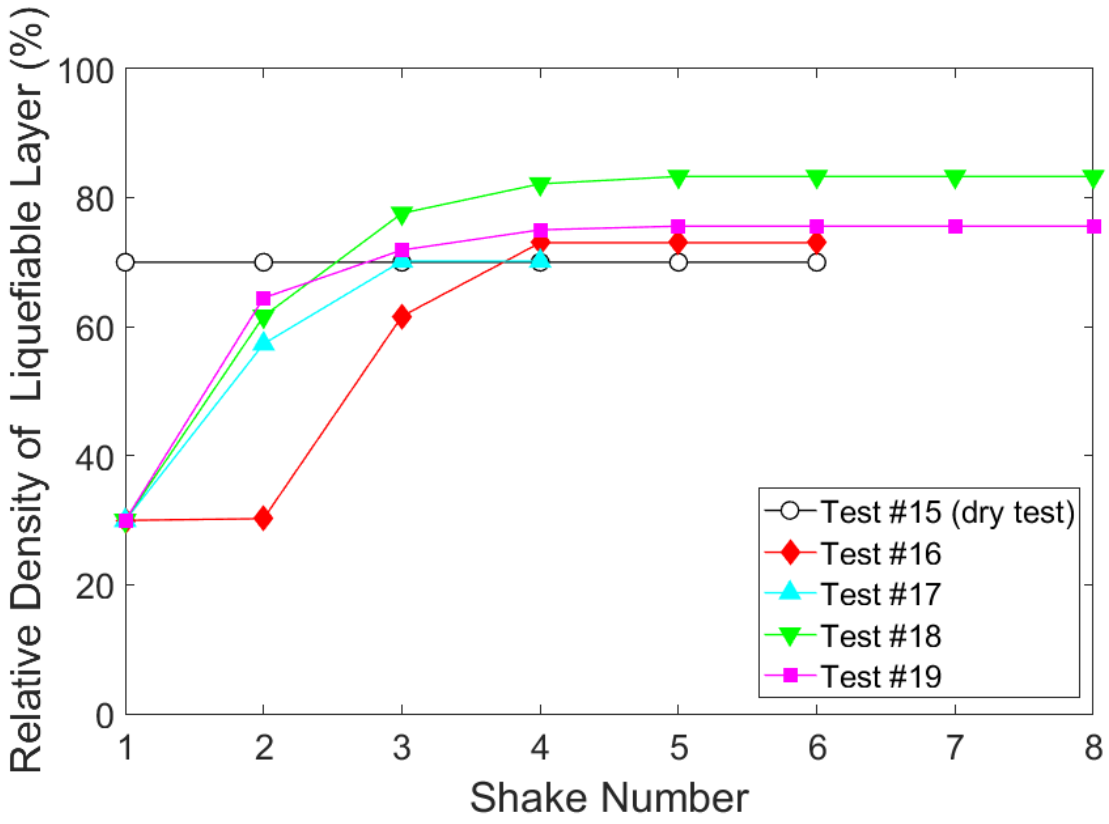

Figure 4.8. Variation of liquefiable layer relative density in each test during multiple shaking sequences

The influence of multiple shakings on the dynamic behavior of helical piles was evaluated based on the bending moment variation along the depth of the slender shaft and the three different types of helical piles. This is summarized in Figure 4.9 for four different shakings with variable relative densities of the liquefiable layer. The legend in the top right corner of each plot indicates the pile type, where P1 represents the slender shaft and P2, P3, and P4 represent the single-, double-, and triple-helix helical piles, respectively. All shakings were conducted under similar ground motion amplitude with the same

superstructure weight on top of each pile. The highest bending moment was observed at the loose-dense layer interface, which is in line with previous research on the seismic behavior of driven piles in layered soils (Abdoun *et al.,* 2003). The variation trend of the bending moment along the depth was similar for all three helical piles and the slender shaft. The multiple shakings led to a higher relative density of the liquefiable layer in the test series, which influenced the bending moment variation along the depth for all the piles. The bending moment difference between the dry sand test (Test #15) and the liquefaction tests (Tests #16-19) at similar depths tended to decrease as the relative density of the liquefiable layer increased. In other words, soil densification due to multiple shakings yielded lower bending moments along the depth for all the piles.

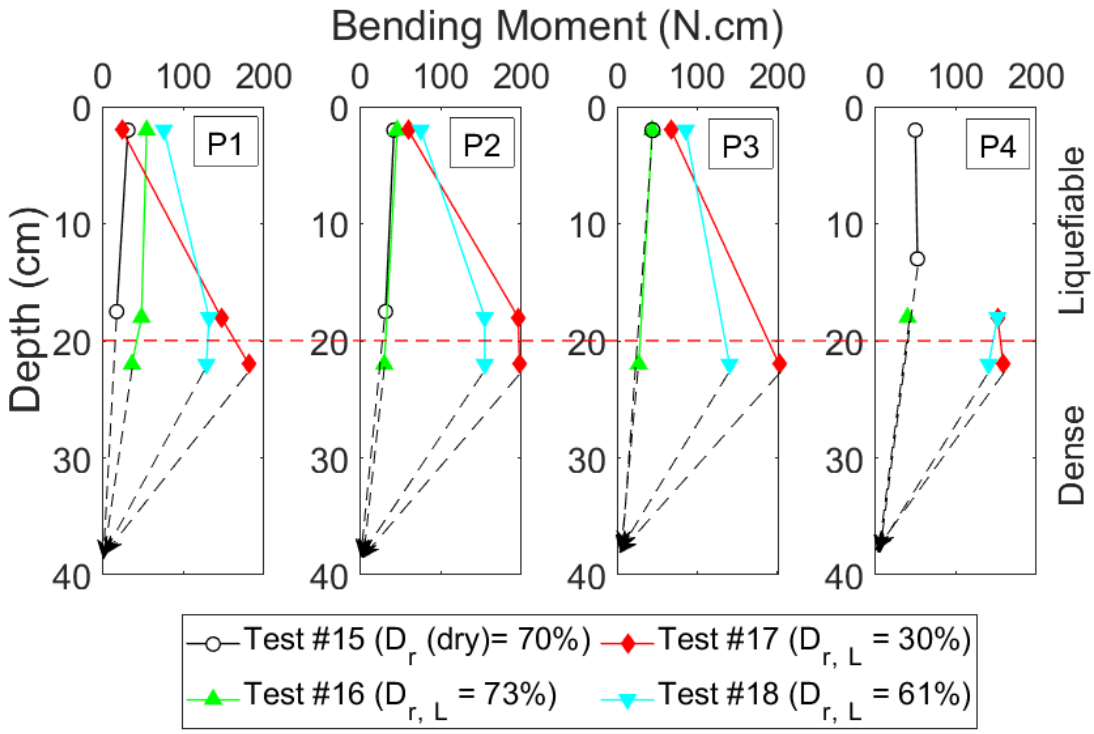

Figure 4.9. Effect of liquefiable layer relative density on bending moment variation for the helical piles and single slender shaft (HWS with peak input acceleration = 0.3*g*)

4.3.2. Effects of Ground Motion Amplitude

This section presents the effects of input motion amplitude on the response of helical piles. The input motion amplitude variation during different shakings resulted in different bending moment variations along the depth for all the piles (see Figure 4.10). The presented shakings in Figure 4.10 were conducted using two different superstructure weights (LWS in Figure 4.10 (a) and HWS in Figure 4.10 (b)) but with a similar relative density of the liquefiable layer. As shown in Figure 4.10 (a), a higher ground motion amplitude led to greater bending moment values at similar depths for all the helical piles and the single slender shaft. The higher motion amplitude led to a higher inertial horizontal force on each helical pile and the slender shaft, which consequently resulted in a greater helical pile response. A similar trend was also observed in the HWS (Figure 4.10 (b)). However, comparing the two test series revealed that peak input acceleration was a stronger determinant of bending moment than superstructure weight.

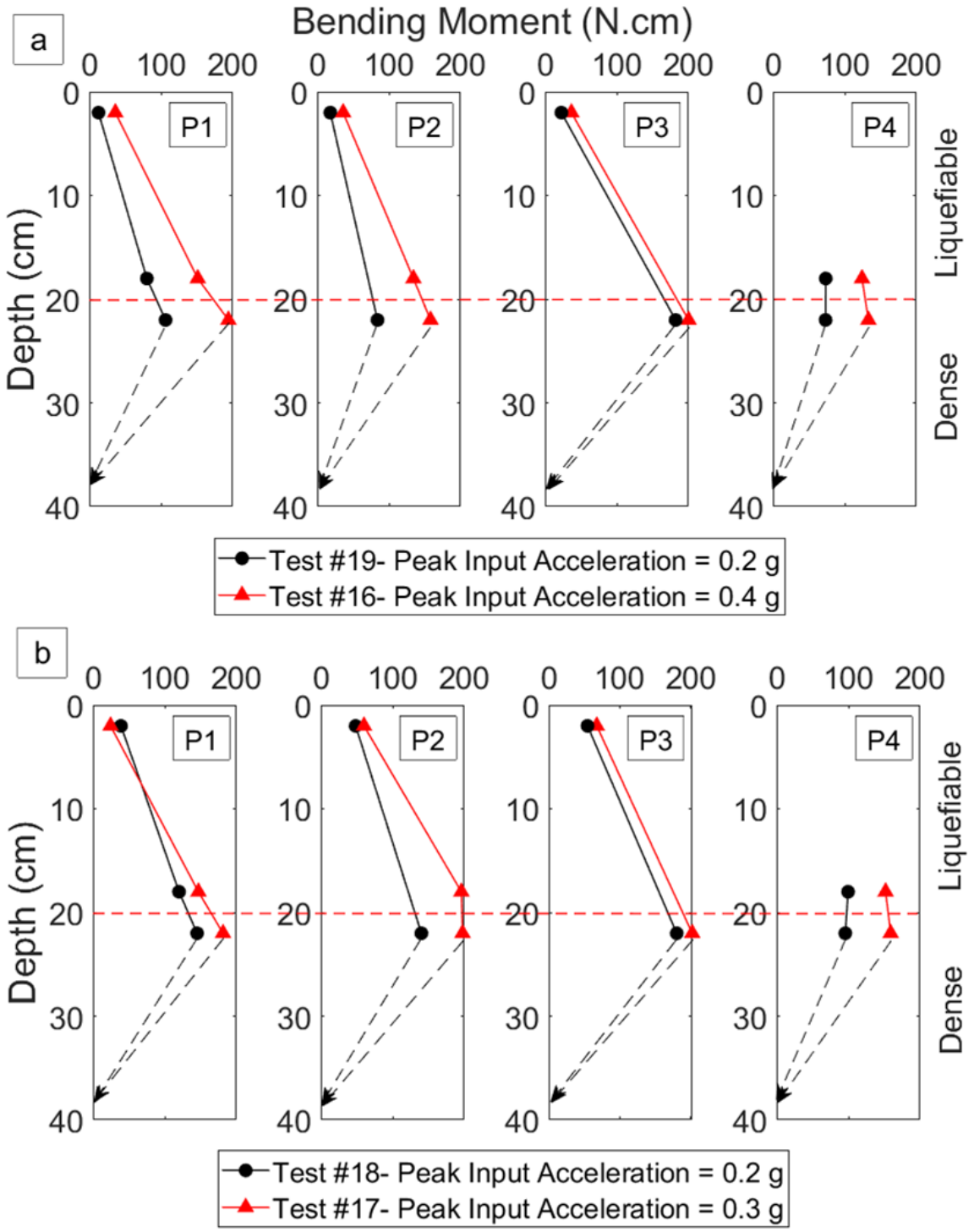

Figure 4.10. Ground motion amplitude effect on bending moment variation along depth for helical piles and single slender shaft during (a) LWS and (b) HWS with $D_{r,L}$ = 30%

4.3.3. Effects of Superstructure Weight

As mentioned earlier, the superstructure weight on top of each pile consisted of two configurations, light weight in the LWS and heavy weight in the HWS. Figure 4.11 illustrates the bending moment variation along the depth for the LWS and the HWS. Each pile carried similar weight during each test series. The results presented in Figure 4.11 were obtained during a peak input acceleration of 0.2*g* (Figure 4.11 (a)) and 0.3*g* (Figure 4.11 (b)) with 30% liquefiable layer relative density. Overall, the HWS resulted in higher bending moments along the depth compared to the LWS in all three helical piles and the slender shaft. Another important observation was the greater difference between the LWS and the HWS at higher peak input accelerations (i.e., the bending moment difference at similar depths between the two test series was higher when the applied peak input acceleration increased from 0.2*g* to 0.3*g*).

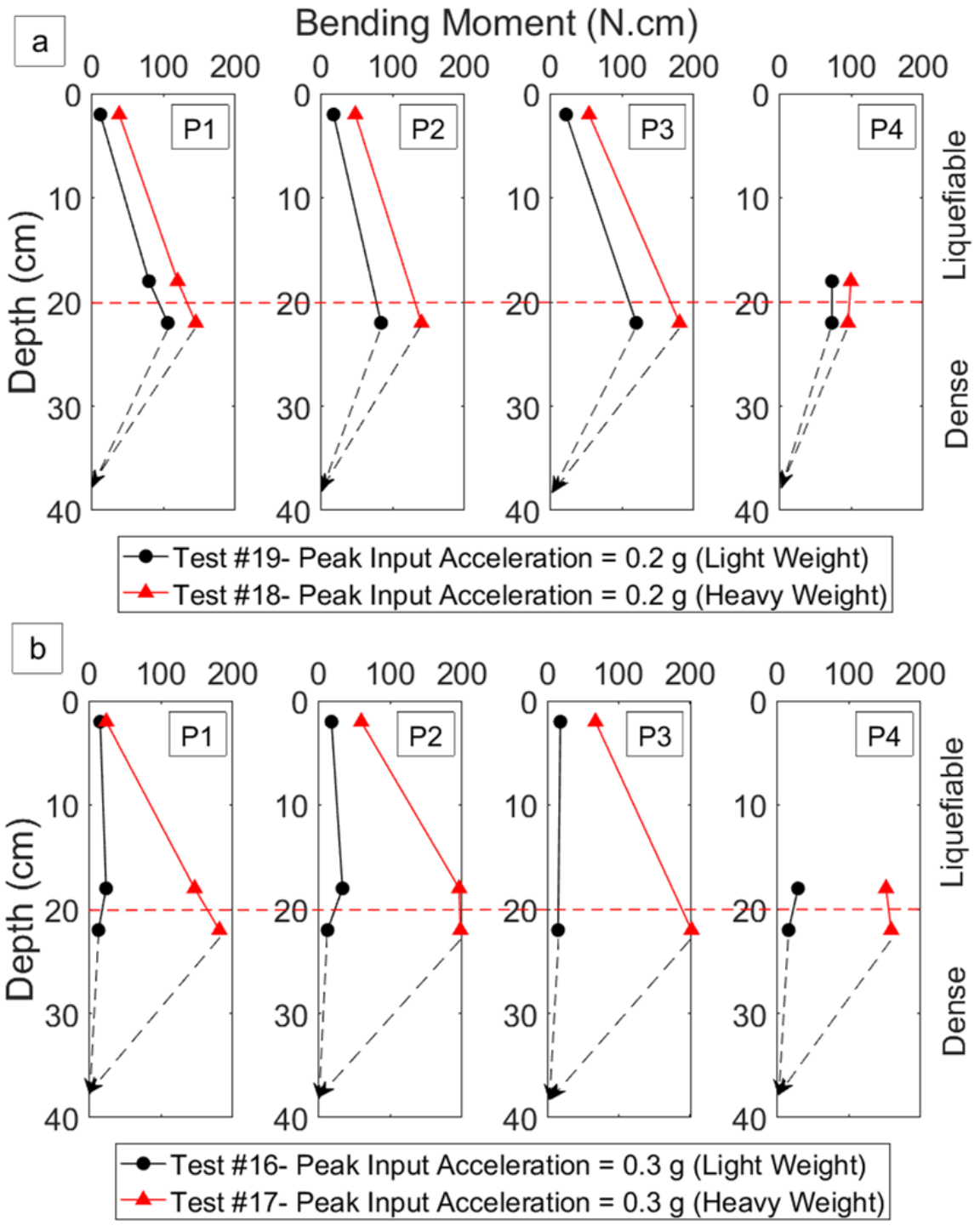

Figure 4.11. Effect of superstructure model weight on bending moment variation along depth for all three helical piles and single slender shaft with $D_{r,L}$ = 30% for (a) peak input acceleration = 0.2g and (b) peak input acceleration = 0.3g

4.3.4. Combined Effects of Relative Density and Superstructure Weight

Results from the combined effects of the liquefiable layer relative density and the superstructure weight on bending moment variation along the depth are presented in Figure 4.12. Both tests were conducted at a similar peak acceleration (0.4*g*). The solid circles indicate Light Weight Series tests with $D_{r,L}$ = 30%, while the solid triangles indicate HWS tests with $D_{r,L}$ = 60%. As shown in Figure 4.12, the bending moment at the top of the liquefiable layer was higher in the HWS with a higher $D_{r,L}$. In contrast, , higher bending moments were observed in the LWS with lower liquefiable layer relative density at the loose-dense layer interface.

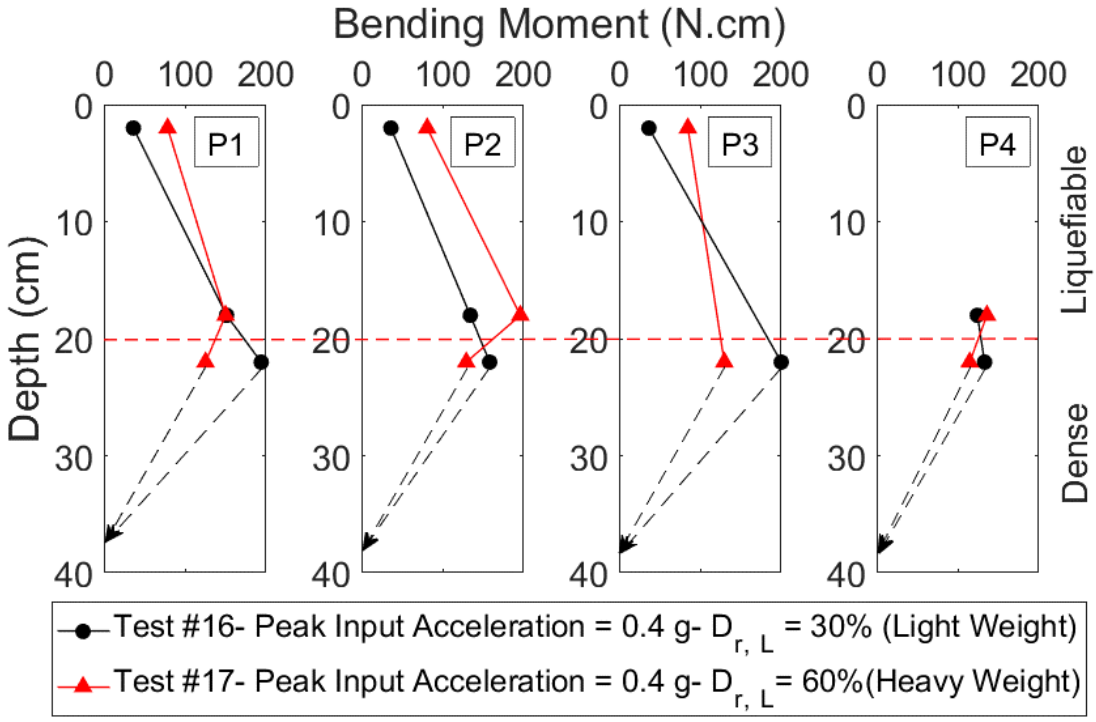

Figure 4.12. Combined effects of superstructure weight and relative density of liquefiable layer on bending moment variation along depth for all piles

4.3.5. Effects of Number of Helices

In this study, four different parameters were used to assess the dynamic response of multi-helix helical piles and a single slender shaft. These parameters included the measured responses at the top of each pile such as maximum horizontal displacement, residual horizontal displacement, maximum acceleration, and maximum bending moment along the depth. The effects of the number of helices on these parameters were quantified based on the percent reduction of each measured parameter in the helical piles with respect to their corresponding values in the slender shaft (no helices). The results from the first shaking in each test are summarized in Figure 4.13. In all of the evaluated helical pile cases, the relative density of the liquefiable layer was 30% and the ground peak acceleration varied from 0.2 - 0.3*g* for both LWS and HWS tests.

Each parameter was evaluated based on 12 measured corresponding responses on the helical piles and the slender shaft. As shown in Figure 4.13, each parameter improved (meaning that displacement or acceleration decreased) as the number of helices increased. The largest improvement was observed in residual horizontal displacement on top of each pile (Figure 4.13(a)), with a 60% reduction in the triple-helix helical pile compared to the slender shaft. Smaller improvements in the range of 35-40% were observed in M_{max} (maximum bending moment along the piles) along depth (Figure 4.13(c)) and maximum pile top displacement (Figure 4.13(b)), and an approximately 20% improvement was observed in maximum acceleration on top of each pile (Figure 4.13(d)). Overall, these results illustrate that increasing the number of helices leads to better performance under dynamic loading.

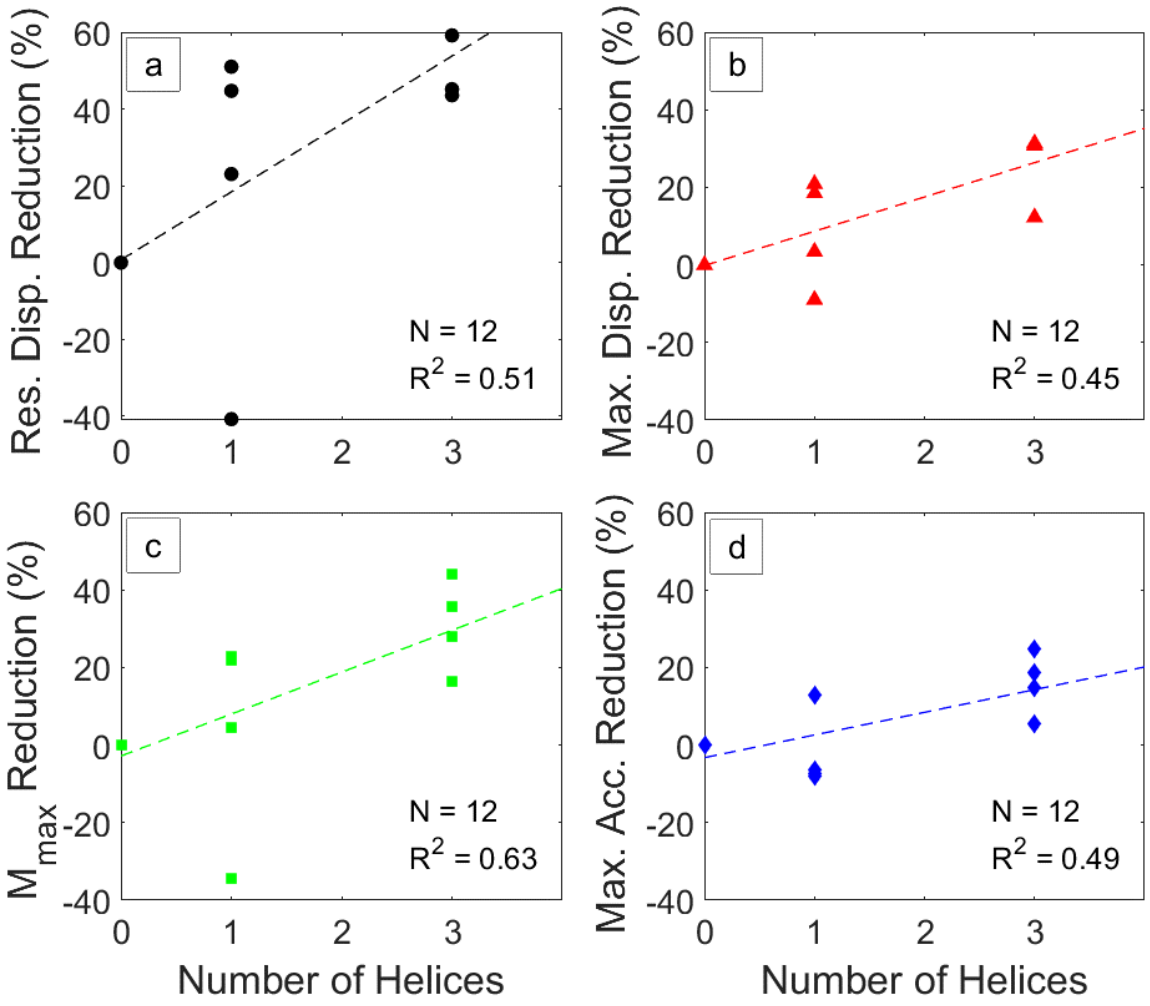

Figure 4.13. Percent reduction in (a) residual horizontal displacement, (b) maximum pile top displacement, (c) M_{max} along depth (with respect to slender shaft), and (d) maximum acceleration on top of piles during first shakings in Tests #16-19

4.3.6. Ground and Pile Settlements

In the experiments, two methods were used to record settlement during and after each shaking. Ground settlement values were measured manually after each shaking, whereas pile settlements were recorded by LVDTs. The manual measurements were conducted at 10 different lines with four measurement points along each line resulting in a total of 40

ground settlement measurements after each shaking. Figure 4.14 illustrates the contour plots obtained through manual ground settlement measurements after four shakings in Test #17. The amount of settlement was higher through the middle third of the soil surface particularly as a result of the boundary effect. The maximum manually measured ground settlement was about 2cm after shaking 1. These settlements of the ground surface indicated the densification of the liquefiable layer due to multiple shaking sequences. The estimated relative density of the liquefiable layer prior to each shaking is also presented in Figure 4.14, which indicates progressive increase in $D_{r,L}$ after each shaking. The effects of multiple shakings appear to diminish beyond Shaking 3, resulting in insignificant settlements.

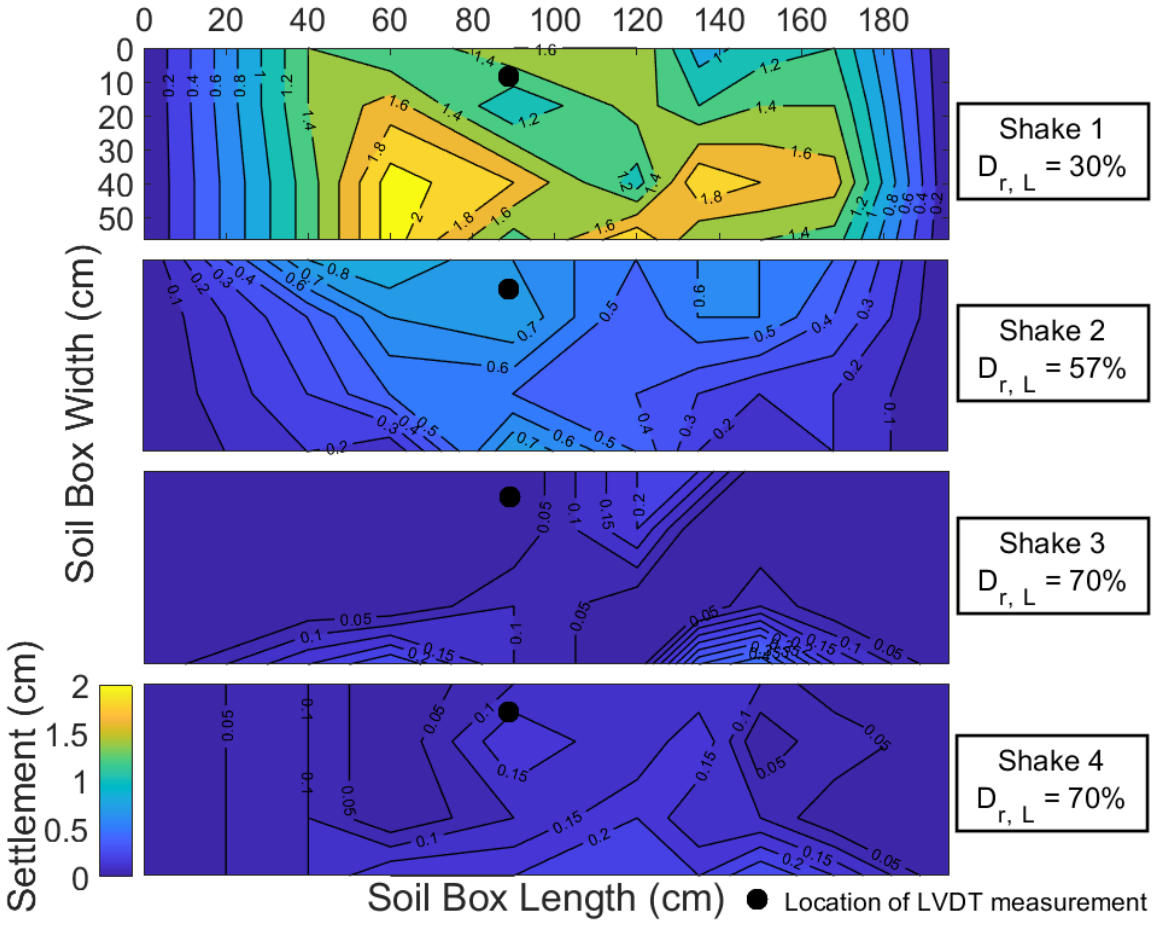

Figure 4.14. Ground settlement contour plots during four shakings in Test #17

In addition to manual measurements of the ground surface settlements, one LVDT was also used to record the ground settlements, summarized in Table 5. The measurements continued until the EPWP completely dissipated. The location of LVDT-measured ground settlement is indicated by solid circles in Figure 4.14. The manual and LVDT-measured ground settlement indicated reasonable consistency at the corresponding ground-LVDT location. Various shaking schemes resulted in different amounts of ground settlement after each shaking. According to the data recorded by LVDTs, there were no observed helical pile or slender shaft settlements in all the shakings during both LWS and HWS tests.

However, the LVDT measured ground settlement as high as 1.2cm. The observed negligible settlement in the helical piles in these test series along with previous large-scale experimental findings illustrate the efficiency of using these deep foundation elements to reduce liquefaction-induced foundation settlement (Jahed Orang *et al.*, 2021a, b).

Table 4.5. LVDT-measured ground settlements in multiple shaking events (all measured values are in centimeters)

Shaking no.	Test #16	Test #17	Test #18	Test #19
1	0.00	0.95	1.10	1.20
2	1.10	0.45	0.56	0.26
3	0.40	0.00	0.16	0.11
4	0.00	0.05	0.05	0.02
5	0.00	-	0.00	0.00
6	0.32	-	0.00	0.00
7	-	-	0.00	0.00
8	-	-	0.00	0.00

4.4. Conclusions

In this study, scaled 1*g* shake table tests were conducted to evaluate the dynamic behavior of a slender shaft and helical piles with different numbers of helices in liquefiable and dry ground models. The shake table experimental results included multiple aspects of the dynamic response of these foundations such as the effects of multiple shakings, ground motion amplitude, superstructure weight, and combined effects of liquefiable layer relative density and superstructure weight, which were investigated based on the bending moment variation along the depth for each of the model piles. In addition, four parameters were used to assess the performance of the helical piles compared to the slender shaft to provide a broader understanding of the efficiency of these deep foundation elements. The major outcomes of this research are summarized hereafter:

- There was no observed difference in the trend of bending moment variation along the depth for different pile types as all of the helical piles and the slender shaft illustrated similar behavior in the variation of bending moment along the depth in all of the test series. The maximum bending moment was observed to be at the loose-dense layer interface, which is in line with previous research.
- Lower bending moments were observed along the depth in the dry test compared to the liquefaction tests. The liquefiable layer relative density played an important role in the dynamic response of the helical piles and the slender shaft. Densification of the liquefiable layer as a result of multiple shakings yielded to similar bending moment values observed in the dry test.
- Higher peak input accelerations resulted in higher moments exerted on the various types of piles. Additionally, Heavy Weight Series (HWS) tests resulted in higher bending moments compared to Light Weight Series (LWS) tests. The increased ground motion amplitude and superstructure weight result in elevated inertial force at the superstructure level. The increased relative density of the liquefiable layer had a major influence in reducing the bending moment along the depth at the loose-dense layer interface in all the piles, even with higher superstructure weight.
- The number of helices influenced the dynamic performance of the helical piles. An increase in the number of helices resulted in an improvement (reduction) in residual horizontal displacement, maximum horizontal displacement, and maximum acceleration (measured on the top of each pile) and maximum moment (measured along the length of each pile). Residual horizontal displacement showed the greatest improvement, with a 60% drop in displacement of the triple-helix helical pile compared to that of the slender shaft.
- During all the shaking events, there were no observed settlements in the helical piles or the slender shaft, while the free-field ground settled as high as 2cm in the proximity of the helical piles through manual measurements post shaking.

This study substantiates the improved performance of various helical piles in liquefiable ground: the use of helical piles resulted in improved dynamic performance

compared to a slender shaft. Nonetheless, care is warranted in the use of helical piles, especially in real field conditions considering variable parameters such as ground condition, depth of liquefiable layer, ground motion characteristics, superstructure specifications, and more importantly soil-pile-structure interaction.

4.5. References

Abd Elaziz, A. Y., & El Naggar, M. H. (2014). Group behaviour of hollow-bar micropiles in cohesive soils. *Canadian geotechnical journal*, *51*(10), 1139-1150.

Abdoun, T., Dobry, R., O'Rourke, T. D., & Goh, S. H. (2003). Pile response to lateral spreads: centrifuge modeling. *Journal of Geotechnical and Geoenvironmental engineering*, *129*(10), 869-878.

Boulanger, R. W., Curras, C. J., Kutter, B. L., Wilson, D. W., & Abghari, A. (1999). Seismic soil-pile-structure interaction experiments and analyses. *Journal of geotechnical and geoenvironmental engineering*, *125*(9), 750-759.

Boulanger, R. W., Kutter, B. L., Brandenberg, S. J., Singh, P., & Chang, D. (2003). Pile foundations in liquefied and laterally spreading ground during earthquakes: centrifuge experiments & analyses. (No. UCD/CGM-03/01). Center for Geotechnical Modeling, Department of Civil and Environmental Engineering, University of California, Davis, California.

Capatti, M. C., Dezi, F., Carbonari, S., & Gara, F. (2018). Full-scale experimental assessment of the dynamic horizontal behavior of micropiles in alluvial silty soils. *Soil Dynamics and Earthquake Engineering*, *113*, 58-74.

Cerato, A.B., Vargas, T.M. & Allred S.M. (2017). A critical review: state of knowledge in seismic behavior of helical piles. *The Journal of the Deep Foundation Institute 11*(1): 39-87.

Dobry, R., O'Rourke, T. D., & Abdoun, T. (2001). Centrifuge-Based Evaluation of Pile Foundation Response to Lateral Spreading and Mitigation Strategies: Research Progress and Accomplishments Report. In Report MCEER-01-SP01,

Multidisciplinary Center for Earthquake Engineering Research (MCEER) (Vol. 2000-2001, pp. 87-101).

Dobry, R., Abdoun, T., O'Rourke, T. D., & Goh, S. H. (2003). Single piles in lateral spreads: Field bending moment evaluation. *Journal of Geotechnical and Geoenvironmental Engineering*, *129*(10), 879-889.

Ebeido, A., Elgamal A., Tokimatsu K., Akio A. (2019). Pile and Pile Group Response to Liquefaction -Induced Lateral Spreading in Four Large-Scale Shake Table Experiments. *Journal of Geotechnical & Geoenvironmental Engineering 145*(10) https://doi.org/10.1061/(ASCE)GT.1943-5606.0002142.

Elkasabgy, M., & El Naggar, M. H. (2018). Lateral vibration of helical and driven steel piles installed in clayey soil. *Journal of Geotechnical and Geoenvironmental Engineering*, *144*(9), 06018009.

Elkasabgy, M., & El Naggar, M. H. (2019). Lateral Performance and p-y Curves for Large-Capacity Helical Piles Installed in Clayey Glacial Deposit. *Journal of Geotechnical and Geoenvironmental Engineering*, *145*(10), 04019078.

El-Marsafawi, H., Han, Y. C., & Novak, M. (1992). Dynamic experiments on two pile groups." *Journal of Geotechnical Engineering*, *118*(4), 576-592.

Elsawy, M.K., El Naggar, M.H., Cerato, A., & Elgamal, A. (2019a). Seismic performance of helical piles in dry sand from large-scale shaking table tests. *Géotechnique*, *69*(12), 1071-1085.

ElSawy, M. K., El Naggar, M. H., Cerato, A. B., & Elgamal, A. W. (2019b). Data Reduction and Dynamic p-y Curves of Helical Piles from Large-Scale Shake Table

Tests. *Journal of Geotechnical and Geoenvironmental Engineering*, *145*(10), 04019075.

Farhangi, V., Karakouzian, M., & Geertsema, M. (2020). Effect of micropiles on clean sand liquefaction risk based on CPT and SPT. *Applied Sciences*, *10*(9), 3111.

Ghayoomi, M., Ghadirianniari, S., Khosravi, A., & Mirshekari, M. (2018). Seismic behavior of pile-supported systems in unsaturated sand. *Soil Dynamics and Earthquake Engineering*, *112*, 162-173.

Iai, S., Tobita, T., & Nakahara, T. (2005). Generalised scaling relations for dynamic centrifuge tests. *Geotechnique*, *55*(5), 355-362.

Jahed Orang, M., Motamed, R., & Toth, J. (2019a). Experimental Evaluation of Dynamic Response of Helical Piles in Dry Sand using 1g Shaking Table Tests. In *7th International Conference on Earthquake Geotechnical Engineering 2019*.

Jahed Orang, M., Bruketta, S., & Motamed, R. (2019b). Experimental evaluation of spatial variability effects on liquefaction-induced settlements. In *Geo-Congress 2019: Earthquake Engineering and Soil Dynamics* (pp. 294-303). Reston, VA: American Society of Civil Engineers.

Jahed Orang, M., Bousheri, R., Motamed, R., Prabhakaran, A., and Elgamal, A., (2020). Large-scale Shake Table Experiment on the Performance of Helical Piles in Liquefiable Soils. *DFI 45th Annual Conference on Deep Foundations*, October 13-16 2020, pp. 576-585.

Jahed Orang, M., Boushehri, R., Motamed, R., Prabhakaran, A., & Elgamal, A. (2021a). An Experimental Evaluation of Helical Piles as a Liquefaction-Induced Building

Settlement Mitigation Measure (Submitted to *Soil Dynamics and Earthquake Engineering*).

Jahed Orang, M., Motamed, R., Prabhakaran, A., & Elgamal, A. (2021b). Large-Scale Shake Table Tests on a Shallow Foundation in Liquefiable Soils. *Journal of Geotechnical and Geoenvironmental Engineering, 147*(1), 04020152.

Lim, H., & Jeong, S. (2018). Simplified p-y curves under dynamic loading in dry sand. *Soil Dynamics and Earthquake Engineering, 113*, 101-111.

Makris, N., Tazoh, T., Yun, X., & Fill, A. C. (1997). Prediction of the measured response of a scaled soil-pile-superstructure system. *Soil Dynamics and Earthquake Engineering, 16*(2), 113-124.

Mashhoud, H. J., Yin, J. H., Panah, A. K., & Leung, Y. F. (2018). Shaking table test study on dynamic behavior of micropiles in loose sand. *Soil Dynamics and Earthquake Engineering, 110,* 53-69.

Motamed, R., & Towhata, I. (2009). Shaking Table Model Tests on Pie Groups behind Quay Walls Subjected to Lateral Spreading. *Journal of Geotechnical and Geoenvironmental Engineering, 136*(3), 477-489.

Motamed, R., Towhata, I., Honda, T., Yasuda, S., Tabata, K., & Nakazawa, H. (2009). Behaviour of pile group behind a sheet pile quay wall subjected to liquefaction-induced large ground deformation observed in shaking test in E-defense project. *Soils and foundations, 49*(3), 459-475.

Motamed, R., Towhata, I., Honda, T., Tabata, K., & Abe, A. (2013). Pile group response to liquefaction-induced lateral spreading: E-Defense large shake table test. *Soil Dyn and Earthquake Eng., 51*, 35-46 http://dx.doi.org/10.1016/j.soildyn.2013.04.007.

Nikolaou, S., Mylonakis, G., Gazetas, G., & Tazoh, T. (2001). Kinematic pile bending during earthquakes: analysis and field measurements. *Geotechnique, 51*(5), 425-440.

Novak, M., & F. Grigg, R. (1976). Dynamic experiments with small pile foundations. *Canadian Geotechnical Journal*, *13*(4), 372-385.

Perko, H.A. (2009). *Helical piles: a practical guide to design and installation*. New York, NY, USA: John Wiley & Sons.

Ridgley, N. (2015). Practice note 28: Screw piles: Guidelines for design, construction & installation. *Wellington, New Zealand: Institution of Professional Engineers New Zealand*.

Shahbazi, M., Cerato, A. B., Allred, S., El Naggar, M. H., & Elgamal, A. (2020a). Damping characteristics of full-scale grouped helical piles in dense sands subjected to small and large shaking events. *Canadian Geotechnical Journal, 57*(6), 801-814.

Shahbazi, M., Cerato, A. B., El Naggar, H. M., and Elgamal, A. (2020b). Evaluation of Seismic Soil–Structure Interaction of Full-Scale Grouped Helical Piles in Dense Sand. *International Journal of Geomechanics, 20*(12), 04020228.

Tokimatsu, K., Suzuki, H., & Sato, M. (2005). Effects of inertial and kinematic interaction on seismic behavior of pile with embedded foundation. *Soil Dynamics and Earthquake Engineering*, *25*(7-10), 753-762.

Wilson, D. W., Boulanger, R. W., & Kutter, B. L. (2000). Observed seismic lateral resistance of liquefying sand. *Journal of Geotechnical and Geoenvironmental Engineering, 126*(10), 898-906.

Zeghal, M., Elgamal, A. W., Zeng, X., & Arulmoli, K. (1999). Mechanism of liquefaction response in sand–silt dynamic centrifuge tests. *Soil Dynamics and Earthquake Engineering, 18*(1), 71-85.

5. Conclusions

5.1. Concluding Remarks

The important outcomes through this research are provided in two different categories including large-scale shake table tests which were conducted at the UCSD Powell Laboratory and scaled 1g shake table tests which were carried out at the UNR SEM 120 Laboratory.

Part 1: Large-Scale Shake Table Tests

Two test series (one without any mitigation and one using helical piles as a mitigation measure) with similar ground conditions and input motions, but with different soil-foundation response characteristics, were conducted at the UCSD Powell Laboratory. In the first test series (i.e., the Baseline test) a shallow rigid foundation was placed atop a three-layer model ground, including a shallow liquefiable medium representing typical soil profiles observed in past earthquakes. In the second test series (i.e., the Helical Pile test) a group of helical piles was used to underpin the shallow foundation in a similar model ground. This study aimed at evaluating the liquefaction-induced settlement of a shallow foundation and assessing the dynamic behavior of helical piles and the effectiveness of using these deep foundation elements in reducing liquefaction-induced foundation settlement and tilt. A summary of major findings throughout this study is provided hereafter:

- This series of shake table tests is the first set of experimental data at this scale exploring the response of a soil-foundation-superstructure system to liquefaction-induced ground movement effects. The produced experimental data in the Baseline test provides researchers and practicing engineers a benchmark dataset to validate

numerical simulations focused on the liquefaction-induced settlement of buildings as well as future evaluation of effective mitigation strategies.

- A dense array of high-resolution accelerometers was utilized for system identification, capturing the fundamental frequency of the model ground (i.e., around 5 Hz) by establishing transfer functions. This set of data was further used to characterize the shear wave velocity profile of the model ground. As we proceeded deeper into the dense layer, the shear wave velocity increased. Two sets of CPT tests were conducted in the Helical Pile test, one before and one after Shake 1, to evaluate further the continuous variations in the relative density of the three-layered soil profile. The variation of cone tip resistance indicated higher values inside the dense layer, in line with the observed elevated shear wave velocity values. Additionally, higher cone tip resistance was measured after Shake 1 especially at the bottom half of the liquefiable layer and the top half of the dense layer.
- The EPWP generation at different depths indicated extensive liquefaction and pore-water pressure buildup in the middle of the dense layer even after shaking ceased. EPWP isochrones became relatively constant along the depth in both the free-field and below the foundation arrays in the Baseline and the Helical Pile tests after Shake 1. Consequently, the transient hydraulic gradients vanished after the end of ground shaking. The calculation of flow velocity, based on Darcy's law and assuming 1D flow inside the ground, indicated the direction of flow on top of the dense layer and on the boundary of the dense/loose layers was toward the dense layer (downward flow), whereas inside the loose layer, the direction of flow was upward. This, especially the downward direction of flow, further explains how

EPWP dissipation at the middle of the dense layer did not occur even after the shaking ended. The upward flow direction in the loose layer was confirmed by the observed sand ejecta after the shaking ceased. Moreover, EPWP contour plots at different time steps indicated reduced pore-water pressure generation in the Helical Pile test. The extent of EPWP reduction was more considerable in the zone of helical pile influence at the top of the dense layer and the bottom of the liquefiable layer. The densification of the area around helical piles, with the changes in the load-carrying patterns of the coupled pile-foundation-ground model system in the Helical Pile test, explains the observed EPWP difference between the two test series.

- The maximum CAV_{dp} was measured at the middle of the dense layer in the case of free-field array, where the corresponding maximum value for the below foundation array was observed at the bottom of the liquefiable layer. This indicates higher acceleration at similar depths in each array, which is in line with the presented acceleration time histories. The CAV_{dp} values were also used for calculating shear-induced settlement of the foundation based on Bray and Macedo's [2017] simplified procedure. The IMs (including CAV_{dp}) were also estimated based on DEEPSOIL version 7.0 analysis assuming free-field no liquefaction condition for shear-induced settlement of the foundation as suggested by Bray and Macedo [2017]. The use of CAV_{dp} at different depths and locations resulted in lower consistency of the estimated settlement values compared with the observed settlement, whereas utilizing IM parameters (i.e., in this case CAV_{dp} and S_{a1}) at the

free-field no liquefaction condition yielded a better estimate for the shear-induced component of the foundation settlement.

- Implementing various protective measures on the strain gauges resulted in high functionality of these strain measuring elements. The bending moments, obtained through the measured bending strains along the depth of the ground model, were used further to inspect the dynamic response of the single-helix helical piles. All the helical piles exhibited a similar trend in their bending moment response in both shakings. The higher bending moment difference between two shakes was observed at the bottom half of the liquefiable layer. The highest bending moment at all of the helical piles observed at the loose-dense layer interface was in line with the observation in the steel-driven piles in layered deposits (i.e., shear discontinuity effect).
- Measured near-foundation and foundation settlement trends displayed a local shear failure mechanism in the Baseline test, which is supported by observed heave in the surrounding ground and excessive punching settlement of the foundation. Post-shaking settlements were carefully quantified and attributed to ground loss due to observed sand boils as well as to post-liquefaction consolidation of the liquefiable layer.
- The measured near-foundation settlements were comparable in both test series during Shake 2, whereas excessive heave was observed in the near-foundation ground due to bearing capacity failure of the unsupported shallow foundation in the Baseline test during Shake 1. A higher portion of the foundation settlement took place during shakings in both the Baseline and Helical Pile tests; however, the

foundation supported by helical piles did not experience any settlement after both shakings. The use of helical piles resulted in almost no measured differential settlement and tilt of the foundation.

- The observed foundation settlement accumulation in both test series shed light on the contribution of different liquefaction-induced settlement mechanisms. The only contributing mechanisms of the foundation settlement during the Helical Pile tests were transient high-hydraulic gradients and SSI ratcheting during shakings. During each shake, the settlement accumulation rate was significantly reduced using a group of helical piles to support the shallow foundation. The contribution of ejecta-induced and volumetric-induced (except high hydraulic transient gradients) components of foundation settlement was eliminated during the Helical Pile tests.
- Two simplified procedures were used to estimate the liquefaction-induced settlement of the foundation, those of Liu and Dobry [1997] and Bray and Macedo [2017]. The normalized settlement versus normalized width of the foundation presented by Liu and Dobry [1997] indicated settlement values in the range of 2.6-22.7 cm, which is lower than the 28 cm measured settlement of the foundation in the case of Shake 1-1. Using Bray and Macedo's [2017] simplified procedure resulted in a total settlement of the foundation ranging from 7.5 cm to 10.9 cm (excluding ejecta-induced settlement), which also is lower than the measured total settlement value (i.e., 28 cm). Both methods underestimated the measured total settlement obtained through this shake table study.

Part 2: Scaled 1g Shake Table Tests

Scaled 1*g* shake table tests were conducted to evaluate the dynamic behavior of a slender shaft and helical piles with different numbers of helices in liquefiable and dry ground models. The shake table experimental results included multiple aspects of the dynamic response of these foundations, such as the effects of multiple shakings, ground motion amplitude, superstructure weight, and combined effects of liquefiable layer relative density and superstructure weight, which were investigated based on the bending moment variation along the depth for each of the model piles. In addition, four parameters were used to assess the performance of the helical piles compared to the slender shaft to provide a broader understanding of the efficiency of these deep foundation elements. The major outcomes are summarized hereafter:

- There was no observed difference in the trend of bending moment variation along the depth for different pile types as all of the helical piles and the slender shaft illustrated similar behavior in the variation of bending moment along the depth in all of the test series. The maximum bending moment was observed to be at the loose-dense layer interface, which is in line with previous research.
- Lower bending moments were observed along the depth in the dry test compared to the liquefaction tests. The liquefiable layer relative density played an important role in the dynamic response of the helical piles and the slender shaft. Densification of the liquefiable layer as a result of multiple shakings yielded to similar bending moment values observed in the dry test.
- Higher peak input accelerations resulted in higher moments exerted on the various types of piles. Additionally, Heavy Weight Series (HWS) tests resulted in higher

bending moments compared to Light Weight Series (LWS) tests. The increased ground motion amplitude and superstructure weight result in elevated inertial force at the superstructure level. The increased relative density of the liquefiable layer had a major influence in reducing the bending moment along the depth at the loose-dense layer interface in all the piles, even with higher superstructure weight.

- The number of helices influenced the dynamic performance of the helical piles. An increase in the number of helices resulted in an improvement (reduction) in residual horizontal displacement, maximum horizontal displacement, and maximum acceleration (measured on the top of each pile) and maximum moment (measured along the length of each pile). Residual horizontal displacement showed the greatest improvement, with a 60% drop in displacement of the triple-helix helical pile compared to that of the slender shaft.
- During all the shaking events, there were no observed settlements in the helical piles or the slender shaft, while the free-field ground settled as high as 2cm in the proximity of the helical piles through manual measurements post shaking.

In the large-scale shake table tests, comparison between various mitigation techniques revealed the salient improved performance of a shallow foundation supported with the helical piles in reducing liquefaction-induced settlement and tilt. Considering the differences in testing conditions, including the type of physical model test, simulated ground model, structural model characteristics, and input motions, the highest settlement and tilting mitigation efficiencies (i.e., SME and TME) were achieved using four single-helix helical piles in shallow liquefiable deposits. Nonetheless, measured acceleration time

histories and the calculated transfer functions in both tests indicated amplified response due to increased stiffness of the soil-pile-foundation system in the Helical Pile test. This research, in conjunction with previous research, suggests a holistic strategy in exploring the efficiency of different liquefaction-mitigation measures taking into account the amplified demand for the superstructure. Similar to large-scale test results, the findings through scaled shake table tests also substantiate the improved performance of various helical piles in the liquefiable ground: the use of helical piles resulted in improved dynamic performance compared to a slender shaft. However, care is warranted in the use of helical piles, especially in real field conditions considering variable parameters such as ground condition, depth of the liquefiable layer, ground motion characteristics, superstructure specifications, and more importantly, soil-pile-structure interaction.

5.2. Research Impact

Overall, this study demonstrated the significant contribution of 1g shake table tests in providing a broader understanding of the liquefaction-induced building settlement phenomenon by reproducing all the controlling mechanisms. Prior centrifuge tests have not captured the eject-induced mechanism, which can extremely affect the amount of the liquefaction-induced foundation settlement. The reproduction of this mechanism through shake table experiments will result in a better simulation of the real ground conditions where considerable amounts of sediment ejecta were observed during field observations in past earthquakes. Additionally, this series of large-scale shake table tests provided useful insight into the efficiency of helical piles as a reliable countermeasure in liquefaction-induced foundation settlement and rotation. This series of large-scale tests was focused on evaluating the effects of a shallow liquefiable layer on the response of a shallow

foundation, consistent with the observed damage during past earthquakes. However, the limitation for shake table experiments is the inability to reproduce higher confining pressures observed at deeper depths, which should be considered in utilizing the results of this study for deeper liquefiable deposits. Finally, the results of this study were obtained on a specific ground condition, foundation contact pressure, and input motion characteristics. Caution should be taken in the real built environment since any change or combined variation of these factors can ultimately affect the performance of helical piles in liquefiable grounds.

5.3. Future Research Directions

A comprehensive series of shake table tests was conducted through the course of this research and provided salient insights on the performance of shallow foundations in liquefiable grounds, application of helical piles as a liquefaction mitigation measure, and the effect of various helical pile specifications on their dynamic response to simulated ground motions. These observations lay the ground for further future research including liquefaction-induced foundation settlement mechanisms, dynamic behavior of helical piles in liquefiable grounds, and more importantly, the effective application of various ground improvement measures such as the use of helical piles in liquefaction-induced settlement and tilt mitigation. Some of the key prospective research directions are provided hereafter:

- There is still an existing knowledge gap concerning the influence of the ejecta-induced mechanism and its contribution to the liquefaction-induced settlement of the shallow foundations. More shake table studies along with proper evaluation of recent case histories could provide a deeper understanding regarding the effect of sand ejecta by quantifying the amount of sand ejecta to guide researchers and

practitioners to better estimates of total liquefaction-induced foundation settlements.

- The current large-scale shake table study entailed a shallow foundation with constant contact pressure in a specific ground condition including a shallow liquefiable layer. More physical modeling tests including shake table and centrifuge experiments are required to replicate a wide variety of ground conditions, input motions, and structural components to provide a holistic dataset along with the observed foundation settlement during past earthquakes. This will assist in improving the foundation tilt and settlement estimates after strong ground shakings.
- The application of helical piles in liquefiable grounds is only limited to this study. A larger number of physical tests is essential to gather reliable information regarding the dynamic performance of helical piles and their overall efficacy in reducing foundation tilt and settlement in various ground conditions, earthquake motions, and superstructure effects. This can be achieved using various configurations of helical piles either in a single or group setup with different specifications (e.g., different number of helices) to underpin different shallow foundations (i.e., with different dimensions and foundation contact pressures) to gain deeper insight into the efficiency of helical piles in liquefiable grounds.
- Numerical simulations also need to be improved to include the effects of soil-pile-foundation-superstructure interaction in order to perceive the mechanisms of helical pile inclusion in various liquefiable deposits. Various simulation software can be utilized to model the different combinations of soil, helical pile, shallow

foundation, and superstructure to predict the liquefaction-induced foundation settlement and tilt. These can be further verified using physical test models described earlier to introduce a holistic approach (i.e., considering numerical simulations, physical model tests, and observed field case histories) in assessing the performance of shallow foundations and the overall system in response to devastating liquefaction effects.

5.4. References

Bray, J. D. & Macedo, J. (2017). “6th Ishihara lecture: Simplified Procedure for estimating liquefaction-induced building settlement.” Soil Dyn. Earthquake Eng., (102) 215-231 http://dx.doi.org/10.1016/j.soildyn.2017.08.026.

Liu, L., and Dobry, R. (1997). “Seismic response of shallow foundation on liquefiable sand.” J. Geotech. Geoenviron. Eng., 123(6), 557–567.